

**AN OPTIMIZATION TECHNIQUE FOR SMART
SELF-HEALING MICROGRIDS**

BY
Maad Mohammed Abdullah Al-Owaifeer

A Thesis Presented to the
DEANSHIP OF GRADUATE STUDIES

KING FAHD UNIVERSITY OF PETROLEUM & MINERALS

DHAHRAN, SAUDI ARABIA

In Partial Fulfillment of the
Requirements for the Degree of

MASTER OF SCIENCE

In

ELECTRICAL ENGINEERING

May 2015

KING FAHD UNIVERSITY OF PETROLEUM & MINERALS
DHAHRAN- 31261, SAUDI ARABIA
DEANSHIP OF GRADUATE STUDIES

This thesis, written by **Maad Mohammed Abdullah Al-Owaifeer** under the direction of his thesis advisor and approved by his thesis committee, has been presented and accepted by the Dean of Graduate Studies, in partial fulfillment of the requirements for the degree of **Master of Science in Electrical Engineering**.

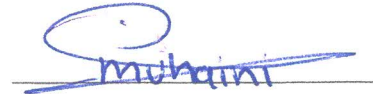


Dr. Ali A. Al-Shaikhi
Department Chairman



Dr. Salam A. Zummo
Dean of Graduate Studies

31/5/15
Date



Dr. Mohammed M. Al-Muhaini
(Advisor)



Dr. Ibrahim M. El-Amin
(Member)



Dr. Mohammad A. Abido
(Member)

© Maad Mohammed Abdullah Al-Owaifeer

2015

Dedicated to my parents and my future wife and kids

ACKNOWLEDGMENTS

First and foremost, I would like to thank Allah for blessing me with his mercy, guidance, health, strength, and many other uncountable graces.

I would also like to express my appreciation to my advisor, Dr. Mohammed, for his invaluable assistance and supervision in every step throughout the masters' journey. Thank you for your advices, support, and understanding.

Great thanks to the Electrical Engineering department and my respected thesis committee members for providing all means and resources in conducting this research.

I want to thank my friends, Abdulrahman, Mohannad, and Taisir for their very useful cooperation and suggestions in forming this thesis.

Special thanks to my parents, brothers and sisters, who have always been by my side during the good and bad times. Thank you very much.

TABLE OF CONTENT

ACKNOWLEDGMENTS	v
TABLE OF CONTENT	vi
LIST OF TABLES	x
LIST OF FIGURES	xiii
LIST OF ABBREVIATIONS	xviii
ABSTRACT (ENGLISH)	xx
ABSTRACT (ARABIC)	xxii
CHAPTER 1 INTRODUCTION	1
1.1 Introduction	1
1.2 Thesis Motivation	4
1.3 Thesis Objectives	6
1.4 Background	7
1.5 Thesis Structure	20
CHAPTER 2 IMPACT OF RENEWABLE ENERGY AND LOAD MANAGEMENT ON SYSTEM RELAIBILITY AND RESTORATION	22
2.1 Literature Review	23
2.2 System Modeling	24
2.2.1 Annual Chronological Load Modeling	24

2.2.2 Wind Power Output Modeling	25
2.2.3 PV Power Output Modeling.....	26
2.2.4 Load Management (LM) Modeling.....	27
2.2.5 Fail and Repair Incidents Simulation	31
2.2.6 RBTS-Bus 2 Distribution System	32
2.3 Case Studies	35
2.3.1 Local Load Study	35
2.3.2 System Study	51
CHAPTER 3 LOAD PRIORITY MODELING FOR SMART MICROGRIDS	62
3.1 Introduction	63
3.2 The Prioritizing Factors.....	66
3.3 The Mathematical Formulation of the Prioritizing Strategy	72
3.3.1 Criticality	73
3.3.2 Expected Effects on System Total Reliability Indices	73
3.3.3 Customers with Demand Side Management (DSM) Programs	74
3.3.4 Estimated Cost of interruption.	76
3.4 Prioritizing RBTS Bus 4 Customers.....	78
3.4.1 Case1: Original RBTS Bus 4 Data	81
3.4.2 Case 2: Simulating MG Loads	83
3.5 Conclusions	86

CHAPTER 4 THE SMART SELF-HEALING OPTIMIZATION TECHNIQUE FOR MICROGRIDS	88
4.1 Introduction	89
4.1.1 Restoration Optimization Techniques in the Literature	89
4.1.2 Pure and Mixed Linear Integer Programming	92
4.2 The Proposed Self-Healing Technique Model	94
4.2.1 Control Variables.....	94
4.2.2 Objective Functions	95
4.2.3 Problem Constraint	98
4.3 The MILP Mathematical formulation of the Optimization Problem.....	99
4.3.1 Formulating Problem Constraint.....	100
4.3.2 Formulating Objective Functions of the Problem	118
4.4 Set of Bounds for McCormick’s Envelopes	120
CHAPTER 5 MICROGRIDS SELF-HEALING OPTIMIZATION – CASE STUDIES AND DISCUSSION	130
5.1 Verification of the Proposed Formulation	134
5.2 Comparison Based Study.....	138
5.3 Testing the Prioritizing Methodology	145
5.4 Comparing Conventional Distribution System with Smart Microgrid System.....	155

5.4.1 Case 1 – Conventional Distribution System	156
5.4.2 Case 2 – Microgrid Operation	161
5.5 Sensitivity Analysis.....	176
CHAPTER 6 CONCLUSIONS AND REMARKS.....	179
6.1 Summary	179
6.2 Conclusions	181
6.3 Contributions	183
6.4 Future Work	183
APPENDICES	184
A.1 Chronological Load Modeling Data	184
A.2 Linearization Methods	186
A.2.1 Disjunctive or Decision Constraints	187
A.2.2 Polygonal Inner-Approximation.....	188
A.2.3 Linear Envelopes for Bilinear Products.....	190
A.2.4 Piecewise Linearization and Special Order Sets of Type 2 (SOS2).....	193
NOMENCLATURE.....	198
REFERENCES.....	202
VITAE.....	209

LIST OF TABLES

Chapter 1

Table 1.1 IIT project cost analysis	19
---	----

Chapter 2

Table 2.1 Load point data	34
---------------------------------	----

Table 2.2 Total case studies	37
------------------------------------	----

Table 2.3 Interruptions information	37
---	----

Table 2.4 Reliability indices - first stage	38
---	----

Table 2.5 Reliability indices – second stage - wind turbine	38
---	----

Table 2.6 Reliability indices – second stage - PV	39
---	----

Table 2.7 Reliability indices – second stage – WT+PV	40
--	----

Table 2.8 Different specifications for PV/WT sizes and LM factors	54
---	----

Table 2.9 Case I restoration results	55
--	----

Table 2.10 Case I reliability indices	55
---	----

Table 2.11 Case I - combining RE and LM	55
---	----

Table 2.12 Case II restoration results	58
--	----

Table 2.13 Case II reliability indices	58
--	----

Table 2.14 Case II – combining RE and LM	58
--	----

Chapter 3

Table 3.1 Weights and levels of criticality	73
---	----

Table 3.2 DSM programs and associated factors	75
---	----

Table 3.3 Number of components and customers for RBTS Bus 4	80
---	----

Table 3.4 Number of customers and load type for all LPs in RBTS Bus-4 system.....	81
---	----

Chapter 5

Table 5.1 IEEE three feeder 16 bus system node data.....	132
Table 5.2 IEEE 3 feeder 16 bus system line data	133
Table 5.3 IEEE 3 feeder 16 bus system - loss minimization results and coparison	137
Table 5.4 Fault at feeder 2-8.....	140
Table 5.5 Restoration process for fault at feeder 2-8.....	141
Table 5.6 Computational time comparison.....	143
Table 5.7 Load points information.....	147
Table 5.8 Intruption information.....	148
Table 5.9 Case studies.....	149
Table 5.10 Case 1 simulation results	150
Table 5.11 Case 2 simulation results	150
Table 5.12 Case 3 simulation results	150
Table 5.13 Case 4 simulation results	151
Table 5.14 Case 5 simulation results	151
Table 5.15 Case 6 simulation results	151
Table 5.16 Summary of results	153
Table 5.17 Load point priority weights.....	156
Table 5.18 Fault incidents.....	156
Table 5.19 Interruption results - case 1 - fault A	157
Table 5.20 Interruption results - case 1 - fault B	159
Table 5.21 Interruption results - case 1 - fault C	161

Table 5.22 Connected DGs data	162
Table 5.23 Curtailed loads data	162
Table 5.24 DG outputs – case 2 – fault A.....	164
Table 5.25 Interruption results - case 2 - fault A	164
Table 5.26 DG outputs – case 2 – fault B.....	167
Table 5.27 Curtailment data – case 2 – fault B.....	167
Table 5.28 Interruption results - case 2 - fault B	167
Table 5.29 DG Outputs – case 2 – fault C	170
Table 5.30 Curtailment data – case 2 – fault C.....	171
Table 5.31 Interruption results - case 2 - fault C	171
Table 5.32 Coparison between case 1 and case 2	175
Table 5.33 Fault information	176
Table 5.34 Cases of sensitivity study.....	177
Table 5.35 Restoration results for sensitivy cases of study	177
Table 5.36 DGs operation information	177
Table 5.37 Load curtailment information	178

Appendices

Table A.1 Weekly load peak fractions.....	184
Table A.2 Daily fraction of the residential, commercial, and industrial peak load	185
Table A.3 Hourly fraction of the residential, commercial, and industrial peak load	185

LIST OF FIGURES

Chapter 1

Figure 1.1 Self-healing strategy for electric microgrids	7
Figure 1.2 Solar power output variation per unit, Dhahran 2003	9
Figure 1.3 Wind power output variation per unit, Dhahran 2003.....	9
Figure 1.4 Contribution of various storage technologies in the U.S.	13
Figure 1.5 IIT perfect microgrid system	20

Chapter 2

Figure 2.1 Power output curve for a typical wind turbine	26
Figure 2.2 Weibull distribution for the studied wind speed.....	26
Figure 2.3 Monthly averaged solar irradiation for the simulated year	27
Figure 2.4 Load shifting method.....	29
Figure 2.5 Peak clipping method	31
Figure 2.6 Energy conserved versus clipping factor C	31
Figure 2.7 MCS implementation procedure.....	33
Figure 2.8 RBTS-BUS2 distribution system	34
Figure 2.9 General architecture flow chart of the first case study	36
Figure 2.10 Unavailability vs. curtailment level (WT).....	39
Figure 2.11 Unavailability vs. curtailment level (PV).....	40
Figure 2.12 Unavailability vs curtailment level (WT and PV).....	41
Figure 2.13 Comparison between WT and PV with different rated power	42
Figure 2.14 Comparison between base case and the second stage of study	42

Figure 2.15 ENS vs. shifting factor	44
Figure 2.16 ENS vs. clipping factor.....	44
Figure 2.17 ENS vs. shifting factor - hybrid system.....	45
Figure 2.18 Unavailability vs. shifting factor - 50% curtailment	46
Figure 2.19 Unavailability vs. shifting factor - 75% Curtailment	47
Figure 2.20 Unavailability vs. shifting factor - 100% curtailment	47
Figure 2.21 ENS vs clipping factor - hybrid system.....	48
Figure 2.22 Unavailability vs. clipping factor - 50% curtailment	49
Figure 2.23 Unavailability vs. clipping factor - 75% curtailment	49
Figure 2.24 Unavailability vs. clipping factor - 100% curtailment	50
Figure 2.25 Faults locations	52
Figure 2.26 Hybrid renewable system location	53
Figure 2.27 Case I - load voltage profile with different hybrid system sizes	56
Figure 2.28 Case I – load voltage profile interchanging load shifting factor	56
Figure 2.29 Case I – load voltage profile interchanging peak clipping factor.....	57
Figure 2.30 Case I – load voltage profile combining RE and LM.....	57
Figure 2.31 Case II - load voltage profile with different hybrid system sizes.....	59
Figure 2.32 Case II – load voltage profile interchanging load shifting factor	59
Figure 2.33 Case II – load voltage profile interchanging peak clipping factor	60
Figure 2.34 Case II – load voltage profile combining RE and LM	60
 Chapter 3	
Figure 3.1 Flow chart of the prioritizing method.....	79
Figure 3.2 Single line diagram of RBTS Bus 4 distribution system	80

Figure 3.3 Case 1: loud points ENS, SAIDI, SAIFI, and cost weights	82
Figure 3.4 Case 1: load points total priority weights	82
Figure 3.5 Case 2.A: load points ENS, SAIDI, SAIFI, and cost weights.....	84
Figure 3.6 Case 2.A: load points total priority weights	85
Figure 3.7 Case 2.B: load points ENS, SAIDI, SAIFI, and cost weights	86
Figure 3.8 Case 2.B: load points total priority weights	87

Chapter 5

Figure 5.1 IEEE 16 bus test system	132
Figure 5.2 IEEE 16 bus voltage magnitudes – original configuration.....	134
Figure 5.3 IEEE 16 bus voltage phase angles – original configuration.....	134
Figure 5.4 Optimal configuration for loss reduction of the IEEE 3 feeder 16 bus system	136
Figure 5.5 Voltage magnitudes – optimal configuration	137
Figure 5.6 Phase angles – optimal configuration.....	138
Figure 5.7 Effects of removing the capacitor banks on voltage profile.....	139
Figure 5.8 Fault incident at feeder 2-8.....	140
Figure 5.9 Optimal system configuration after service restoration.....	141
Figure 5.10 Comparison in voltage magnitude between method [68] and the proposed method	142
Figure 5.11 Comparison in voltage angle between method [68] and the proposed method	142
Figure 5.12 Solution process using formulation [68]	143
Figure 5.13 Solution process of the proposed formulation.....	144

Figure 5.14 Load curves for each load type.....	148
Figure 5.15 ENS comparison between all cases - dashed bar for base case - solid bar for proposed method	152
Figure 5.16 SAIDI comparison between all cases - dashed bar for base case - solid bar for proposed method	152
Figure 5.17 SAIFI comparison between all cases - dashed bar for base case - solid bar for proposed method	153
Figure 5.18 Interruption cost comparison between all cases - dashed bar for base case - solid bar for proposed method.....	153
Figure 5.19 Restoration configuration result - case 1 - fault A	157
Figure 5.20 Voltage magnitudes - case 1 - fault A	158
Figure 5.21 Voltage angles - case 1 - fault A	158
Figure 5.22 Restoration configuration result - case 1 – fault B.....	159
Figure 5.23 Voltage magnitudes - case 1 - fault B	160
Figure 5.24 Voltage angles - case 1 - fault B.....	160
Figure 5.25 Restoration configuration result - Case 2 – Fault A	163
Figure 5.26 Voltage magnitudes - case 2 - fault A	164
Figure 5.27 Voltage angles - case 2 - fault A	165
Figure 5.28 Restoration configuration result - case 2 – fault B	166
Figure 5.29 Voltage magnitudes - case 2 - fault B	168
Figure 5.30 Voltage angles - case 2 - fault B.....	168
Figure 5.31 Restoration configuration result - case 2 – fault C	170
Figure 5.32 Voltage magnitudes - case 2 - fault C	171

Figure 5.33 Voltage angles - case 2 - fault C.....	172
Figure 5.34 ENS comparison.....	173
Figure 5.35 SAIDI comparison.....	173
Figure 5.36 SAIFI comparison	174
Figure 5.37 Associated cost comparison	174

Appendices

Figure A.1 Polygonal inner approximation for a circle with radius=1 considering different number of edges.....	188
Figure A.2 Error probability in polygonal inner approximation.....	190
Figure A.3 Actual function of bilinear product	192
Figure A.4 Lower bound McCormick's envelopes	192
Figure A.5 Upper bound McCormick's envelopes.....	193
Figure A.6 Piecewise linearization	195

LIST OF ABBREVIATIONS

MILP	:	Mixed Integer Linear Programming
DG	:	Distributed Generator
IEEE	:	Institute of Electrical and Electronics Engineers
IT	:	Information Technology
DER	:	Distributed Energy Resources
LM	:	Load Management
PDF	:	Probability Distribution Function
PV	:	Photovoltaics
WT	:	Wind Turbine
AMI	:	Advanced Metering Infrastructure
DSM	:	Demand Side Management
LS	:	Load Shifting
PC	:	Peak Clipping
RBTS	:	Roy Billinton's Test System
MG	:	Microgrid
MCS	:	Monte Carlo Simulation

LP	:	Load Point
RE	:	Renewable Energy
STRI	:	System Total Reliability Indices
MTTR	:	Mean Time to Repair
ENS	:	Energy not Supplied
SAIDI	:	System Average Interruption Duration Index
SAIFI	:	System Average Interruption Frequency Index
SOS2	:	Special Order Set of type 2

ABSTRACT

Full Name: Maad Mohammed Abdullah Al-Owaifeer

Thesis Title: An Optimization Technique for Smart Self-Healing Microgrids

Major Field: Electrical Engineering

Date of Degree: May, 2015

Typical distribution systems are rapidly facing enormous changes. High technological equipment have been invented and magnificently designed allowing operators to have full vision and control over the system. Integrating these equipment into a conventional distribution system increases the level of reliability and transfers the system to be the so-called “a microgrid”. However, and due to the increased control variables and complexity of such networks, the decision for an operator, especially at emergency and fault cases, becomes a very difficult task, thereby, impacting system reliability. Sophisticated algorithms need to be applied in order to guarantee the optimum restoration solution for any interruption incident.

In this study, a smart self-healing optimization strategy for electrical microgrids is proposed that depends on several factors such as, available power supply, system configuration and load demand. Also, a load priority model is proposed which is merged into the self-healing strategy. The strategy of self-healing is formulated as a Mixed Integer Linear Programming (MILP) problem which is then solved mathematically ensuring global optimality of the solution. The strategy is implemented and studied on the IEEE 3 feeder 16 bus distribution system. The systems to be studied is assumed in this thesis to be a smart

microgrid distribution systems equipped with automation devices and IT infrastructure including automated switches, sensors and fault detection and isolation devices.

Simulation results demonstrate the effectiveness of the proposed strategy in restoring the system after any fault by optimizing system configuration, DGs power output, and amount of load curtailment. Further, remarkable results in terms of accuracy and computational time of the strategy are recorded.

ملخص الرسالة

الاسم الكامل: معد محمد عبدالله العوفير

عنوان الرسالة: تقنية لتحسين الشفاء الذاتي لشبكات التوزيع الذكية

التخصص: الهندسة الكهربائية

تاريخ الدرجة العلمية: جمادى الآخرة، ١٤٣٦ هـ

تواجه نظم التوزيع الكهربائية التقليدية تغيرات هائلة في الفترة الحالية. أخترت معدات عالية التقنية وصممت للسماح لمشغلي شبكات الطاقة بالرؤية والتحكم بالنظام الكهربائي بشكل متقن. دمج هذه المعدات عالية التقنية بالنظم الكهربائية يزيد من مستوى الموثوقية ويحول النظام إلى ما يسمى بشبكات التوزيع الذكية. بسبب إزدياد أجهزة التحكم والتعقيد المصاحب لتلك الشبكات الذكية، فإن قرار مشغل الشبكة يصبح صعباً للغاية خصوصاً في حالات الطوارئ وإنقطاع الكهرباء مما يؤثر على موثوقية الشبكة. من أجل ضمان الحل الأمثل لإي حالت إنقطاع، يجب تطبيق العديد من الدراسات والتحليلات الرياضية.

في هذه الدراسة، يتم تقديم إستراتيجية شفاء ذاتي للشبكات الكهربائية الذكية (smart microgrids). هذه الإستراتيجية تعتمد على العديد من العوامل التقنية، كسعة المولدات الجاهزة للتشغيل، هيكل توصيلات الشبكة، و كمية الأحمال الكهربائية. إضافة إلى ذلك، يتم في هذه الرسالة تقديم نموذج لتصنيف أهمية وأولية الأحمال الكهربائية عند إستعادة الطاقة والذي يدمج مع إستراتيجية الشفاء الذاتي. يتم صياغة إستراتيجية الشفاء الذاتي كمسألة MILP والتي تحل بعد ذلك رياضياً لضمات وجود الحل الأمثل. يتم تنفيذ وتطبيق هذه الدراسة على نظام IEEE 3 feeder 16 bus system. النظام المدروس مفترض في هذه الدراسة على أنه ذكي ومجهز بالبنية التحتية عالية التقنية بما في ذلك المفاتيح الآلية، أجهزة الإستشعار الذكية ومعدات كشف وعزل الأخطاء الكهربائية.

نتائج التحليلات تشير بكفاءة الإستراتيجية المقدمة في إستعادة النظام بعد أية إنقطاع عن طريق إيجاد الحل الأمثل لإستعادة الطاقة من ناحية كمية الطاقة الضرورية من المولدات الكهربائية، كمية تقليص الأحمال اللازمة، و تشكيلة شبكة النظام. بالإضافة، سجلت نتائج جديرة بالملاحظة من حيث سرعة تطبيق الإستراتيجية ودقة الحل.

CHAPTER 1

INTRODUCTION

The first chapter of this thesis is divided into five main sections. Section 1.1 provides a general introduction followed by the thesis motivation in section 1.2. Then, section 1.3 states the main thesis objectives. A general background about selected topics that are strongly related to the thesis topic is delivered in section 1.4. Finally, section 1.5 contains the structure and the organization of the thesis.

1.1 Introduction

Due to the increase in electric demand, complexity of power grids and the call for more reliable, sustainable and controllable energy systems and sources, governments and responsible organizations are moving toward building a new efficient power system, the smart grid. According to the U.S. Department of Energy (DoE) “Smart grid” refers to a class of technologies that people are using to bring utility electricity delivery systems into the 21st century, using computer-based remote control and automation. They are beginning to be used on electricity networks, from the power plants, all the way to the consumers of electricity in homes and businesses. They offer many benefits to utilities and consumers, mostly seen in big improvements in energy efficiency and reliability on the electricity grid and in energy users. It can be added that smart grids, from the customer prospective, includes using smart meters appliances to control the electricity consumption and reduce the bill. On the other hand, from utility prospective, smart grid means introducing more

smart technologies and designs to monitor, operate, and control the system with more reliable and more secure service

Many environmental concerns are rising regarding carbon emissions and its footprints. The obvious solution is to replace the conventional fossil energy sources with renewable energy sources and also to start depending on electrical vehicles rather than gasoline vehicles. An important benefit of a smart grid is that it will pave the way in order to apply these technical solutions in order to improve the security and reliability of the future power grid. Moreover, in [1], 15 important issues and concerns that motivated the implementation of smart grids were stated:

- 1) Aging and underinvested infrastructure.
- 2) Electricity demand throughout the world is steadily increasing, causing high power system loading resulting in overstressed system equipment.
- 3) Public interest groups are putting pressure on politicians to reduce CO₂ emissions through the adoption of alternative energy sources and put in place regulations to increase energy efficiency.
- 4) Increasing distance between generation sites and load centers.
- 5) The changing mix of power generation operating central power plants in parallel with large numbers of small, decentralized (distributed) generation DG.
- 6) Intermittent and fluctuating energy availability of renewable energy sources, such as wind and solar, are placing additional strains on existing grids. The intermittence must be counter-balanced with more intelligence in the grid, base load power generation (hydro, nuclear), and storage.

- 7) Additional and new consumption models (smart plug-in vehicles, smart homes (SHs), and smart buildings).
- 8) Increasing cost and regulatory pressures.
- 9) Utility unbundling increased energy trading.
- 10) There is a need for transparent consumption and pricing for the consumer.
- 11) Regulators are pushing for more competitive and lower energy prices.
- 12) There is a need for securing supply and meeting the increase in energy needs.
- 13) Utilities need to adopt information and communication technologies to handle new operational scenarios and challenges while maintaining profitability and retaining the ability to invest in infrastructure
- 14) Efficient and reliable transmission and distribution of electricity is fundamental to maintaining functioning economies and societies.
- 15) Sustainability.

Several issues and obstacles may hinder the progress of building smart grids such as cost and fear from cyber-attacks on the grid communication system. Also, customers may raise the issue of privacy on the data received by utilities from their homes. To overcome these problems and to succeed in implementing smart grids, governments, international organizations, industries and research institutes must work in a cooperative manner in order to accomplish smart grid implementation. In addition, customers and consumers should also be aware about the huge benefits smart grids will offer in terms of cost, quality and reliability.

It is known that for a smart grid system to be effectively efficient in terms of reliability, a restoration scheme must be established in case of emergencies or interruptions. The power restoration problem is usually formulated as a multi-objective multi-constraints optimization problem. The optimum solution can be subjected to several objective functions such as:

- Maximizing number of customers restored.
- Maximizing the total restored energy.
- Minimizing operational cost (i.e. switching operation, DG output, ...etc).
- Minimizing outage cost.
- Minimizing system total losses.

1.2 Thesis Motivation

System reliability has always been a crucial concern in designing and operating current and modern grids. In the US, the total cost of outages in year 2002 was estimated to be around \$79B [2] which equal almost 32% of the total electricity retail revenue of \$249B for the same year [3]. The grid today is facing many problems that negatively affect the reliability. These problems can be summarized in four points:

- 1) Ambiguity of network defects until a failure occurs.
- 2) Utilities are aware of outages only when customers report them.
- 3) Determining the cause of an outage is a challenging issue, thus delaying service restoration.
- 4) Incapability in guiding consumers to conserve energy in peak times, hence jeopardizing reliability.

By utilizing smart grids technologies, these problems can eventually be solved by:

- 1) Using information technology infrastructure to deliver knowledge on potential faults in the network to utilities in order to react before outages occur.
- 2) Employing smart grid automation and smart meters to provide real-time information of the grid's status and to immediately alert utilities in the case of failures.
- 3) Functioning monitoring and control technologies in order to locate faults then re-route power in the grid to isolate faulted areas (islanding).
- 4) Encouraging customers to use less energy during peak times by utilizing AMI and price responses (demand response/load management).

As smart grids can improve the reliability of power systems, they may also contribute in deteriorating it due to the following factors:

- 1) Uncertainty in renewable energies power output such as wind and solar may cause unexpected failures due to the mismatch between power output and load.
- 2) The current grid is operated at its edge due to the aging infrastructure.
- 3) Diversity and complexity in energy sources may cause difficulties in switching configuration which will affect the outage time.

Therefore, in order to fully utilize the benefits that are provided from the smart grid, these previously mentioned factors must be addressed effectively and efficiently including studies that test the reliability and security of smart microgrids. Moreover, a strategic restoration technique must be incorporated in order to be utilized in case of emergencies and outages. The technique must model and take into consideration different aspect that

arise in a microgrid, such as DGs, renewable energy, controlled switches and consumer demand side management DSM programs. In this study, a smart self-healing strategy for microgrids service restoration will be proposed including priority listing. The strategy will be capable to provide the optimum restoration plan as in; optimum system reconfiguration, optimum load shedding and optimum DGs scheduled power output.

1.3 Thesis Objectives

This thesis focuses on achieving three main objectives listed as follows:

- 1) To model and analyze the effects of DGs and renewable energy with the inclusion of demand side management on the reliability and restoration of microgrids.
- 2) To propose a priority list model that is based on different factors such as: type and criticality of the load, cost of interruption, load management programs, and system reliability indices.
- 3) To propose a smart self-healing optimization strategy for the system based on the available supply, system configuration, switching devices, load demand, and finally, the priority listing.

The flow chart in Figure 1.1 demonstrates the procedure of the proposed microgrid self-healing strategy.

Self Healing Strategy for Microgrids

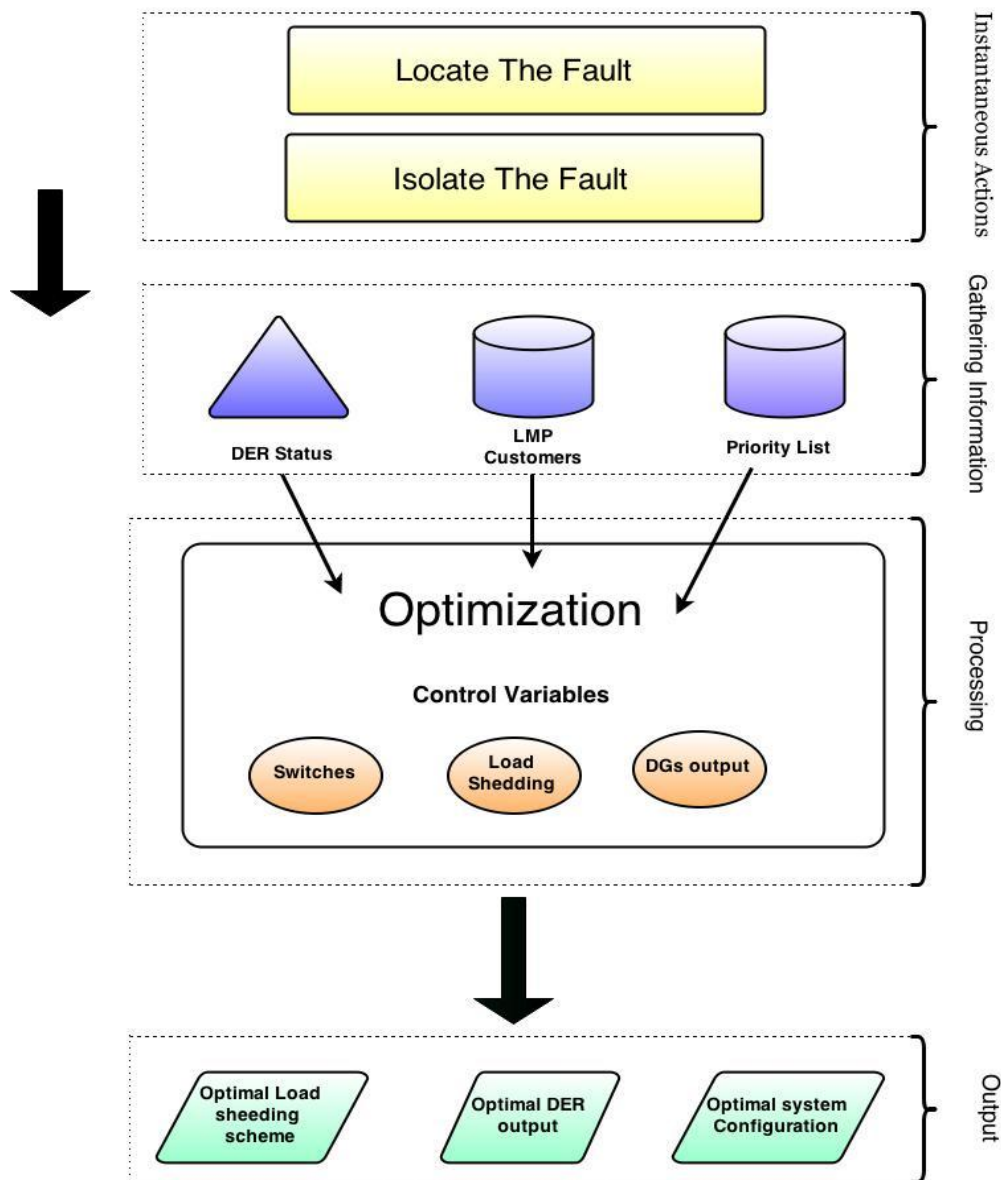


Figure 1.1 Self-healing strategy for electric microgrids

1.4 Background

It was intended when organizing this thesis to include and mention the literature survey whenever needed depending on the subject. For instance, the priority list model is built and modeled in chapter 3. Thereby, literature review related to load prioritizing are

presented in the introduction of the same chapter. It was found that this approach is more convenient to the reader where comparison between thesis proposed studies and studies existing in the literature can be made easily and directly without the need to return to the first chapter each time. However, for the necessity of providing a technical platform and knowledge based discussion, this section presents an overview about selected topics that are highly linked to this thesis such as renewable energy, load management and demand response, power restoration and electric microgrids.

Solar and wind are the most two growing renewable resource due to their high availability. Solar is considered the most abundant source of energy where the annual solar energy reaching earth is almost 1000 times the current world-wide fossil fuel consumption in a year [4]. The cumulative global installed PV capacity is expected to reach 329.8GW by the year of 2020 [5]. In the case of wind power, U.S. government is expecting to increase its wind power generation from 31TWh in 2008 (1.3% of total supply) to 1160TWh (20% of future total supply) by the year of 2030 [6]. One obvious issue of these two renewable sources is the uncertainty and variability of power output which creates a significant problem for the reliability of the power grid. Figures 1.2 and 1.3 show the curves of output power from solar and wind resources in Dhahran, Saudi Arabia for the year of 2003. As it can be seen, the issue of variability is bigger in the case of wind than solar. The forecasting errors for wind power could exceed 25% depending on the methodology [7].

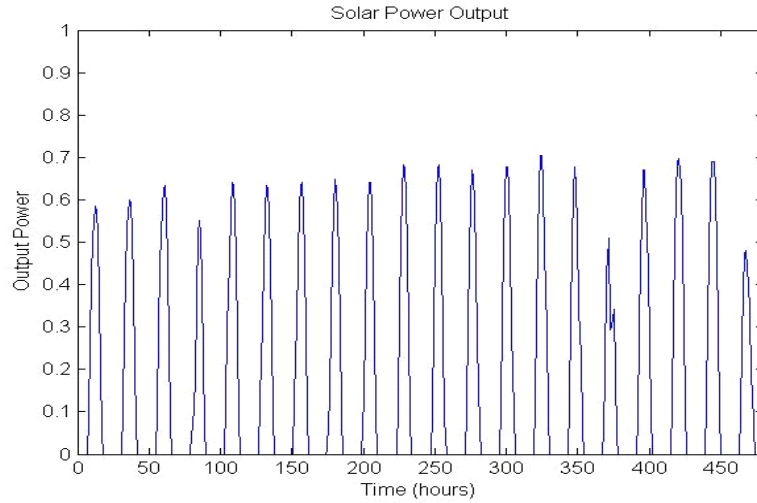


Figure 1.2 Solar power output variation per unit, Dhahran 2003

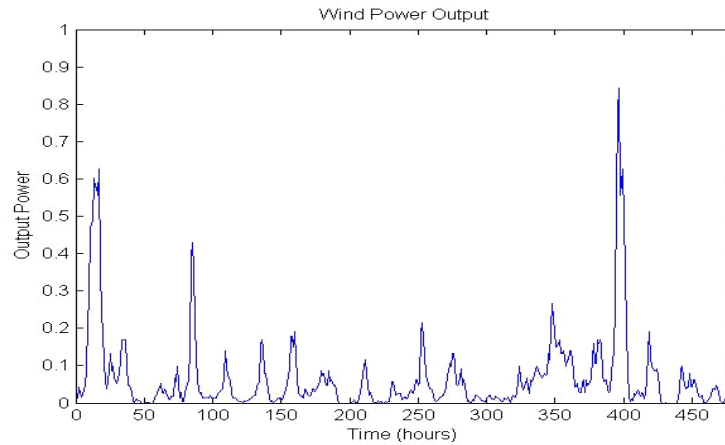


Figure 1.3 Wind power output variation per unit, Dhahran 2003

Certainly, both of their power outputs are affected by the climate, engineering design and the location of installation. Also, large scale resources are usually far away from loads causing transmission lines limitations, thereby affecting the reliability. In general, renewable resources may badly impact grid reliability due to the following summarized reasons:

- 1- Variability and fluctuation of resources.

2- The power output cannot be controlled; hence it is difficult to match the generation with load profile.

3- High forecasting errors in particular in long term forecasting.

4- Transmission limitation in case of remote resources.

It can be seen, while renewable energies can provide more sustained power and relieve several environmental concerns, they may also harm the quality and reliability of the grid due to their uncertain generated power. These issues can be solved by utilizing load management and energy storages to address renewable resources inconsistency in order to obtain a perfect match between load and generated power.

Load management (LM) can be defined as any action taken by the customer and/or the electricity supplier to change the load profile to reduce total system peak load, increase load factor and improve utilization of valuable resources such as fuels or generation, transmission and distribution capacity [8]. Generally, in load management practice, consumers are encouraged to reduce their energy consumption during specific periods (peak times) and to consume energy in a more efficient manner. Usually, this is achieved by increasing the price of electricity at peak times and reducing it at times where the demand is low in order to smooth-out the load profile. LM can also be obtained by methods other than altering the price such as increasing the awareness of customers about conserving energy and lowering demand. It is worth mentioning that in LM exercise, the total energy consumption is not necessarily reduced since in most cases, load is rather shifted from on-peak times to off-peak times.

Demand Response is a type of LM where it refers to the ability of customers to reduce or alter their electricity consumption in response to events based on electrical market or reliability needs.

The U.S Department of Energy (DOE) defines demand response as "Changes in electric usage by end-use customers from their normal consumption patterns in response to changes in the price of electricity over time, or to incentive payments designed to induce lower electricity use at times of high wholesale market prices or when system reliability is jeopardized".

Demand response can be categorized into two primary types [9]:

- Incentive-based demand response
 - o Direct load control
 - o Interruptible/curtailable rates
 - o Demand bidding/buyback programs
 - o Emergency demand response programs
 - o Capacity market programs
 - o Ancillary-services market programs
- Time-based rates
 - o Time-of-use
 - o Critical-peak pricing

- o Real-time pricing

By implementing LM and DR, substantial benefits can be accomplished, especially at peak times, in reducing the need for additional resources and generators.

To protect the grid from overloading, in some cases, load shedding is used where the utility disconnect the power on customers without even informing them in order to reduce total demand. In smart grids, by the use of LM/ DR and the communication system between the utility and customers, overloading problems can be resolved including customer participation. Utility can require customers to turn-off unnecessary loads at particular time where the total load is high; hence, LM and DR can be seen as an ancillary resource where it could eventually work on improving grid reliability. In addition, combining load management schemes with electrical storage systems could further improve grid reliability by addressing peak demand and load variability in an efficient manner.

The European Directorate-General for Energy states that "Energy storage can supply more flexibility and balancing to the grid, providing a back-up to intermittent renewable energy. Locally, it can improve the management of distribution networks, reducing costs and improving efficiency. In this way, it can ease the market introduction of renewables, accelerate the decarbonization of the electricity grid, improve the security and efficiency of electricity transmission and distribution (reduce unplanned loop flows, grid congestion, voltage and frequency variations), stabilize market prices for electricity, while also ensuring a higher security of energy supply".

Traditionally, large scale pumped hydro storage systems were widely used in the network but with the high emerging penetration of renewable resources in the grid, smaller more flexible storage devices are required to be applicable at all system levels. Various energy storage technologies are being implemented in order to meet the grid needs such as thermal storage, compressed air, flywheel and batteries. The contribution of each storage technology to the overall capability in the U.S. in year 2013 is shown in Figure 1.4.

In general, applications of energy storage in the grid differs depending on the level of the electrical system:

- 1) Generation level: Increasing generation capacity and balancing it with the demand.
- 2) Transmission level: Controlling frequency and voltage level and as a black start.
- 3) Distribution level: Supporting capacity and controlling voltage level.
- 4) End-user level: peak shaving, islanding supply, cost utilization.

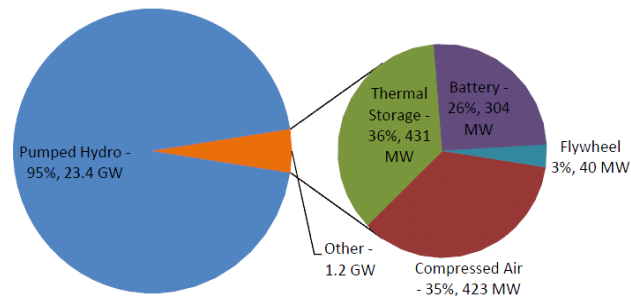


Figure 1.4 Contribution of various storage technologies in the U.S. [10]

Batteries appear to be the most promising technology to be implemented in the grid due to its flexibility in operation and cost. Batteries provide mobility as well as elasticity

in storage capacity which makes them flexible to be installed in several places in the grid, including:

- A renewable energy source (RES) feeder such as photovoltaic and wind.
- High, medium or low voltage substations.
- Connect it to RES supplying homes.

All storage devices tend to make load profile seen by the utility flat and constant where they fill generation gaps in peak times. Batteries in particular, respond very fast, in fraction of a second, which makes them beneficial sources in fast control schemes in the smart grid. These two properties when achieved efficiently, can improve grid reliability and substantially.

An effective combination between these three resources, renewable energies, load management and storage devices, in the grid will most certainly raise the level of reliability to meet all network challenges. A perfect grid with wide IT infrastructure that provides control, communication and coordination is necessary needed in order to perfectly achieve these reliability challenges.

There exists several studies in the literature analyzing the impact of renewable energy and load management on system reliability. Dange Huang and Roy Billinton in [11] mainly focused on the effects of one aspect of the various demand side management measures, which is load shifting, on reliability indices, reliability index probability distributions and peak load carrying capabilities for a bulk electric system. The interactive impacts of demand side management programs and the consideration of load forecast uncertainty on system reliability were also investigated. The conventional system

reliability indices, Loss of Load Expectation (LOLE), Loss of Energy Expectation (LOEE) were used to illustrate the reliability effects of DSM applied to the IEEE-Reliability Test System (IEEE-RTS). The sequential Monte Carlo simulation technique was utilized in their study.

The load shifting procedures examined in [11] improved the system reliability by modifying the load model. System reliability indices decrease with the application of load shifting measures. The lower the pre-specified peak load, the lower the system indices. Not only are the system indices improved by implementing DSM measures, the index probability distributions are also affected. The relative frequency of encountering zero load curtailment increases with a decrease in the pre-specified peak load. The standard deviation and the range of the index probability distribution decreases significantly with the application of load shifting measures. This implies that the system reliability performance becomes less variable from year to year and the indices are less dispersed by implementing load shifting programs.

The system peak load carrying capability increases as the pre-specified peak load in the load shifting procedure decreases. System reliability indices are affected negatively with increasing load forecast uncertainty. The application of demand side management tends to counteract the effects of load forecast uncertainty and therefore, reduce the inherent increase in the system reliability indices due to the load forecast uncertainty.

In [12], Chenye Wu, Hamed Mohsenian-Rad, Jianwei Huang, and Yuexuan Wang propose a novel demand side management method to tackle the intermittency in wind power generation. Their focus is on an isolated microgrid with one wind turbine, one fast

responding conventional generator, and several users. Using dynamic potential game theory, they analyze and coordinate the interactions among users to efficiently utilize the available renewable and conventional energy resources to minimize the total energy cost in the system. The intertemporal variations of the available wind power were modeled as a Markov chain based on real field data.

Using techniques from dynamic potential game theory, they first derive closed-form expressions for the best responses for the users that participate in demand side management. Then, they investigate the efficiency of the constructed game model at the equilibrium. Finally, the system performance is assessed using computer simulation. In particular, their proposed scheme saves 38% generation cost compared with the case without demand side management.

Moreover, in [13], the effect of generation system on the load point reliability was considered, so it was supposed that transmission system is fully reliable. This paper proposed a New Equivalent Multistate Generation Provider (NEMGP) to include the effect of wind generating units besides conventional generators in the reliability evaluation. A novel technique was proposed to determine the maximum generation capacity delivered to each load point. The proposed technique uses the maximum deliverable capacity to determine load point reliability indices. In this progress, it was assumed that customers behave as dispatchable loads. This technique is based on Optimal Power Flow (OPF) approach. Generalized Reduced Gradient (GRG) method was employed to solve the nonlinear programming problems. The proposed techniques were illustrated using deregulated Roy Billinton Test system (RBTS).

The deregulated RBTS with a wind farm connected to a single bus was analyzed in [13] to demonstrate the effectiveness of the proposed techniques. Using these techniques, more realistic results were obtained in comparison with old approaches. Two different cases were applied at which the customers bid different prices per MWh. The results show the effect of changes in the customer's bid price on the reliability of each load point. Because of network configuration and different distances between customers and different generators, some customers may have lower reliability. As it was expected, the results indicate that the customers with low reliability should pay more money to reach to higher reliability.

Power restoration process is considered to be a major factor that plays an important role in the increase or decrease of system reliability. In order to reach a satisfactory level of reliability, power restoration must be fast, secure and reliable in case of interruptions or even blackouts. Even though blackouts can be categorized as rare events, but when they occur, they could cause a huge loss in commercial and industrial activity. For that reason, traditionally, many electric utilities have established some specific guidelines and strategies that an operator should follow in order to restore the energy in the case of a blackout or an interruption. Many restoration attempts tend to be unsuccessful using this technique, and the reason behind that is the uncertainty and unknown condition of the interrupted system at the moment when the restoration plan was developed. In most cases, the prevailing conditions of interrupted system differ significantly than the assumed conditions of the restoration plan [14].

Recently, several new techniques to improve solving the restoration issue have been proposed in the literature. Mainly, these techniques can be categorized into three types: heuristic or Expert Systems (ES), Soft Computing (SC) and Mathematical Programming (MP). Mathematically speaking, power restoration is a combinatorial problem with the objective of maximizing the power supply for as many customers as possible while satisfying source, line/cable loading, and often radial network constraints [15]. A final configuration for the restored system must be found which is typically presented as the status for all breakers in the system as well as the sequence of switching to avoid over loading the network components. Before implementing this configuration onto the system, a load flow analysis is crucial in order to examine the operating feasibility of the proposed system configuration. The process of finding the optimal configuration and then checking the load flow can consume a huge amount of time when applied to large a transmission/distribution system. The topic of power restoration and the methods that are applied to solve this problem will be further discussed in chapter 4 when proposing the restoration optimization strategy of this thesis.

In the introduction of this chapter, the benefits, definition and advantages of smart grids was stated. Similarly, microgrids are considered to be modern, small-scale versions of the centralized smart grid systems. They consist of cluster of loads and microsources that can be operated in an efficient fast manner. Typically, all switches and equipment in the microgrid are assumed to function remotely by the operator or a control system. A MicroGrid can operate in synchronism to the bulk system or as an isolated single entity. Microgrids provide several technical advantage, such as reliability, carbon emission reduction, diversification of energy sources, and cost reduction seen by the consumer side.

From the utility point of view, a MicroGrid can be thought of as a controlled cell of the power system. For example this cell could be controlled as a single dispatchable load, which can respond in seconds to meet the needs of the transmission system [16]. From the customer point of view, a MicroGrid can be designed to meet their special needs; such as, enhancement of reliability, supporting voltage level, fast restoration during service interruption, and reduction of electric bills especially those customer participating in load management programs.

The Galvin Center premier project at Illinois Institute of Technology (IIT) [17] is considered to be the first perfect microgrid system. The total funding of the project cost around \$12 million with a payback period of only 5 years as seen in Table 1.1. The system network is shown in Figure 1.5. The system is equipped with high reliable building load controllers that is connected to a master controller in order mitigate the changes of utility prices and to reduce peak loading. Also, roof-top PV panels, wind generation units, energy storage systems and an 8MW natural gas power plant are all included in the system. Hence, in case of a blackout or a major interruption, the IIT microgrid is able to disconnect from the utility and run as a self-supported network. The system consists of 7 underground cable loops that are equipped with high performance switches in order to detect, then isolate faults and provide rerouting to the power supply.

Table 1.1 IIT project cost analysis [17]

Estimated Perfect Power Costs and Savings	
System Cost	\$12M
One time savings	\$5M
Annual savings	\$1.3M
Simple payback period	5 years

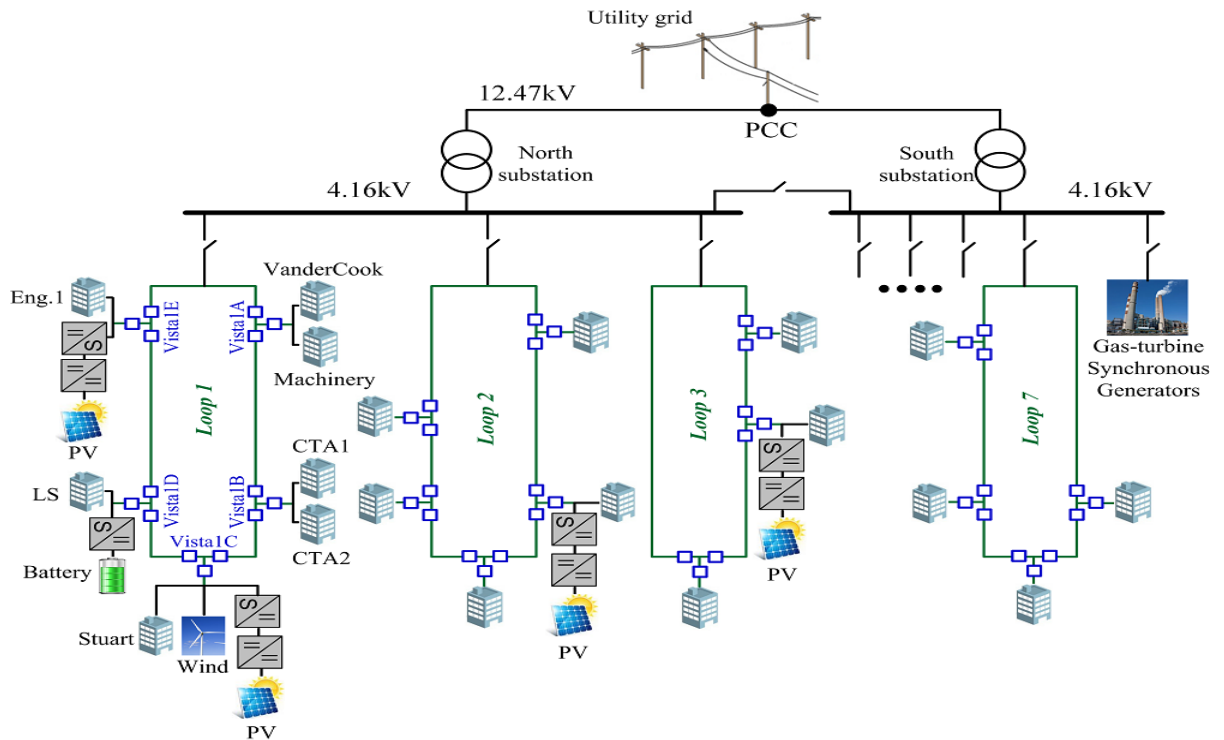


Figure 1.5 IIT perfect microgrid system [17]

1.5 Thesis Structure

The rest of the thesis is organized as follows:

- Chapter 2 provides analytical studies about the impact of RE based DGs and the practice of LM on the reliability and restoration of the network. It starts with providing the modeling and formulation of renewable outputs, load management, and Monte Carlo fault simulation. Then, two case studies are presented to measure the improvement of reliability and restoration after the integration of RE and LM.
- In chapter 3, a load prioritizing method is proposed. The method intend to assign a calculated priority weight to each customer in the system based on

criticality, load amount, cost of interruption, and reliability measures. This weight will be used when optimizing the restoration process.

- Chapter 4 is considered the main contribution of this thesis where the objective, constraint, and parameters of the self-healing optimization problem are discussed. The full mathematical formulation of the problem is introduced in this chapter.
- Chapter 5 contains selected case studies verifying and implementing the proposed technique. The priority weight and the optimization formulation are integrated together.
- Finally, conclusions and suggestions for future work are presented in chapter 6.

CHAPTER 2

IMPACT OF RENEWABLE ENERGY AND LOAD

MANEGEMENT ON SYSTEM RELAILBILTY AND

RESTORATION

Power reliability and restoration are considered significantly challenging issues in the development of future smart grids. Different characteristics can impact the reliability and restoration process of the future power distribution system. Two of the main characteristics of future smart grids are the integration of hybrid renewable resources and the implementation of load-side management (LM) programs.

In this chapter, the impact of integrating wind and solar energy sources and the application of LM programs on the reliability and restoration process are examined. Actual wind speed data and solar irradiation are used in modeling wind and solar power outputs to include seasonal variations. Then, the LM concept will be implemented to assess the increase in load reliability. Two main LM aspects are studied and simulated which are load shifting and peak clipping aspects. In order to generalize the study to include several LM measures, two LM modeling methods are introduced and explained in this chapter. The Monte Carlo Simulation (MCS) will be utilized to simulate fail and repair incidents and to evaluate the reliability for residential, commercial, and industrial loads.

Two case studies are illustrated. One relating the reliability assessment of local load and the other case examine reliability impacts system-wise using RBTS-Bus 2 system. This chapter was intended to be written in order to provide case studies that shows analytical illustration of the benefits gained from microgrids over traditional distribution systems.

In section 2.1, a literature review related to the case studies subject is presented. Section 2.2 contains the modeling of load curves, wind and solar outputs, load management, and fault and repair simulation which are all needed in forming the cases studies that are shown in section 2.3.

2.1 Literature Review

Although several papers study the effect of RE and DSM, separately, on the reliability, the literature still lacks researches combining the two aspects together. Very few papers addressed the impacts of combining RE and DSM [18-20]. Reference [18] examined the effect of selected load management techniques with wind power on the individual load point and system reliability indices. However, when modeling load shifting technique, the load was assumed to be constant at peak hours which limits the practicality. In [19], simulation studies have been performed on real Italian distribution network, showing the effects of DSM actions on the growth of DGs. However, the wind generator used in the study was assumed to be equivalent to a constant generator excluding the stochastic nature of wind speed. In [20], the effect of LM with solar power on outage incidents is examined. However, the study only covers scheduled power outage where loads are simply shifted intentionally before and/or after the fault period by applying load shifting. This for sure does not simulate the practice of LM in a practical way, where load

shifting should be applied based on the load curves without knowing the time of interruption.

2.2 System Modeling

2.2.1 Annual Chronological Load Modeling

The mechanism of building the hourly load model used in this study is explicitly illustrated in [21]. This model simulates the hourly load behavior for different sectors based on the hour of the day, the day of the week, and the week of the year. The per unit hourly load model can then be extracted by the following equation:

$$L_k(t) = P_w \cdot P_d \cdot P_h \quad (2.1)$$

where $L_k(t)$ is the k^{th} load at hour t in per unit, P_w, P_d , and P_h are the load factors for hour t in the year, $w = \{1,2, \dots, 52\}$, $d = \{1,2, \dots, 7\}$, and $h = \{1,2, \dots, 24\}$.

The values of weekly, daily, and hourly factors are tabulated in Appendix A.1. To further simulate the uncertainty of the load, a different approach is used. Each load point is generated randomly based on a normal distribution function with the mean equal to the multiplication of the factors (weekly, daily, and hourly) for that load point. Usually, in long-term load forecasting, the relative errors between the actual and the forecasted values range below 15% ([22-24]). To simulate that error, 15% of the mean at each load point is set to equal three standard deviations meaning that the maximum deviation from the mean value is $\approx 15\%$. The following equations are used to simulate the load for different sectors such as residential, commercial, and industrial loads:

$$\begin{aligned}
mean(t) &= P_w \cdot P_d \cdot P_h \\
3\sigma(t) &= 15\% \times mean(t) \\
L_k(t) &= normrand(mean(t), \sigma(t))
\end{aligned} \tag{2.2}$$

where $mean(t)$ is the mean used to generate the load at hour t , $\sigma(t)$ is the standard deviation for hour t , and "*normrand*" is a normal random generator.

2.2.2 Wind Power Output Modeling

Figure 2.1 shows the power output curve of a typical wind turbine, which can be expressed by the following sub-functions [25]:

$$P_{out}^{WT}(v) = \begin{cases} 0, & v \leq v_{ci} \cup v \geq v_{co} \\ P_R \frac{v^3 - v_{ci}^3}{v_R^3 - v_{ci}^3}, & v_{ci} < v < v_R \\ P_R, & v \geq v_R \end{cases} \tag{2.3}$$

where v is the wind speed, v_{ci} is the cut-in speed (minimal speed for output power), v_R is the rated output speed, v_{co} is the cut-out speed (maximum speed for outputting power), P_R is the rated output power, and P_{out} is the output power of the wind turbine.

For this study, actual hourly wind speed data were analyzed to extract wind power output. Figure 2.2 shows the simulated wind speed data in a Weibull distribution function. Note that the Weibull Probability Distribution Function (PDF) was simulated only to provide a general overview about the behavior and probabilities of the studied wind speed. Equation (2.3) was used to convert the actual wind speed into power output.

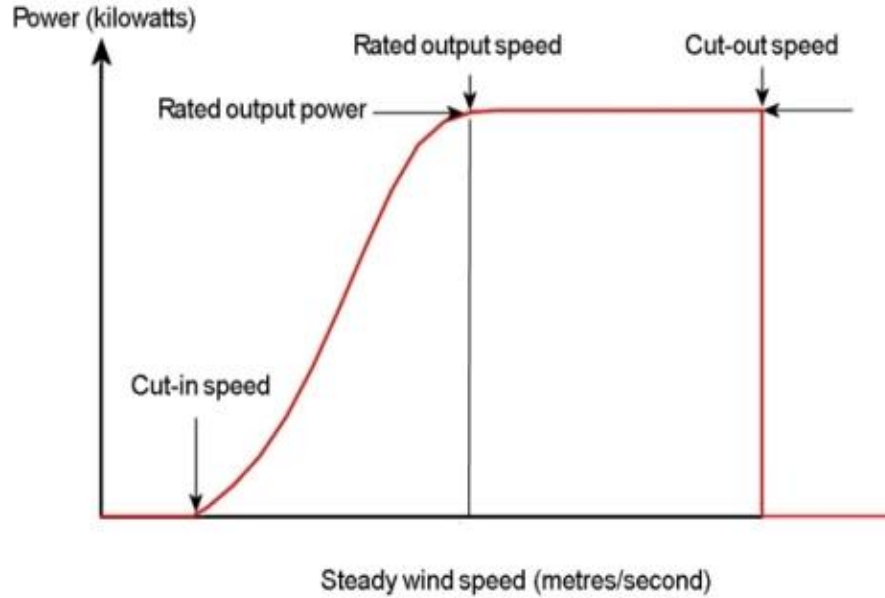


Figure 2.1 Power output curve for a typical wind turbine

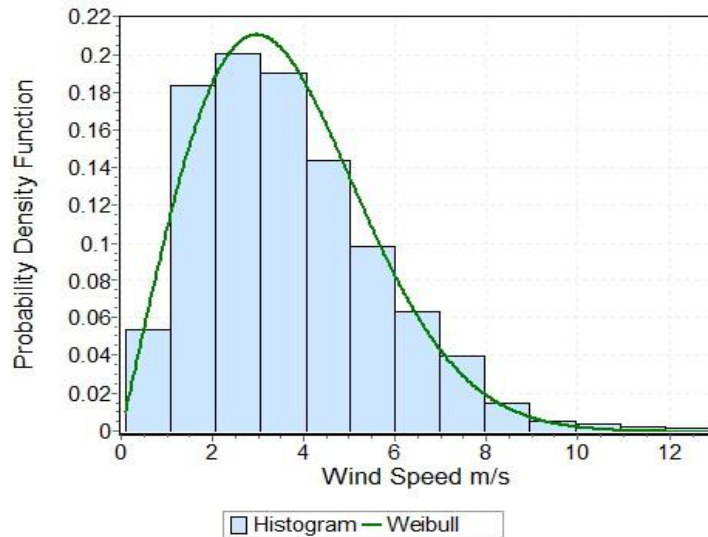


Figure 2.2 Weibull distribution for the studied wind speed

2.2.3 PV Power Output Modeling

Power output from PVs is influenced by many external factors such as ambient temperature and sunlight intensity. A simplified equation relating sun irradiation to PV power output is [25]:

$$P_{out}^{PV} = P_{STC} \frac{G_{AC}}{G_{STC}} \quad (2.4)$$

where P_{STC} is the maximum test power for the used PV panel at the standard test conditions (STC) (intensity of sunlight of 1,000W/m² and ambient temperature of 25° C); G_{AC} is the intensity of the light; and G_{STC} is light intensity for the STC.

Actual solar irradiation data were used in this study. Figure 2.3 shows the monthly averaged solar irradiation of the simulated year 2003. Equation (2.4) was used to convert the solar irradiation into power output.

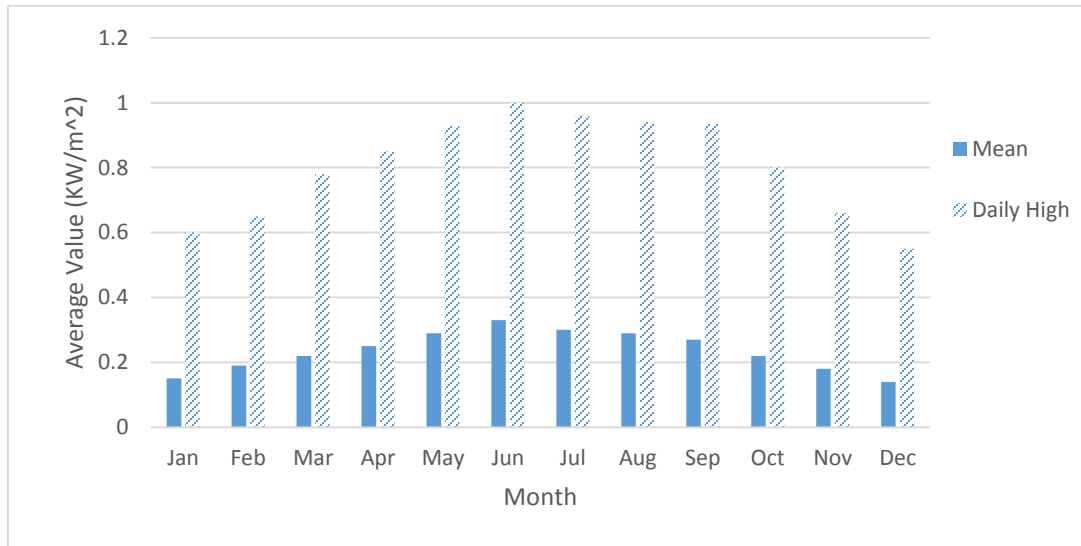


Figure 2.3 Monthly averaged solar irradiation for the simulated year

2.2.4 Load Management (LM) Modeling

Before introducing the modeling, it is important to mention the main factors that usually derive the actions of LM. These are, Energy efficiency (EE), energy conservation (EC), and demand response (DR) [26]. EE is related to technological solution by replacing or repairing electrical devices in order to enhance their energy efficiency. EC depends highly on the consumer behavior to use less resources in general. Finally, DR activities are

based on the electricity market and price signals that are sent to customers by utilizing Advance Metering Infrastructure (AMI).

The impact of introducing LM to the system will be studied in terms of reliability assessment. Two main aspects of the various DSM measures will be considered in this study, load shifting and peak clipping.

2.2.4.1 Load Shifting (LS) Method

Basically, in this type of LM, the total energy demand will not decrease, but the load curve will change where peak loads move from on-peak times to off-peak times. In this thesis, the LM simulation is done by a process of comparing and shifting for N times for all load points where the value of N represents the effectiveness of LM. The simulation steps are as follows:

Step 1: comparing $L_k(t)$ with $L_k(t - 1)$ (2.5)

$$\text{If } L_k(t) < L_k(t - 1) \rightarrow L_k(t) = L_k(t) + \varepsilon \times L_k(t - 1)$$

$$L_k(t - 1) = L_k(t - 1) - \varepsilon \times L_k(t - 1)$$

else if $L_k(t) \geq L_k(t - 1) \rightarrow$ no change

Step 2: comparing $L_k(t)$ with $L_k(t + 1)$ (2.6)

$$\text{If } L_k(t) < L_k(t + 1) \rightarrow L_k(t) = L_k(t) + \varepsilon \times L_k(t + 1)$$

$$L_k(t + 1) = L_k(t + 1) - \varepsilon \times L_k(t + 1)$$

else if $L_k(t) \geq L_k(t + 1) \rightarrow$ no change

where $L_k(t)$ is the k^{th} load at hour t , ε is the shifting amount per step chosen to be 0.01 in order to shift the loads gradually and study the impacts clearly and precisely.

The two steps are simulated for all t chronologically and load values are updated after each step. The whole process including the two steps is repeated N times.

Figure 2.4 shows the studied residential load before and after LS, with different values of N . The number N will be referred to as “shifting factor” in the rest of the paper.

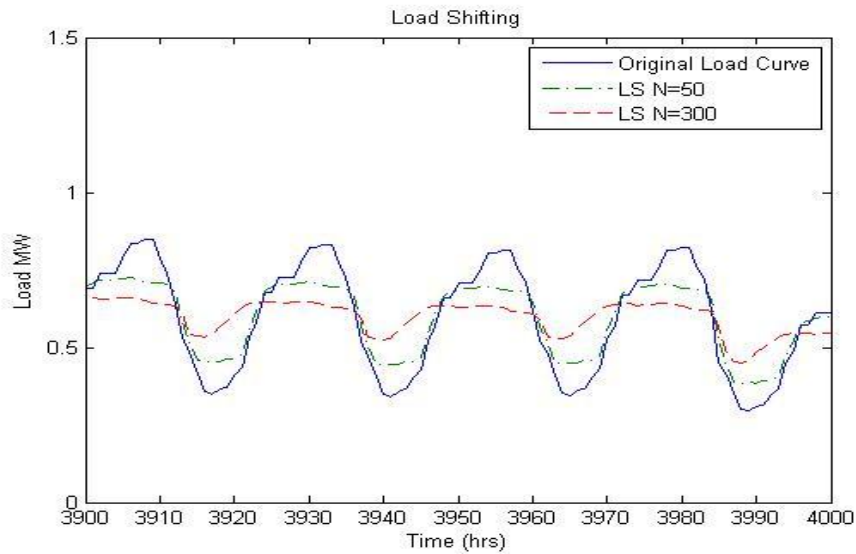


Figure 2.4 Load shifting method

As seen in Fig 2.4 as the value of N increases, a larger amount of the load is shifted. Obviously, if N is further increased (raising the effectiveness of LM), the load will eventually be constant, which is what utilities are striving to reach to ensure higher reliability and less generation cost. This simulates what happens in reality, where depending on the amount of incentives and obligations related to the consumer, load curve will vary to reach utilities requirements.

2.2.4.2 Peak Clipping (PC) Method

Unlike load shifting, in the peak clipping method, the total energy demand is reduced. Load values that are considered to be peaks are clipped and brought down to a certain level. The issue lies in defining peaks. Generally, peaks are defined as load values that are significantly higher than the average load. In this study, different cases were examined in which the peak was defined to be a factor of the load average. The following equation illustrates the clipping procedure:

$$L_k^{PC}(t) = \begin{cases} L_k(t), & L_k(t) \leq A_k \times C \\ A_k \times C, & L_k(t) > A_k \times C \end{cases} \quad (2.7)$$

where $L_k^{PC}(t)$ is the k^{th} load at hour t after peak clipping, A_k is the load average of load k , and C refers to the clipping factor.

Figure 2.5 shows an example for one of the studied load curves, obtained from the data in Appendix A.1, before and after peak clipping with changing the clipping factor C . Clearly, as the clipping factor increases, less total energy is conserved. Notice that all three curves in Figure 2.5 have similar values in off-peak regions and they only differ in on-peak regions. Figure 2.6 shows the total energy conserved (per unit of the original load peak value) versus the value of the clipping factor for the same load example. It is noticed that the curve in Figure 2.6 approaches zero at 1.7, which indicates that the peak load is less than $1.7 \times$ load average. In other words, no clipping will occur if $C \geq 1.7$.

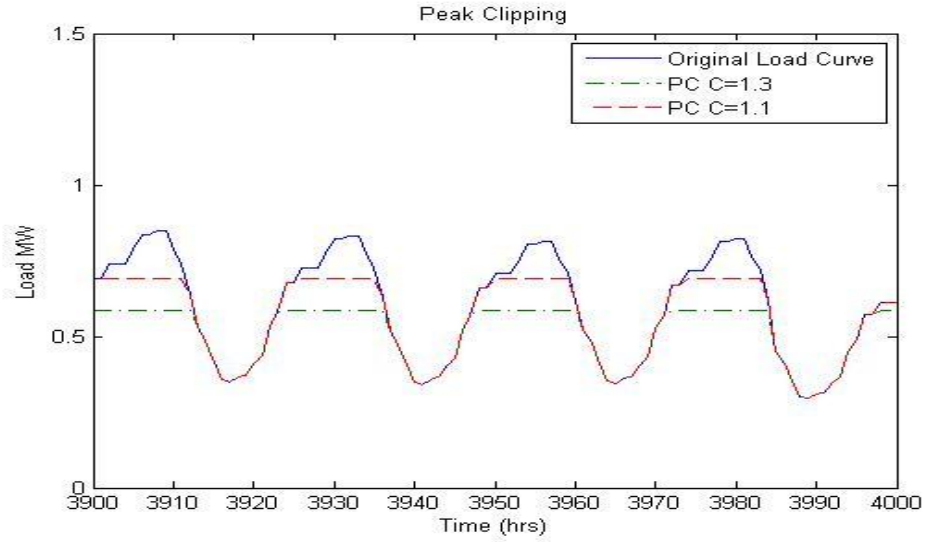


Figure 2.5 Peak clipping method

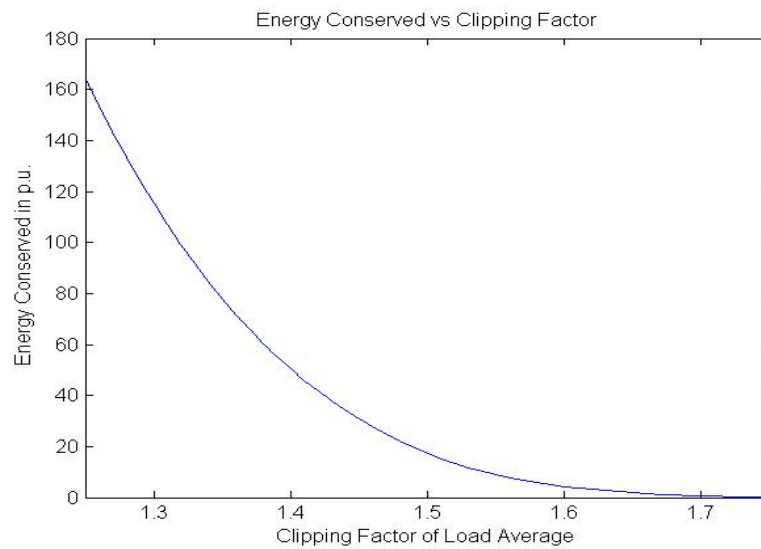


Figure 2.6 Energy conserved versus clipping factor C

2.2.5 Fail and Repair Incidents Simulation

In order to examine the reliability and restoration of the studied load/system, fail incidents and repair actions of the system were simulated using Monte Carlo Simulation (MCS). Generally, the probability to fail or repair for an electrical system follows an exponential distribution, which is what will be used in the simulation process. It is assumed

that the system will have a failure rate of 4 f/yr and a mean time to repair of 4 hours. The sample simulation procedure is conducted as follows:

$$\begin{aligned} \mathbf{if} \ CDF(t) > random(0 - 1) &\rightarrow \mathbf{incident\ occur} & (2.8) \\ \mathbf{else} &\rightarrow \mathbf{incident\ did\ not\ occur} \end{aligned}$$

where CDF is the Cumulative Distribution Function of the exponential distribution, " $random$ " generates a random number between (0,1) uniformly distributed, and t is time in hours.

This procedure applied for all t for a complete year. The detailed implementation of the MCS is illustrated in a flow chart in Figure 2.7. This procedure will be used to simulate and extract the fail and repair hours for the case studies. The following abbreviations are used in the flow chart shown in in Figure 2.7.

t : simulated hour in the year

T : Total number of simulated hours in the year.

U : normal random generator between 0-1.

$F(t)$: failure CDF = $1 - e^{-\lambda t}$; λ : failure rate of the local load.

$R(t)$: repair CDF = $1 - e^{-\mu t}$; μ : repair rate of the local load.

2.2.6 RBTS-Bus 2 Distribution System

The RBTS-Bus 2 distribution system has been used frequently in the literature to study system reliability [27]. The system is radial in nature and supplied by two 33/11 kV, 16 MVA transformers. Both high voltage and low voltage customers are included in the

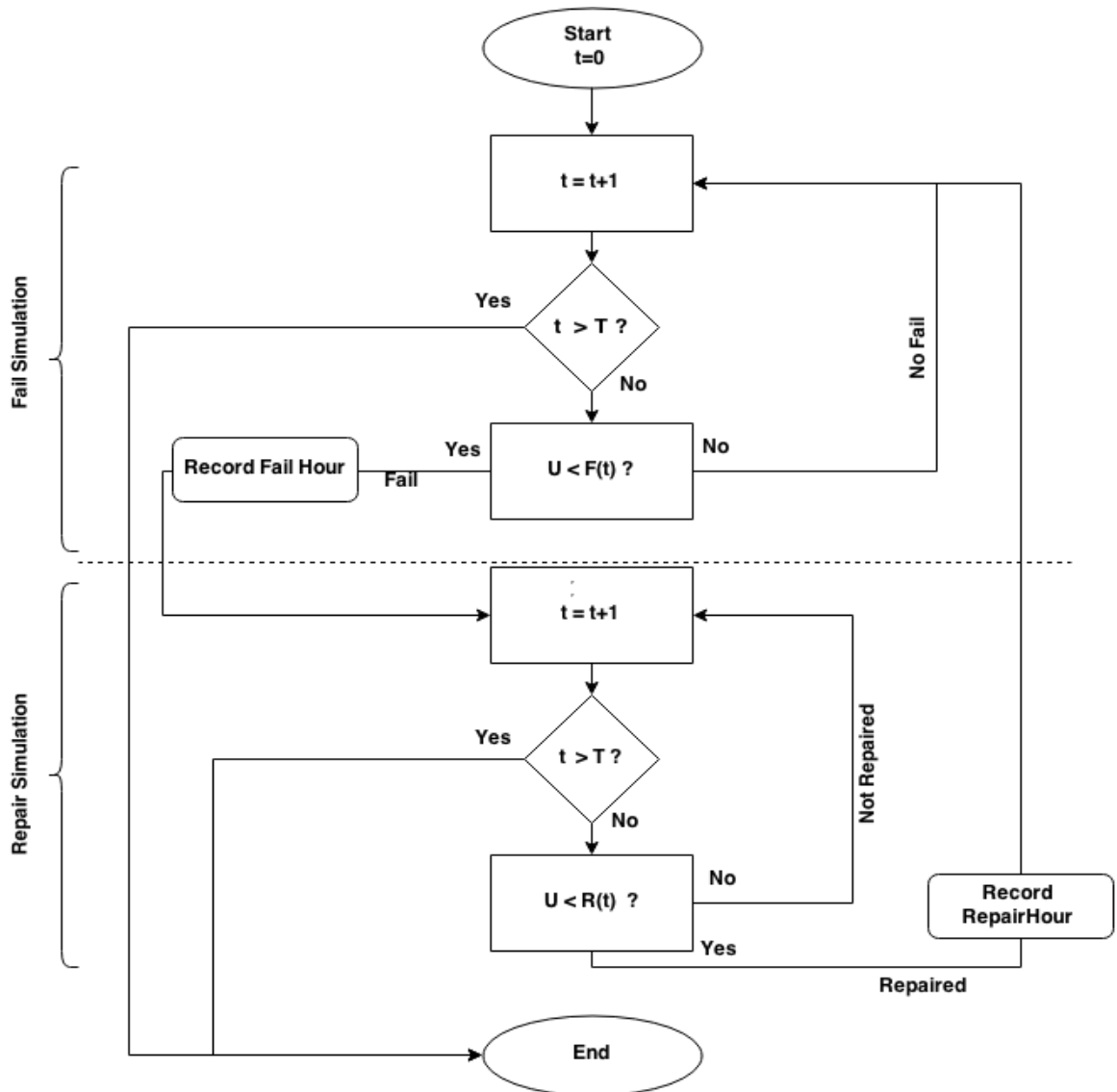


Figure 2.7 MCS implementation procedure

distribution system, where the 0.415 kV low voltage customers are supplied via 11/0.415 kV transformers and the 11 kV customers are supplied directly. For the purpose of this study, only loads connected to feeders 1 and 2 are considered. A total of 9 load points consist of various types of customers. In general, the customers are divided into four groups: residential, governmental/institutional, commercial and industrial. Additionally, it is assumed that the normally open switch (NO) connecting load point 7 to load point 9 is

an automated switch that will automatically close immediately at interruption of one of the two feeders. Figure 2.8 shows the studied distribution system, and Table 2.1 presents additional information about the load points.

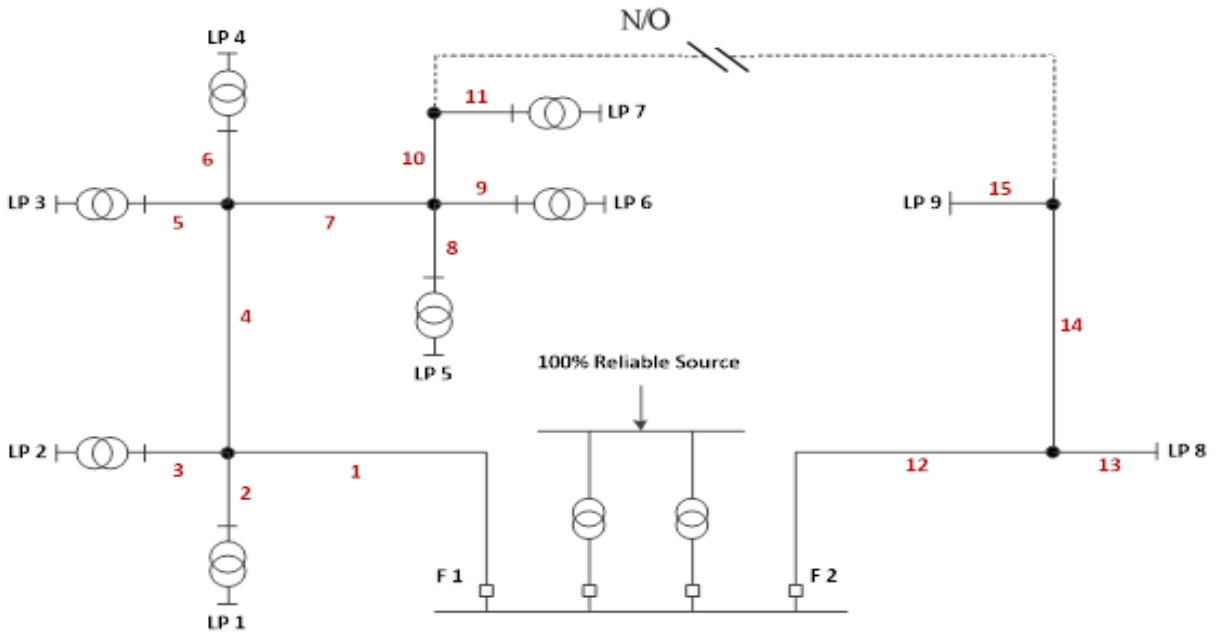


Figure 2.8 RBTS-BUS2 distribution system [27]

Table 2.1 Load point data

Load Point	Type	Average Load (MW)	No. Customers /LP
1-3	Residential	0.535	210
4,5	Cov/Inst	0.566	1
6,7	Commercial	0.454	10
8	Small user	1	1
9	Small user	1.15	1

Two case studies are presented in this chapter. A local load study and a system based study. Note that in the former, only three loads are tested using the load information of the RBTS-BUS 2 system. However, in the latter case, the whole system is used and analyzed.

2.3 Case Studies

2.3.1 Local Load Study

Three local load types, residential, commercial, and industrial that are assumed to be connected through the same feeder are studied. Four main stages are considered in this study: the base case, renewable energy integration, implementing DSM, and finally, applying DSM while including the hybrid renewable system. Note that the term DSM is similar to LM. At each stage, the reliability will be evaluated using two indices as a measure. These two indices are Unavailability in hours and Energy Not Supplied (ENS) in per unit considering the load energy peak to be the base. The unavailability at each hour is calculated as follows:

$$U_k(t) = \begin{cases} 0, & P_k(t) \geq R \times L_k(t) \\ 1, & P_k(t) < R \times L_k(t) \end{cases} \quad (2.9)$$

for all t .

where $U_k(t)$ is the unavailability at hour t for the k^{th} load, $P_k(t)$ is the available power supply at hour t for load k , $L_k(t)$ is the demand at hour t for load k , and R is the curtailment level in %.

By summing all $U_k(t)$, we get the total unavailability in hours for load k . The curtailment level represent the measure of when to consider a load as unavailable. For example, if only 1% of the load was unserved, are we considering the load to be unavailable? To generalize the study, the value of R will be altered while evaluating the reliability as will be shown.

The ENS at each hour is calculated as follows:

$$ENS_k(t) = \begin{cases} 0, & P_k(t) \geq L_k(t) \\ L_k(t) - P_k(t), & P_k(t) < L_k(t) \end{cases} \quad (2.10)$$

for all t .

where $ENS_k(t)$ is the energy not supplied at hour t .

Then, by summing all $ENS_k(t)$, we get the total ENS in p.u for load k .

A flow chart that summarizes the study procedure is shown in Figure 2.9. Renewable energy stage will include integrating wind turbine and PV cells. Also, DSM stage will include LS and PC methods. A total of 8 cases are studied by interchanging the integrated RE and the applied DSM method as illustrated in table 2.2.

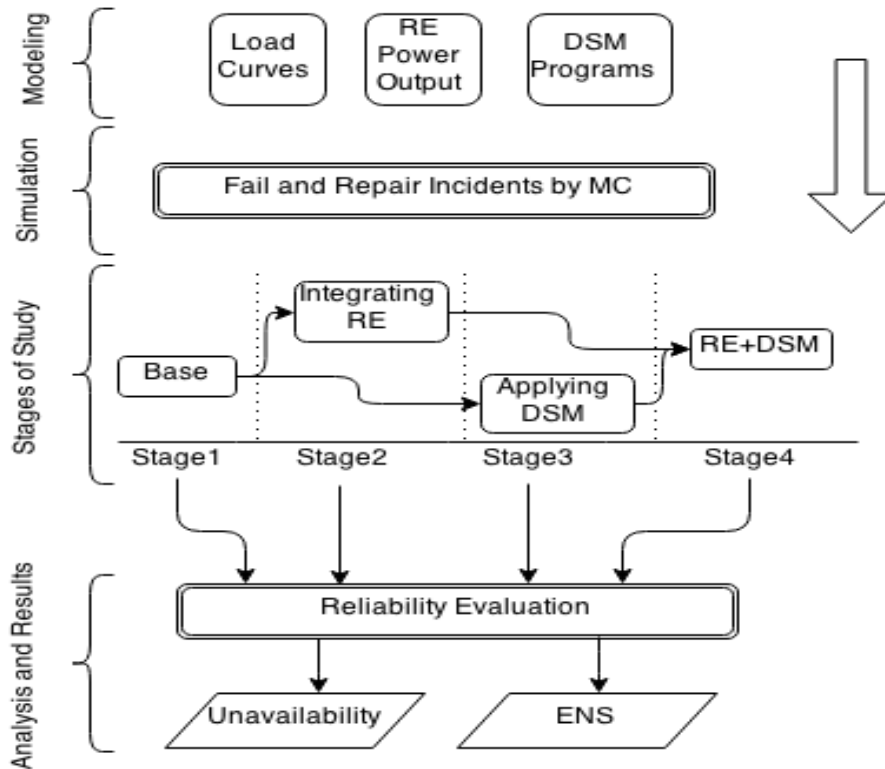


Figure 2.9 General architecture flow chart of the first case study

Table 2.2 Total case studies

	Case	RE		DSM	
		WT	PV	LS	PC
Stage1	1				
Stage2	2	✓			
	3		✓		
	4	✓	✓		
Stage3	5			✓	
	6				✓
Stage4	7	✓	✓	✓	
	8	✓	✓		✓

2.3.1.1 Stage 1. Base Case; Load Connected to Utility Only

The system in this stage is considered to be the base, where there is no DG connected and the DSM is not yet included. After running the fail and repair simulation shown in the flow chart procedure in Figure 2.7, 6 failures occurred with 5 hours of repair time on average. Table 2.3 lists in detail the time of each interruption. Table 2.4 shows the total unavailability and the ENS during the failures for each load type. Obviously, ENS differs for each load type since they consume different amount of energies at different times. Also, note that the unavailability is equal the summation of all faults periods since there is no external source of power at this stage.

Table 2.3 Interruptions information

Interruption No.	Date	From	To
1	June 15	06:00 a.m.	10:00 a.m.
2	July 9	03:00 a.m.	10:00 a.m.
3	August 25	03:00 p.m.	08:00 p.m.
4	October 15	10:00 a.m.	03:00 p.m.
5	October 30	09:00 a.m.	12:00 p.m.
6	November 8	09:00 a.m.	03:00 p.m.

Table 2.4 Reliability indices - first stage

	Unavailability (hrs)	ENS p.u.
Residential Load	30	15.56
Commercial Load	30	18.54
Industrial Load	30	24.83

2.3.1.2 Stage 2. Integrating Renewable Energy

1) Wind Turbine

After integrating the wind turbine into the system, the ENS decreased where the energy generated from the wind turbine had covered some parts of the interrupted loads.

Table 2.5 lists the ENS for all three loads.

Table 2.5 Reliability indices – second stage - wind turbine

	ENS p.u.
Residential Load	10.72
Commercial Load	14.98
Industrial Load	18.80

From Table 2.5, the ENS has decreased by 31.1% for the residential load, 19.2% for commercial, and 24.2% for the industrial load due to the wind power output. Regarding the measure of unavailability, the number of unavailable hours depends on the level of curtailment to be undertaken. Figure 2.10 shows the Unavailability index versus level of curtailment for the case of adding a wind turbine.

At 100% curtailment (100% load coverage), all three loads had improved in terms of unavailability from 30 hrs to 20 hrs for residential, to 23 hrs for commercial, and to 26 hrs for industrial.

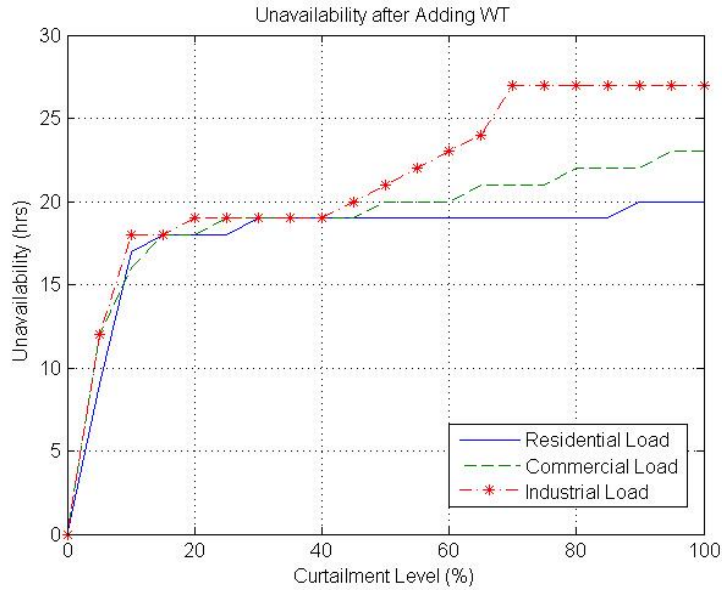


Figure 2.10 Unavailability vs. curtailment level (WT)

2) PV System

For this stage, instead of adding a wind turbine to the system, PV panels are added.

Table 2.6 shows the ENS for all three loads after PV cells have been integrated into the system.

Table 2.6 Reliability indices – second stage - PV

	ENS p.u.
Residential Load	4.99
Commercial Load	7.59
Industrial Load	13.79

It can be seen by comparing Tables 2.5 and 2.6 that adding PV improved the ENS of the system more than adding a WT, where in this case the ENS decreased by 67.9% for the residential load, 59.1% for commercial, and 44.4% for the industrial load. This is due to the fact that the simulated faults occurred at day hours where the availability of studied

solar power output is larger than the availability of the studied wind power output. On the other hand, WT showed slightly better results in terms of the Unavailability at 100% level of curtailment. Figure 2.11 shows the Unavailability index versus level of curtailment for the case of adding PV panels.

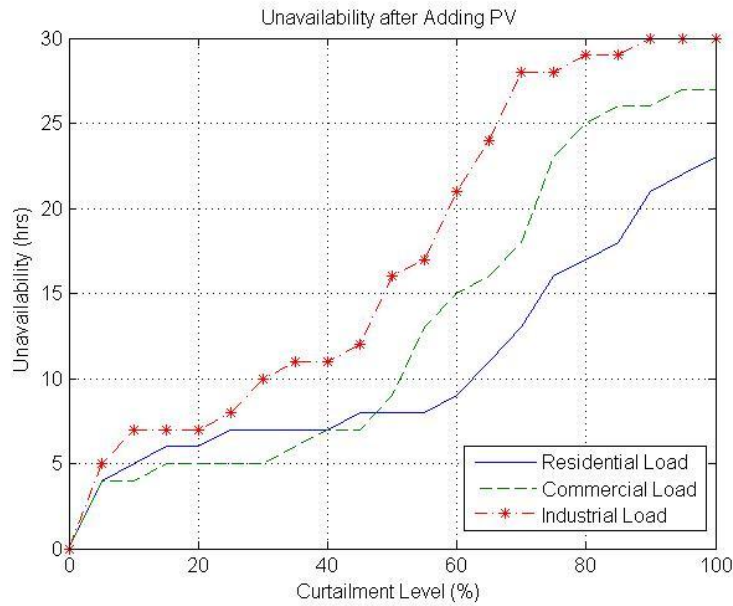


Figure 2.11 Unavailability vs. curtailment level (PV)

3) Hybrid WT and PV

In this section, the reliability of the system will be examined after integrating both the WT and PV together into the grid. Table 2.7 lists the ENS, and Figure 2.12 shows the Unavailability.

Table 2.7 Reliability indices – second stage – WT+PV

	ENS p.u.
Residential Load	2.58
Commercial Load	5.73
Industrial Load	8.30

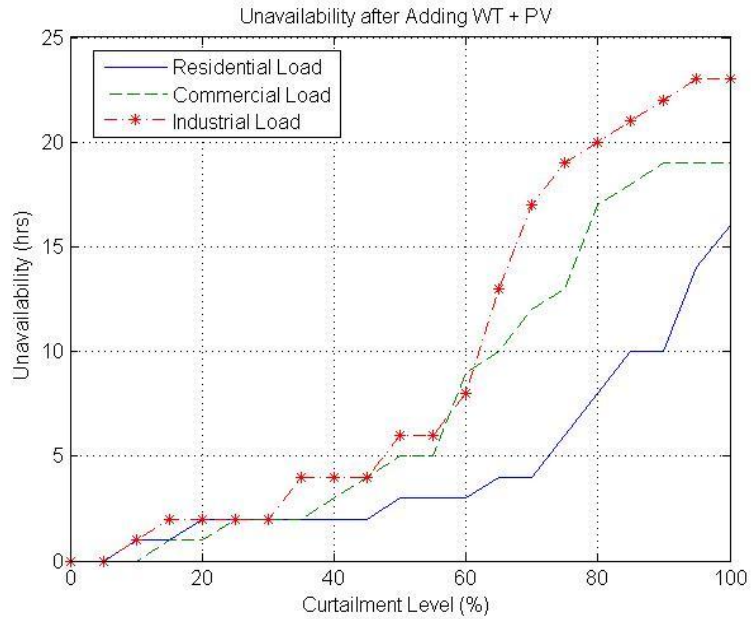


Figure 2.12 Unavailability vs curtailment level (WT and PV)

From Table 2.7 and Figure 2.12, it can be clearly seen that the hybrid system (WT and PV) showed the best results among the three sub-cases. The ENS decreased for the residential, commercial, and industrial loads by 83.42%, 69.1%, and 66.6%, respectively.

It is essential to mention that the energy covered by the connected DGs can largely be affected by the rated power output of these generators. In this case of study, it was assumed that both DGs (WT and PV) had rated power equal to load peak (1 p.u.). The reliability of the system will definitely alter when changing the rated values since the generated power will differ. Figure 2.13 shows a comparison, in terms of total ENS, between WT and PV with different rated outputs. It can be seen that increasing the rated power for the WT did not affect the ENS effectively, which means that the availability of wind power during some faults was ineffectual. On the contrary, PV panels coverage increased significantly with increasing rated power, meaning that the amount of power generated from

the panels, at 1 p.u. rated power, during some faults was insufficient. When the rated power was doubled to be equal 2 p.u., ENS decreased by 62%.

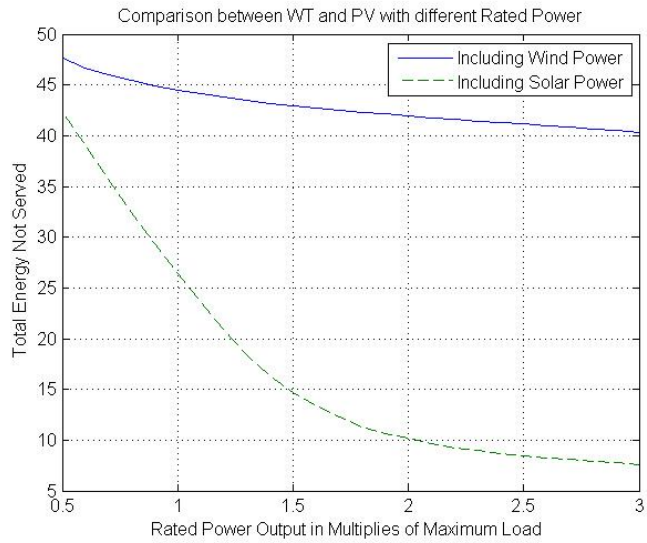


Figure 2.13 Comparison between WT and PV with different rated power

A comparison between all previous study cases in terms of ENS is shown in Figure 2.14 for all three load types.

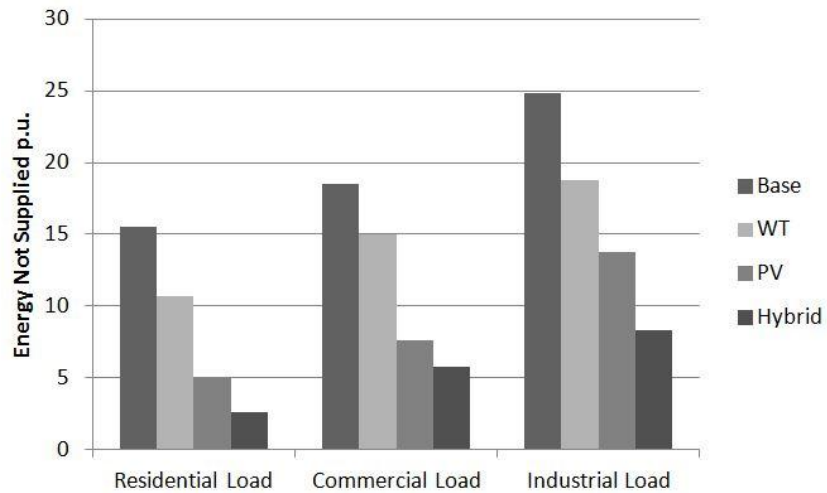


Figure 2.14 Comparison between base case and the second stage of study

2.3.1.3 Stage 3. Applying Demand Side Management (DSM)

The DSM practice will be included in the system at this stage. As mentioned previously, two types of DSM will be examined: load shifting and peak clipping. The reliability of the system will be examined at each case. The Unavailability index will not be affected in both cases (30 hrs) since there is no added power generation in this stage. Another major reason for the unavailability to remain unchanged is that failures did not depend on the load amount in our case. In practice, failures do depend on the load demand. So the use of DSM may avoid some expected interruptions, thereby enhancing the availability of the system.

1) Load Shifting

In this case, since the load shape depends on the value of shifting factor N , ENS will also be a function of the shifting factor N . Figure 2.15 shows the ENS for the system versus the shifting factor. It can be seen from that figure that, unlike the commercial and the industrial loads, the residential load did not show any significant improvement. The reason lies in the fact that ENS depends on load curve and failure time. If the failure time occurs at a peak, ENS will improve. Otherwise, if the fail occurs at off-peak times, ENS will increase. This is because load shifting moves amounts of load from on-peak times to off-peak times. In more practical cases, failures are more likely to happen at peak times, which means that load shifting will definitely decrease the ENS.

1) Peak Clipping

In this method, the ENS will depend on the clipping factor. A low clipping factor means a large amount of peak load is clipped (conserved). Hence, if the fail occurs at a

peak, a low clipping factor yields low ENS and a high clipping factor results in a small or no change in the ENS. This can be seen clearly in Figure 2.16, where the ENS is plotted versus the clipping factor. Note that as we decrease the clipping factor, more load is shaved (refer to equation (2.7)).

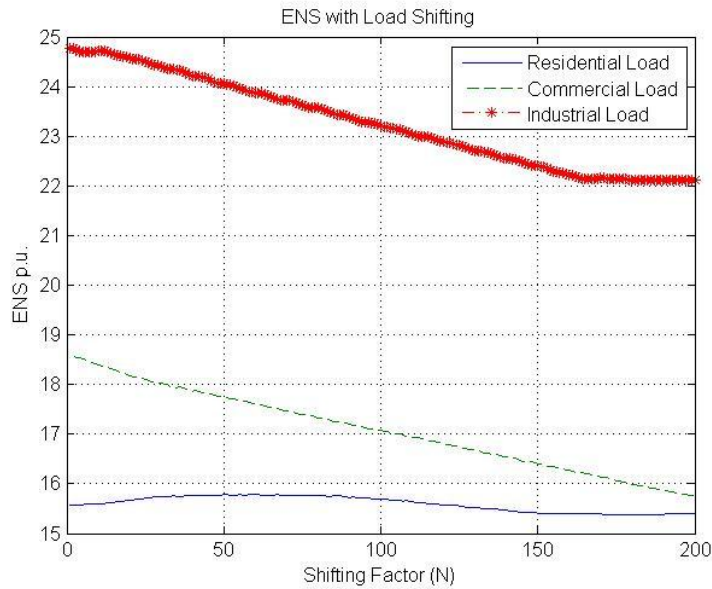


Figure 2.15 ENS vs. shifting factor

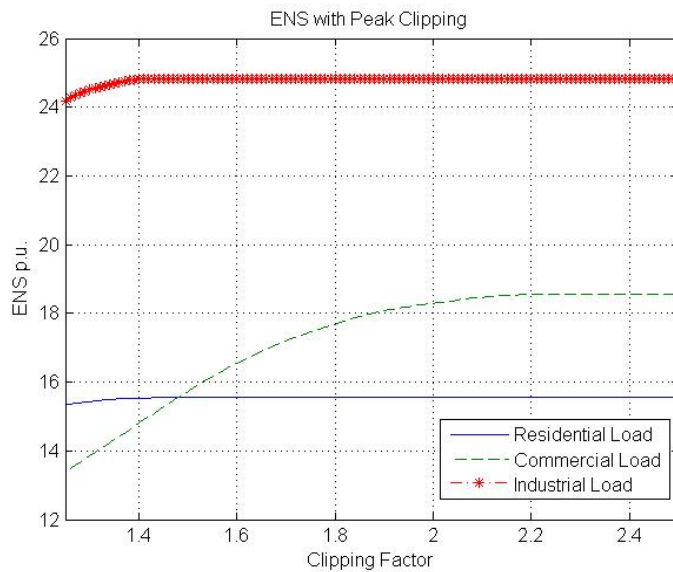


Figure 2.16 ENS vs. clipping factor

2.3.1.4 Stage 4. Integrating Renewable Energy and Demand Side Management (DSM)

In this stage, the impact of DSM on the reliability of the system including hybrid renewable power is studied. Both load shifting and peak clipping methods are implemented.

1) Load Shifting with Hybrid Renewable System

Comparing the values of ENS in Table 2.7 with the values indicated in Figure 2.17, it can be seen that DSM improves the reliability of the hybrid system. As the shifting factor is increased (higher effectiveness of DSM), less energy will not be supplied.

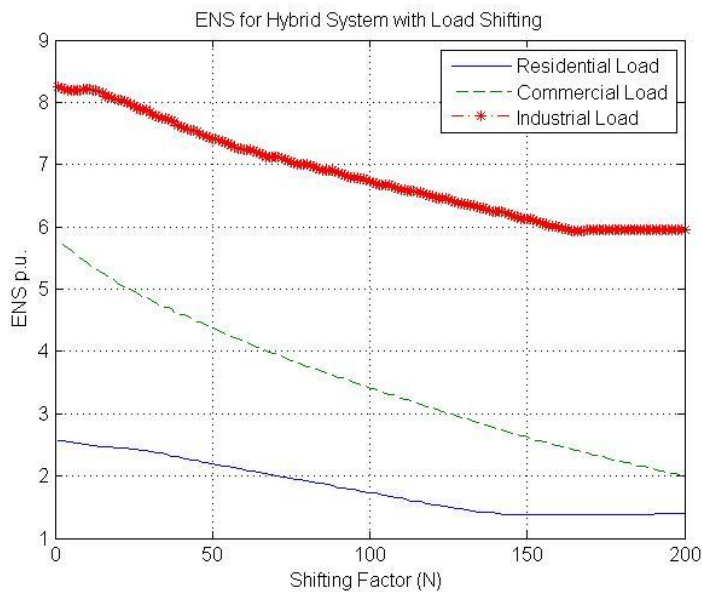


Figure 2.17 ENS vs. shifting factor - hybrid system

Figures (2.18-2.20) show the unavailability versus shifting factor at 50%, 75%, and 100% levels of curtailment, respectively. It can be seen that by changing the shifting factor, the unavailability can be affected positively or negatively. In some cases, when failures

occur at off-peak periods, increasing the shifting factor will cause the unavailability to increase since more load is moved to these periods. On the other hand, if all failures occur during peak periods, increasing the shifting factor will further improve the availability for the same reason (more load is now moved from these periods). Since in our case some faults took place at peak times and others at off-peak times, altering the shifting factor may increase or decrease the hours of unavailability, depending on the amount of lost load at each fault. Residential, commercial, and industrial loads have peaks at different times with different amounts, which cause the rise and fall in Figures (2.18-2.20). Generally, comparing the base case (shifting factor=0) with the maximum case (shifting factor=200), the unavailability of the hybrid system decreases in all cases except the case of industrial load with 100% level of curtailment, in which load shifting negatively affects availability.

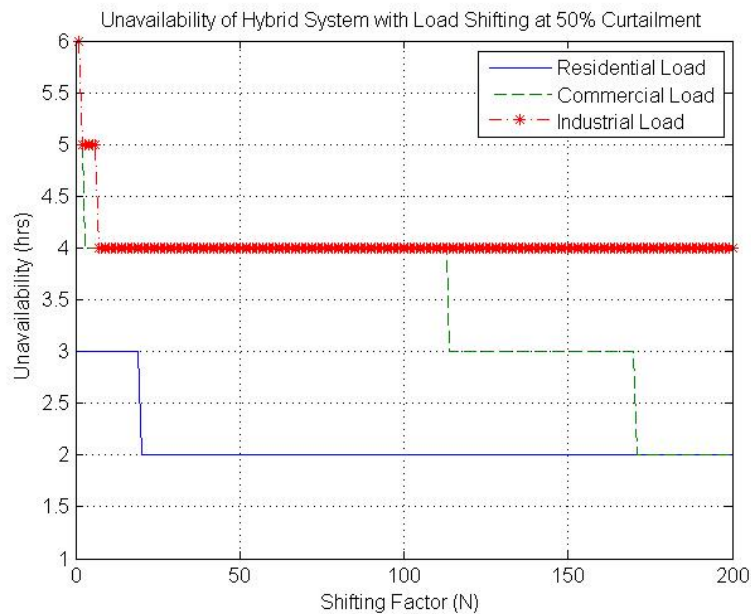


Figure 2.18 Unavailability vs. shifting factor - 50% curtailment

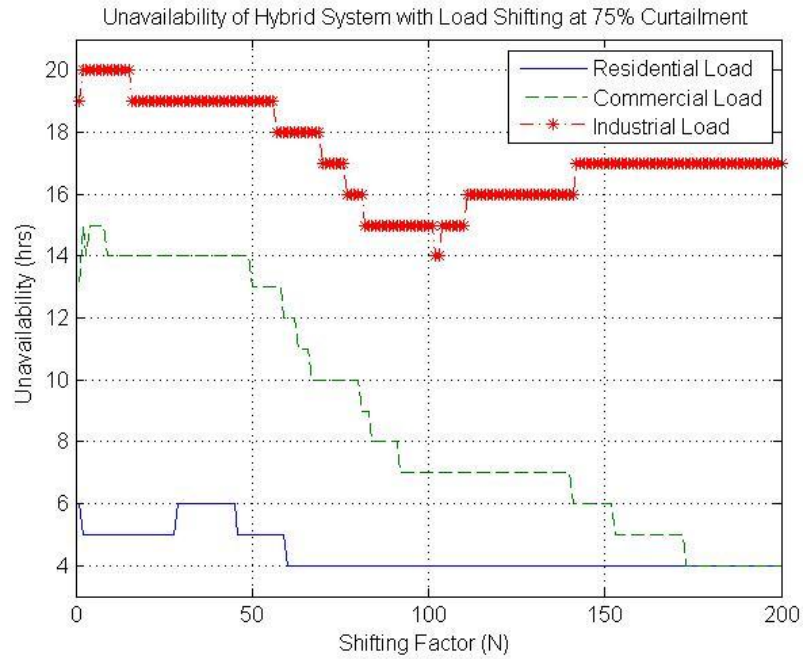


Figure 2.19 Unavailability vs. shifting factor - 75% Curtailment

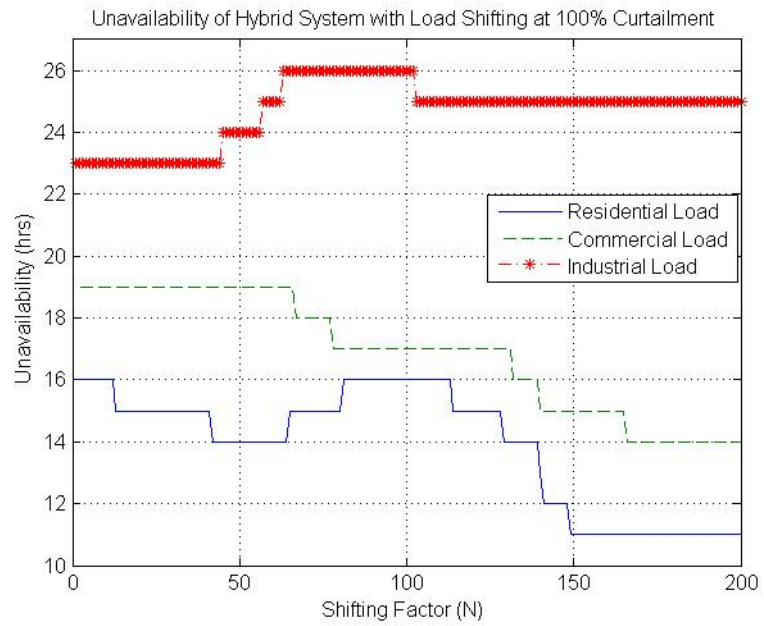


Figure 2.20 Unavailability vs. shifting factor - 100% Curtailment

2) Peak Clipping with Hybrid Renewable System

The ENS for the hybrid system is shown in Figure 2.21 as a function of the clipping factor. The commercial load shows the best result, which indicates that most of the faults occurred at commercial peak times.

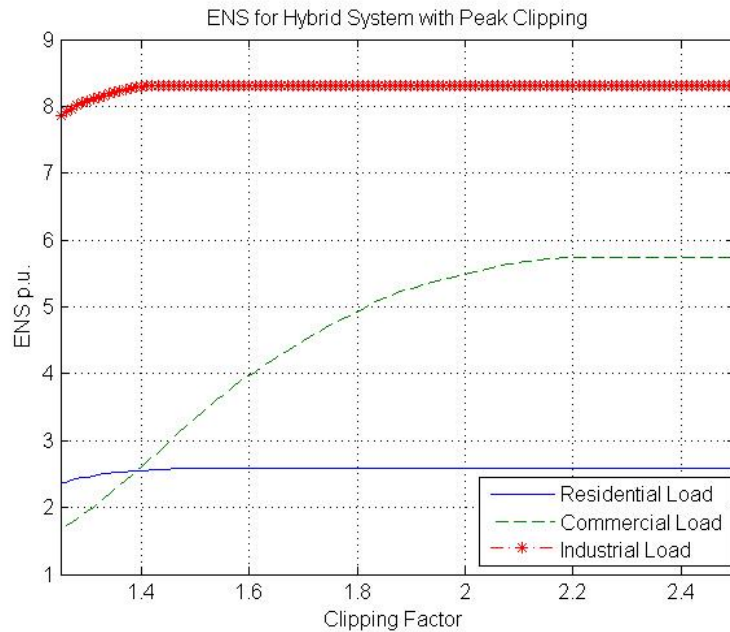


Figure 2.21 ENS vs clipping factor - hybrid system

Figures (2.22-2.24) show the unavailability versus clipping factor at 50%, 75%, and 100% levels of curtailment, respectively. From these graphs, it can be realized that in contrast to the load shifting method, peak clipping can never negatively impact the figure of unavailability. It is either improved or it remains unchanged, as in the case for the residential load in Figures 2.20 and 2.22.

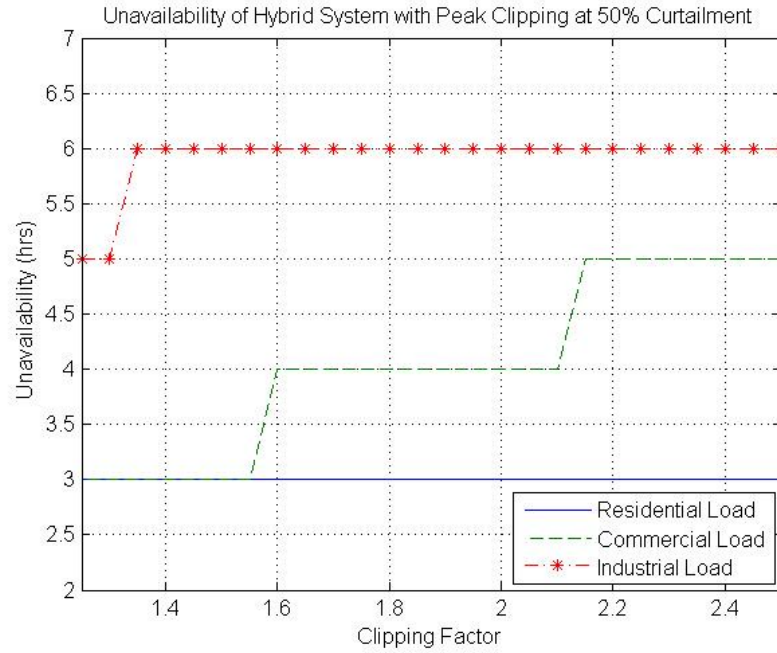


Figure 2.22 Unavailability vs. clipping factor - 50% curtailment

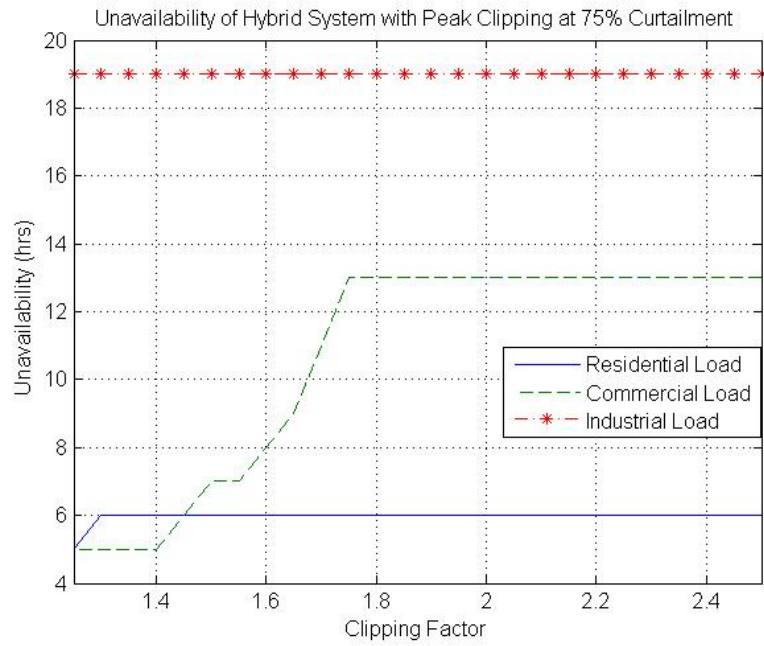


Figure 2.23 Unavailability vs. clipping factor - 75% curtailment

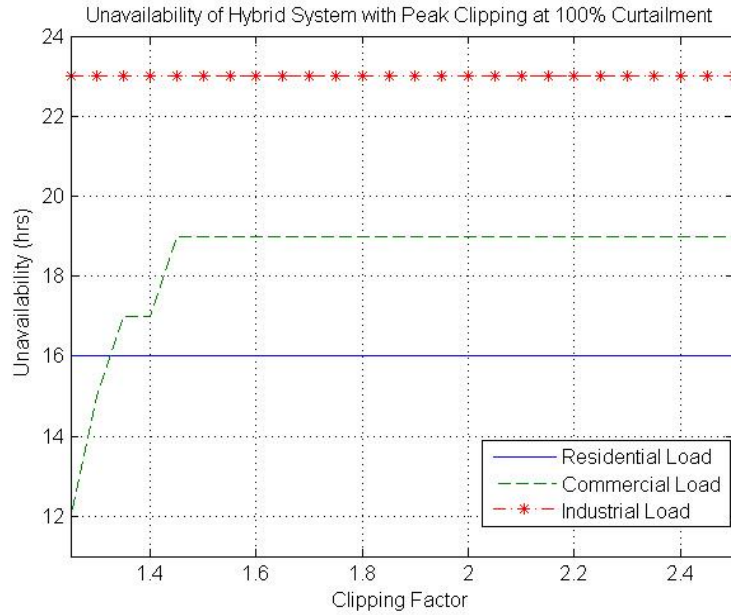


Figure 2.24 Unavailability vs. clipping factor - 100% curtailment

2.3.1.5 Summary and Discussion of the Local Load Study

The reliability of a local load, including residential, commercial, and industrial sectors, was examined in four stages. The first stage consisted of the loads connected only to the utility. In the second stage, hybrid wind turbines and PV panels were integrated into the system. The third stage included the DSM and in the fourth stage DSM was included along with the hybrid renewable system. At each stage, the reliability was assessed in terms of unavailability in hours and ENS. From the study results, ENS decreased by 83%, 69%, and 66% for the residential, commercial, and industrial loads, respectively, after integrating the hybrid system. Two DSM types were introduced, load shifting and peak clipping. The ENS decreased as more DSM is applied by interchanging the introduced shifting and clipping factors. Finally, after combining RE with DSM in stage four, the reliability of the local load was further improved depending on DSM factors. For example, at shifting factor=200, 48%, 66%, and 27% decrease in ENS for the residential, commercial, and

industrial loads were measured compared to the RE stage excluding DSM (stage 2). In general, after studying all the four stages, it was recorded that integrating RE or applying DSM highly impact the level of reliability. Moreover, combining the two aspect simultaneously, as the case in smart grids, results in more enhancement to the level of reliability and dependency.

2.3.2 System Study

The reliability evaluation of the RBTS-BUS2 system indicated previously in section 2.2.6 will be performed. The system will be studied during a restoration process and evaluated in terms of SAIFI, SAIDI and ENS indices. To include the transfer capacity of the system in this study, the voltage profile level for the connected loads will be analyzed. If the voltage drops below 0.95 p.u., the load will be considered lost or disconnected. The methodology of studying DGs and LM impacts on system reliability evaluation is as follows:

- 1) Modeling the loads using equation (2.1).
- 2) Simulating interruptions using MCS.
- 3) Calculating system reliability indices and recording lost LP (evaluating system reliability).
- 4) Integrating renewable DGs.
- 5) Re-evaluating system reliability.
- 6) Applying LM techniques to load curves excluding DGs.
- 7) Re-evaluating system reliability.
- 8) Applying LM techniques including renewable DGs Integration.

9) Re-evaluating system reliability.

2.3.2.1 Case Studies

Two fault incidents are simulated. The fault locations are shown in Figure 2.25.

These are:

Case I: Fault at Branch 1

Case II: Fault at Branch 12

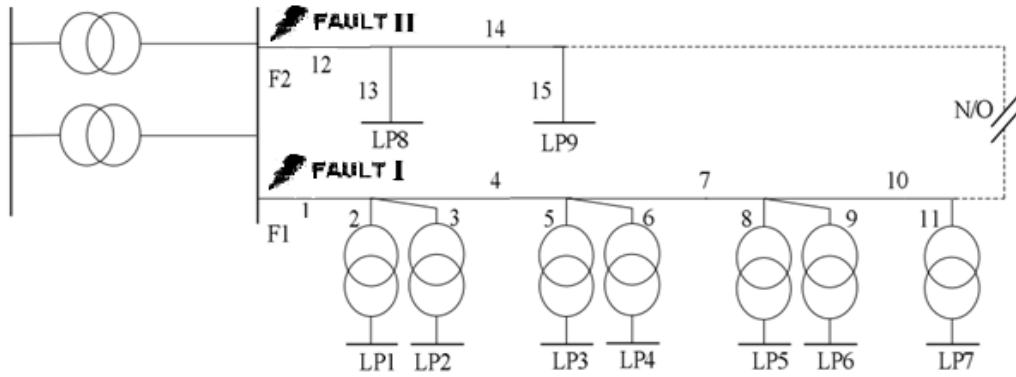


Figure 2.25 Faults locations

In both cases, the failure duration was assumed to be 5 hours based on the mean time to repair (MTTR) value of the faulted branches indicated in [27]. The time to fail was specified using MCS. The established chronological hourly load model provides the peak loads at the simulated interruption hours for each point. After disconnecting one of the branches, the possibility of load restoration is assessed by solving the load flow problem of the RBTS system. The reliability of the grid will be further studied by connecting RE with different sizes as percentages of the total connected load peak in order to examine their effect on the restoration process. The power outputs for the solar panels and the wind

turbine at failure time are extracted from their simulated hourly output data. Figure 2.26 shows the connection location of the hybrid renewable system.

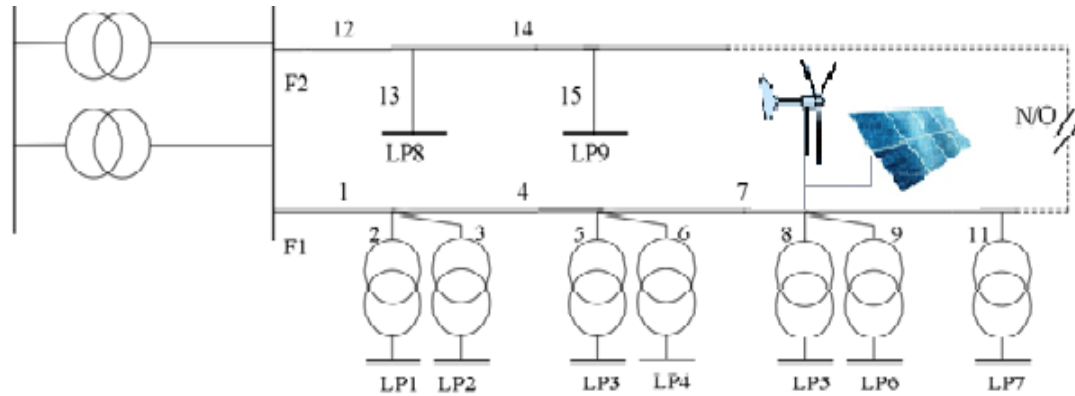


Figure 2.26 Hybrid renewable system location

The system is then re-assessed by applying LM techniques on the residential, governmental, and commercial customers of the network. Two LM methods are applied, which are load shifting and peak clipping. The load shifting and peak clipping factors are varied to measure their effect on load restoration. The system will be analyzed after applying different renewable resource integration and load management improvements. Table 2.8 summarizes the different sizes of wind turbines and PVs in the hybrid system, and the LM factors that will be studied. Note that the wind turbine and the PVs are connected simultaneously, while load shifting and peak clipping are applied separately. Also note that the last sizes of the hybrid system shown in Table 2.8 will be used only for the second case since greater generation will be needed due to faults occurring near high demand load points (LP 8 and LP 9).

Table 2.8 Different specifications for PV/WT sizes and LM factors

Hybrid Sizes (%of total load peak)			Load Management Shifting/Clipping	
	WT	PV	LS factors	PC factors
Size1	1%	0.6%	N=100	C=1.3
Size2	2%	1.25%	N=200	C=1.2
Size3	3%	1.9%	N=300	C=1.1
Size4	4%	2.5%		

2.3.2.2 Results and Analysis

Two main case incidents are presented in study. Different scenarios were applied to improve the system restoration for each case as illustrated in Table 2.8. The scenarios were compared based on SAIFI, SAIDI, ENS, and the interrupted loads with their average voltage levels. In total, 10 scenarios for each main case were studied, with changes in the hybrid system size, load shifting with different N shift factors, and peak clipping with different C clipping factors. Finally, for each case, two extra scenarios were analyzed in which hybrid renewable system and LM were both integrated into the system.

1) Case I: Failure at Branch 1

Considering the failure of Branch 1, load flow analysis was performed to calculate the voltage level for all loads. As discussed above, loads with a voltage level below 0.95 p.u. were considered lost or disconnected while loads with voltage within the limits were restored. Table 2.9 lists interrupted load points and their average voltage levels for case I. Table 2.10 shows the reliability indices for scenarios with lost loads.

Table 2.9 Case I restoration results

Scenario		Interrupted LPs	Lost LP Voltage Avg.
Hybrid	Base	L1-6	0.9434
	Size 1	L1-4	0.9464
	Size 2	None	-
	Size 3	None	-
LS	N=100	L1- 2	0.9493
	N=200	None	-
	N=300	None	-
PC	C=1.3	L1-2	0.9492
	C=1.2	None	-
	C=1.1	None	-

Table 2.10 Case I reliability indices

Scenario	SAIFI	SAIDI (hrs)	ENS (MWh)
Base	0.981	4.9	23.531
Size 1	0.965	4.8	15.6676
LS-N=100	0.642	3.21	6.5202
PC-C=1.3	0.642	3.21	6.9092

It can be noted from Table 2.10 that SAIFI and SAIDI are highly affected due to a high number of customers connected near the fault location. Two extra scenarios were examined by combining renewable energy and LM for residential, governmental/institutional and commercial loads. This resulted in the complete recovery and restoration of all loads. Table 2.11 indicates the results after combining the scenarios with lost loads.

Table 2.11 Case I - combining RE and LM

Scenario	Lost LP
Size 1 + LS (N=100)	None
Size 1 + PC (C=1.3)	None

In order to observe RE and LM effects more clearly, Figures 2.27-2.30 show the voltage profile curves for all loads at each scenario for incident case I. In Figure 2.27, the voltages are shown for each size of the hybrid system. In Figures 2.28 and 2.29, the voltages are shown for each LS/ PC factor. Figure 2.30 shows the voltage profile after combing RE and LM. The dashed line across the figures represents the minimum permissible voltage (0.95 p.u.).

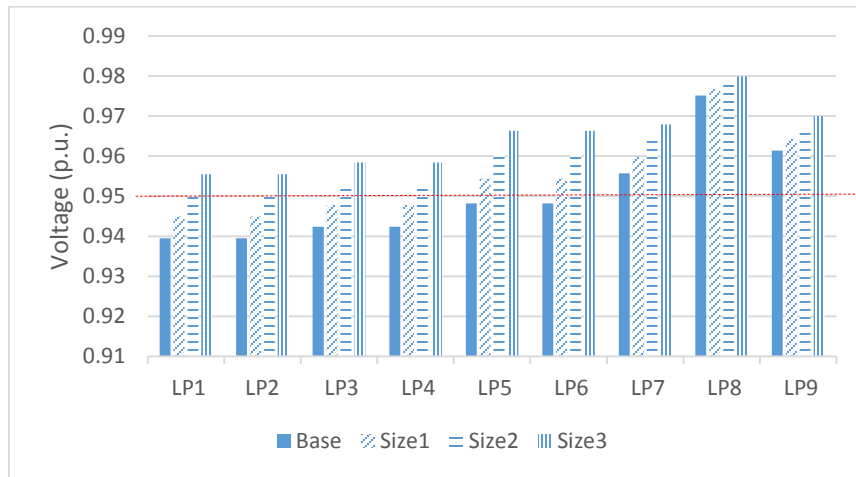


Figure 2.27 Case I - load voltage profile with different hybrid system sizes

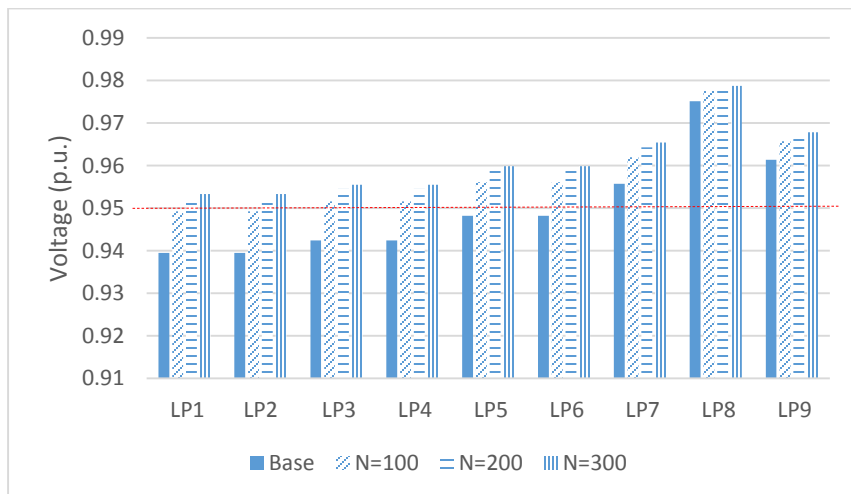


Figure 2.28 Case I – load voltage profile interchanging load shifting factor

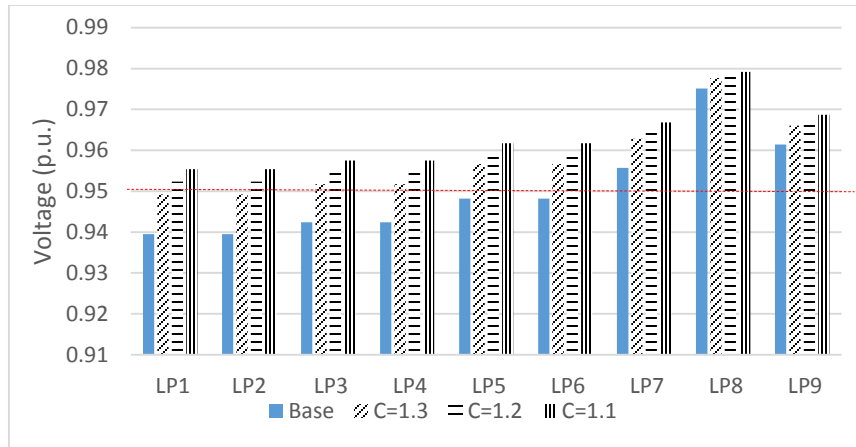


Figure 2.29 Case I – load voltage profile interchanging peak clipping factor

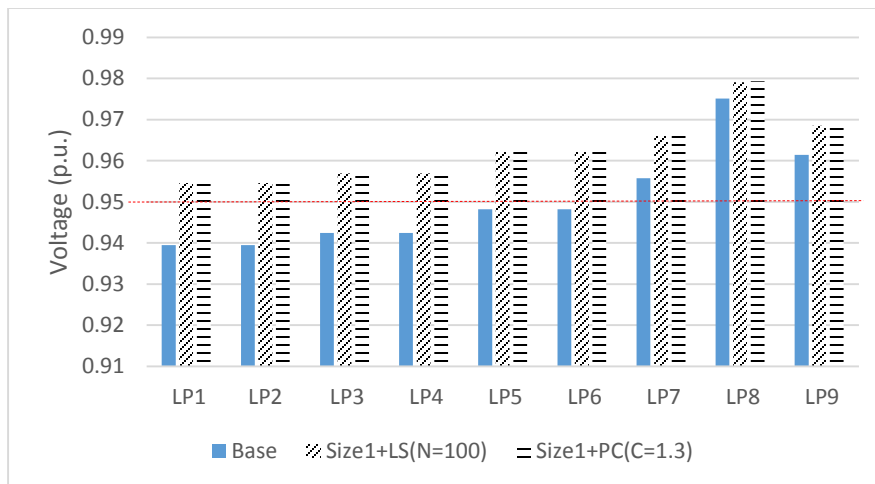


Figure 2.30 Case I – load voltage profile combining RE and LM

2) Case II: Failure at Branch 12

In this incident case, Branch 12 is the one experiencing an outage. Tables 2.12 and 2.13 show the results. It can be noted that SAIDI and SAIFI are less affected now because the faults occurred near the small users where they account for only 0.3% of total number of customers. None of the scenarios completely restored all load points, but this can be achieved by combining RE and LM, as shown in Table 2.14.

Table 2.12 Case II restoration results

Scenario		Interrupted LP	Lost LP Voltage Avg.
Hybrid	Base	L5-L9	0.93504
	Size 2	L7-L9	0.9379
	Size 3	N8,L9	0.93865
	Size 4	L8,L9	0.94335
LS	N=100	L7-L9	0.9334
	N=200	L7-L9	0.93567
	N=300	L7-L9	0.93693
PC	C=1.3	L7-L9	0.93483
	C=1.2	L7-L9	0.9365
	C=1.1	L7-L9	0.93823

Table 2.13 Case II reliability indices

Scenario	SIAFI	SAIDI (hrs)	ENS (MWh)
Base	0.0352	0.176	29.1435
Size 2	0.0183	0.0915	21.28
Size 3	0.003	0.015	17.5
Size 4	0.003	0.015	17.5
N=100	0.0183	0.0915	20.7101
N=200	0.0183	0.0915	20.2559
N=300	0.0183	0.0915	19.9252
C=1.3	0.0183	0.0915	20.151
C=1.2	0.0183	0.0915	19.9471
C=1.1	0.0183	0.0915	19.7432

Table 2.14 Case II – combining RE and LM

Scenario	Lost LP
Size 4 + LS (N=300)	None
Size 4 + PC (C=1.1)	None

Similar to case study 1, voltage profile of the system at different scenarios are shown in Figures 2.31-2.34. It can be seen from these figures that fault case II caused larger effect on the voltage profile due to the outage location which is near loads with high demand.

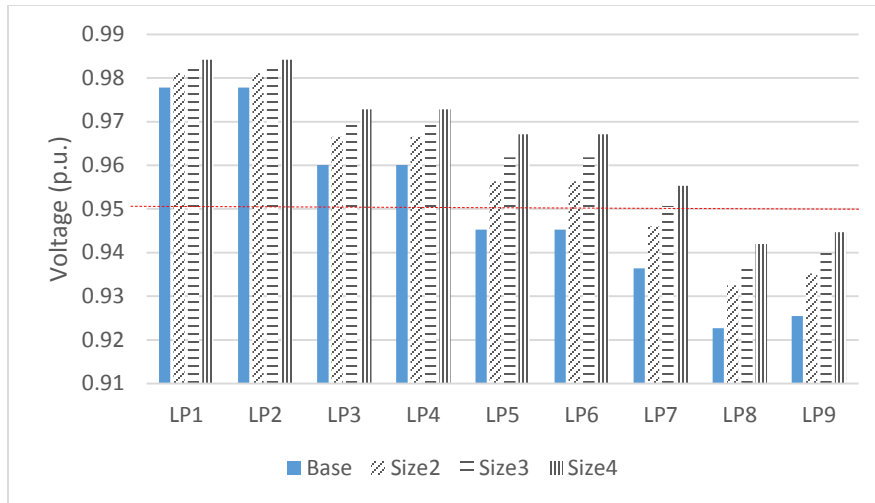


Figure 2.31 Case II - load voltage profile with different hybrid system sizes

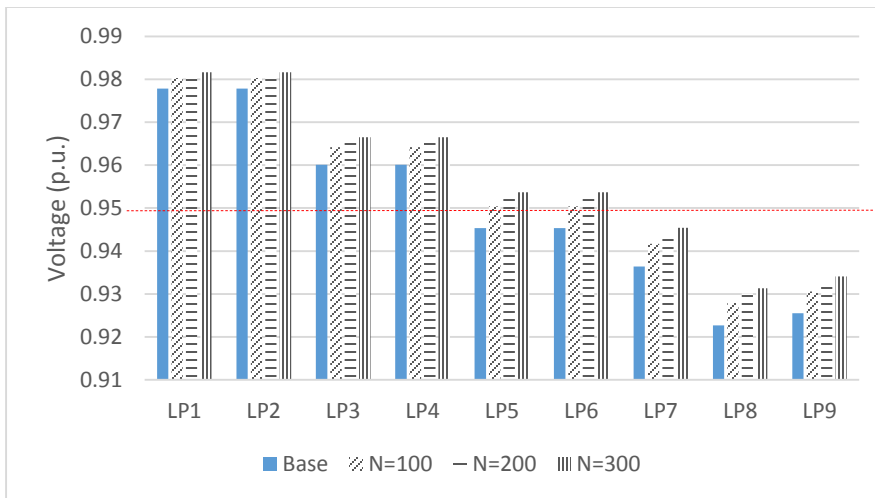


Figure 2.32 Case II – load voltage profile interchanging load shifting factor

2.3.2.3 Summary and Discussion of the System Study

In this case of study, the impact of LM and the integration of renewable energy on the restoration process was studied. Two faults on two different locations of the RBTS-BUS2 distribution system were simulated. Several scenarios were analyzed by connecting different hybrid system sizes and by interchanging the LM factors. SAIFI, SAIDI and ENS indices of the system were obtained at each incident case. The voltage profiles were also

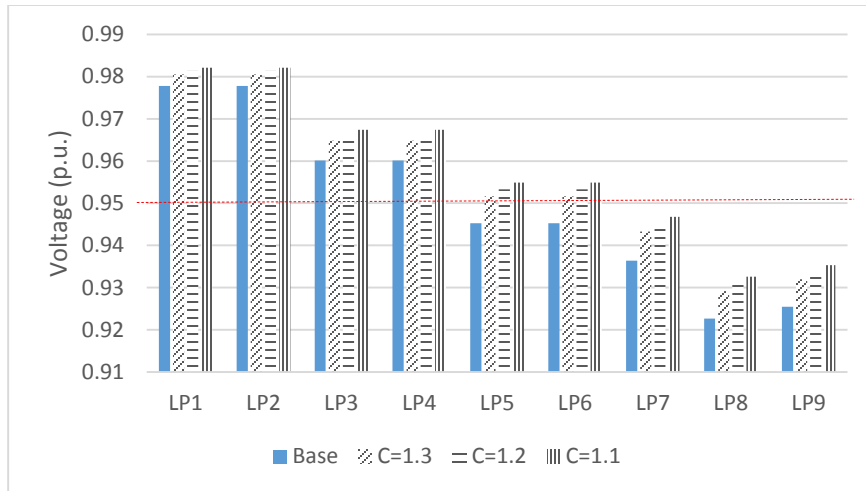


Figure 2.33 Case II – load voltage profile interchanging peak clipping factor

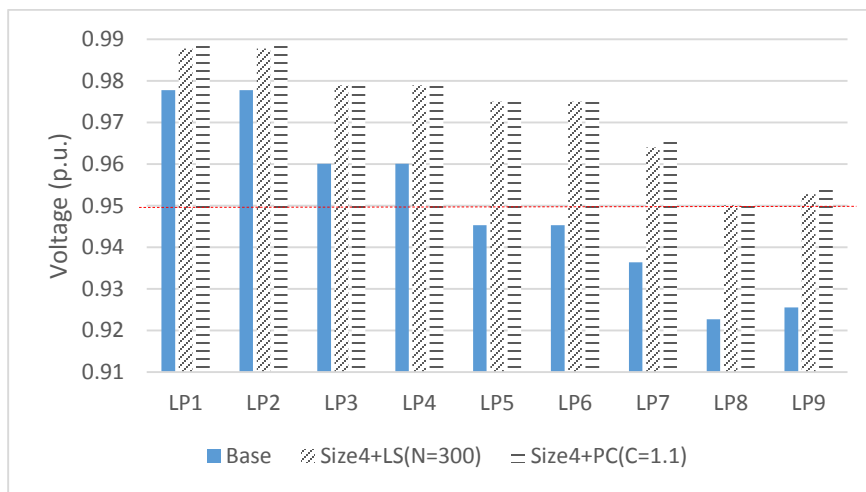


Figure 2.34 Case II – load voltage profile combining RE and LM

examined in order to test system restoration capability. It was realized that the integration of a wind turbine and solar panels to the system can largely improve the restoration process during an interruption. Furthermore, applying LM techniques on connected customers can also affect the reliability and system restoration.

From the local load study and the system study, the following can be concluded:

- 1) DGs and RE can largely enhance the level of reliability and the efficiency of the restoration process.
- 2) Load management practice also provided improvements to the figure of reliability especially when combined with RE based DGs.
- 3) Loads unserved during an intrusion are random and depend on fault location.

Points 1 and 2 should be convenient to the reader at this stage. The word random in point three refers to the fact that an operator has no control over which loads to be served and which are disconnected during the occurrence of an intrusion. This is fully dependent on the fault location. Fortunately, in a smart microgrid, this is not the case. By utilizing the advanced control schemes existing in smart microgrids, an operator can curtail a specific amount of load from specific customers in order to serve others. This raises another issue which is rarely discussed in the literature. On what basis does an operator or a control system prioritize one load over another? There are many aspects that can influence the choice of the operator such as load amount, number of customers and cost of intrusion. In the next chapter, this issue is resolved where a prioritizing methodology is proposed that encompasses several aspects that might influence customer prioritizing.

CHAPTER 3

LOAD PRIORITY MODELING FOR SMART

MICROGRIDS

As a result of society's dependence on electric power and the high costs associated with service interruptions, enhancing the reliability of distribution systems has become a necessity. One key technique for improving system reliability is to apply an efficient power restoration methodology. For a restoration methodology to be effective and resilient, it must make strategic load prioritization a systematic procedure.

In this chapter, a load prioritization method for service restoration in distribution systems is presented. The method ranks loads by priority and assigns a calculated weight for each load in the system. These weights are ranked and used as an input to the restoration optimization problem. The weights are dynamic (i.e., time-dependent), and the priority list can be updated at any time point of interest. The load prioritization procedure takes into account the criticality of the load, the amount of energy consumption, the number of connected customers, and the cost of interruption. Additionally, customers participating in demand side management (DSM) programs are addressed via prioritization and weighting. The RBTS Bus 4 system is used as a case study to implement this method.

The subject of prioritizing is considered both, a technical and a managerial issue. Thereby, detailed discussion must be provided before introducing the mathematical

formulation. Hence, this chapter starts with an introduction about load prioritizing and its current consideration in the literature in section 3.1. Then, section 3.2 delivers the factors and the strategy of the proposed method. The mathematical formulation is demonstrated in section 3.3 and finally, section 3.4 illustrates an example of load prioritizing.

3.1 Introduction

Distribution systems (DS) are obligated to operate in a reliable and secure manner. Even with advanced-technology DS equipment and reliability improvements in recent years, interruptions are inevitable. In fact, 80% of all network interruptions are located and caused within DS [28].

The development of the microgrid (MG) concept has produced many technical solutions that have improved the reliability and resilience of DS. However, the increased new aspects and controls, such as demand side management (DSM) and distributed generators (DG), have also increased the complexity of MG systems. Therefore, the development of a robust strategic method for MG DS power service restoration (PSR) is needed that can take into account multiple technical requirements including maximizing the total load amount to be restored, maximizing the total number of customers served, implementing DSM programs, and reducing outage time, all while satisfying power quality constraints. Moreover, in the case of MGs the overall impact of an interruption on society must be minimized by applying special attention in the PSR process to certain types of loads that strongly affect the community in general.

It is very common for MGs to include customers that cannot mitigate a loss of electricity and therefore require restoration as soon as possible. These so-called priority

customers (PCs) include hospitals, security departments, banks, and large steel factories. Power restoration for hospitals, for instance, is favored over many other loads that might have larger energy demands or more customers. Furthermore, loads within the PC classification may also differ in their level of importance. For example, the restoration of a fire station is more important than the restoration of a bank, even though both are considered to be PCs.

The procedure of listing and ranking loads must take into account multiple characteristic factors such as demand amount, number of customers connected, expected outage duration, cost of interruption and load criticality. Additionally, the listing criteria should be dynamic to reflect the possibility that priorities will change over time. For example, a governmental load may be prioritized during workdays rather than over weekends, and in the morning rather than at night. It is intuitive that prioritization of loads becomes an even more sophisticated problem when many loads exist. The process of PSR in MGs becomes much more effective and far-reaching when a priority list is implemented. The result is not only a reduction in failure-associated financial losses but also an increase in total system reliability. Therefore, the formation and modeling of a strategic solid methodology that lists and prioritizes loads in an efficient manner is extremely desirable.

Currently, prioritization is performed by the utilities depending on operator judgment, which may be based on an existing non-dynamic list. The resulting decisions may negatively affect the efficiency and reliability of PSR because—in reality—load prioritization is a function of time; some loads may be considered to be PCs at only specific

hours of the day, days of the week or weeks in the year. Schools, for example, are considered to be PCs only on workday mornings and not on weekends or vacations.

Regarding the evaluation of PCs in the literature to address the PSR problem, research has been divided into three main categories:

- 1) Ignoring PC classification during restoration [29-31].
- 2) Classifying PCs with only one level of importance [32, 33].
- 3) Assigning limited levels or arbitrary general weights representing PCs [34, 35].

In [29-31] PCs were not considered in the restoration process because the process was based only on maximizing the amount of total load restored. This approach reduces the efficiency and robustness of the restoration process, however. References [32 & 33] assumed only one level of priority. In [32], one of the objective functions in the restoration process was to maximize restoration of all PCs, which were lumped into a single higher-priority group. Reference [33], also included PCs in the problem constraints, which specified that all PCs must be restored. Of course, by applying such a constraint, many efficient restoration plans and configurations would be neglected if they were unable to restore every last PC. References [34 & 35], considered only three priority grades, which were assigned based on reliability requirements. This approach is arguably the best of the three, but it still lacks precision, especially when dealing with large-scale distribution systems. When large numbers of customers are included in the prioritization process, it becomes difficult to determine a grade for each load, and decisions based on intuition are inherently qualitative. Moreover, loads within the same grade may actually differ in priority, a point that has not been addressed in previous work.

3.2 The Prioritizing Factors

To build a well-structured prioritization method, the following question must be answered: “On what basis should a utility or an operator prioritize one load over another?”

Many factors can be included to answer this question. They can be summarized by the following:

- 1) Load criticality.
- 2) Load demand (KW) at the time of prioritization.
- 3) Expected energy not served (EENS).
- 4) Number of customers.
- 5) Expected outage duration for each load.
- 6) Demand side management (DSM) programs.
- 7) Effect on system total reliability indices (STRIs).
- 8) Cost of interruption.
- 9) Time of prioritization.

These are the factors to consider when prioritizing one load over another. To include them all in the prioritization process, an efficient methodology must be developed. The proposed method contains all of the factors listed above. The method not only ranks the loads by priority but also assigns a calculated weight for each load in the system. This weight expresses the priority of that load and constitutes a quantitative measure that can be used in the ranking process and in the restoration optimization problem.

The weights are dynamic and time-dependent, allowing the priority list to be updated at any time point of interest.

To include the system total reliability indices in prioritization, the effect of each load on these indices is calculated and included in the weighting process. The proposed method of prioritization and weighting is divided into two levels. Each level contains certain factors associated with each load in the system as follows:

Level 1:

- Criticality.

Level 2:

- Expected effects on system total reliability indices (STRIs) that include
 - . Energy not served (ENS).
 - . System average interruption duration index (SAIDI).
 - . System average interruption frequency index (SAIFI).
- Customers with demand side management (DSM) programs.
- Estimated cost of interruption.

At the first ranking level, loads are prioritized based on their criticality, which is independent from their energy need, number of customers, and cost of interruption. If two loads have the same level of criticality, the second level is used to differentiate between them. Additionally, all other non-critical loads are ranked based on the second level. The second level of prioritization relies the effects of load interruption on the ENS, SAIDI and SAIFI metrics, along with the cost of load interruption. Customers with DSM programs are integrated by adjusting their ENS, SAIDI and SAIFI factors. Finally, by combining all four factors for each load, the final priority weights for each load can be obtained.

Consequently, rather than assigning arbitrary importance weights to each load, weights can now be systematically calculated and modeled—as will now be illustrated.

A. Load Criticality (LC)

Some loads are considered inherently critical without including or measuring any other factors. Such critical loads are given the highest priority regardless of their energy consumption or cost of interruption. When an outage occurs, the restoration of such loads is crucial and should be achieved as fast as possible. Those types of loads must be prioritized over all other loads in the system. Note that the criticality as defined here does not depend on the load demand, number of customers, or cost of interruption, but instead depends on the type of the load itself. Such loads include hospitals, fire stations, and police departments.

B. Expected Effects on System Total Reliability Indices (STRIs)

It is very important for utilities to keep their STRIs as high as possible. Three main indices are commonly used to represent the reliability of a system: energy not served (ENS), system average interruption duration index (SAIDI), and system average interruption frequency index (SAIFI). SAIFI and SAIDI have been widely used in North America as measures of the effectiveness of distribution systems [36]. Most utilities must report their reliability indices to regulatory sectors. In a 2008 survey, public utility commissions in 35 U.S. states required routine reporting of reliability indices from utilities [37]. Therefore, one of the key aspects in prioritizing loads is to measure their effects, when interrupted, on the STRIs. Certain loads, when subjected to an outage, can severely harm the reliability metric of a system, whereas others do not. One strategy is therefore to

prioritize the most impactful loads. This approach not only improves STRIs but also prioritizes loads with higher demand and larger number of customers because they are more likely to affect the STRIs.

Three main Indices are what commonly represent the reliability of a system. These are, Energy Not Served (ENS), System Average Interruption Duration Index (SAIDI), and System Average Interruption Frequency Index (SAIFI). Loads that affect these three indices will be prioritized over other loads that barely mitigate the indices. This will not only improve STRI, but will also prioritize loads with higher demand and larger number of customers since they are more capable to affect STRI.

1) Expected Effects on System ENS

The load effect on system ENS can be calculated using the expected energy not served (EENS) for the load when a fault occurs. It is more convenient to rank the loads depending on their EENS when experiencing an outage rather than ranking them depending on their current power consumption. The mean time to repair (MTTR) for the faulted section can be used to represent the expected failure duration (EFD), where MTTR is the average time required to repair and restore the section when experiencing a sustained interruption. Of course, load EENS will change with time depending on the demand forecast and the MTTR value of the faulted section. As a result, in this example of prioritization, loads can be ranked and weighted depending on their EENS (t) value. Applying this criterion in prioritization minimizes the system total ENS because loads that are expected to have a larger effect on system ENS are prioritized.

2) *Expected Effects on System SAIDI*

The SAIDI metric represents the average time that customer power is interrupted in minutes (or hours) in 1 year and can be calculated as follows:

$$\begin{aligned} SAIDI &= \frac{\text{Total duration of all interruptions}}{\text{Total number of customers}} \\ &= \frac{N_1 * FD_1 + N_2 * FD_2 + \dots + N_f FD_f}{N_T} \end{aligned} \quad (3.1)$$

where N_1, N_2, \dots, N_f are the number of customers interrupted at fault 1, 2, ..., f, FD_1, FD_2, \dots, FD_f are the durations associated with each fault, and N_T is the total number of customers in the system.

From equation (3.1), it can be seen that the main factor associated with a load point (LP) that could affect SAIDI is the product of the number of customers and the load outage duration. As with the case of ENS, the load outage duration can be represented using the MTTR of the faulted section at the time of prioritizing. Finally, loads can be prioritized and weighted depending on the numerical value of the number of connected customers multiplied by load MTTR.

3) *Effects on System SAIFI*

The SAIFI metric represents how often interruptions occur on average for each customer and is calculated as follows:

$$SAIFI = \frac{\text{Total number of all interruptions}}{\text{Total number of customers connected}} \quad (3.2)$$

$$= \frac{N_1 + N_2 + \dots + N_f}{N_T}$$

The SAIFI figure entirely depends on the number of customers associated with a load. Hence, with this metric, loads are prioritized according to their number of customers.

C. DSM Programs

DSM includes any incentive made by the utility to influence the customer's load. There are many different types of DSM programs depending on load sector, utility agreement, requested level of reliability and many other factors. The DSM programs that influence load prioritization can be categorized into two types. The first represents customers that pay the utility a surcharge to receive a higher level of reliability and to be prioritized in restoration when an interruption occurs. The second represents customers that benefit from reduced electricity bills from the utility but receive a lower priority and may forgo part or all of their power in emergency cases. The former type can be incorporated into the priority list by increasing the ENS, SAIDI, and SAIFI priority weights that are associated with these participating customers. Similarly, the latter type is incorporated by reducing their weights, as will be illustrated more specifically in the formulation section.

D. Estimated Cost of Interruption

An important prioritization factor is the estimated cost of interruption for each load in the system. The cost of interruption depends on several measured and unmeasured factors. Many methods are used to estimate the cost of interruptions including survey-based methods, scaled macro-economic indicators (e.g., gross domestic product or wages), and

market-based indicators (e.g., incremental value of reliability derived from studies of price elasticity of demand for service offered under non-firm rates) [38].

According to Sullivan et al., “Survey-based methods have become the most widely used approach and are generally preferred over other measurement methods due to their ability to quantify outage costs for a wide variety of reliability and power quality conditions that are usually not observable using other techniques.” [39].

Load prioritization in this case can be achieved by weighting the loads depending on their estimated cost of interruption, which depends on the time of prioritization. The estimated costs of interruption used in this research are collected from an Assessment of Publicly Available Information Reported to State Public Utility Commissions in the U.S. [40]. In [40], the cost of interruptions for different types of loads at different times and seasons were estimated based on surveys of the economic losses customers experience as a result of electric service interruptions along with surveys of customers’ willingness to pay to avoid (or willingness to accept compensation for) problems.

Finally, by calculating, normalizing and then combining all previously mentioned weights for each load in the DS, the final associated priority weights for all loads at any time can be extracted. The mathematical formulation is described in the next section.

3.3 The Mathematical Formulation of the Prioritizing Strategy

The time segment that will be considered in this study is one hour. This means that the priority weights and lists are updated at each hour.

The time segment assumed in this study is 1 hour; equivalently, the priority weights and lists are updated each hour.

3.3.1 Criticality

Load criticality is modeled by assigning the weight $L_{critic}^i(t)$ (referred to as the criticality weight) to each load i in the system depending on the level of criticality, which can range between 0–2 as shown in table I. Most of the loads are classified as low criticality with $L_{critic}^i(t) = 0$ and are subsequently prioritized based on level 2. Note that this weight is a function of time, whereas criticality of each load depends on the time of evaluation and prioritization.

Table 3.1 Weights and levels of criticality

Level of criticality	$L_{critic}^i(t)$	Examples
High	2	Hospitals, Fire Stations, ..., etc.
Medium	1	Schools
Low	0	All other loads

3.3.2 Expected Effects on System Total Reliability Indices

In this part, loads are prioritized and weighted depending on their forecasted energy consumption which is what effects system total ENS. The total effect of load i when interrupted on system ENS is calculated as follows:

$$L_{ENS}^i(t) = \sum_t^{t+MTTR^f} D^i(t) \quad (3.3)$$

where $L_{ENS}^i(t)$ is the expected effects of load i , when interrupted at hour t , on system ENS (referred to as ENS weight), $D^i(t)$ is the forecasted demand of load i at hour t , and $MTTR^f$ is the mean time to repair of the faulted section.

For SAIDI, loads are weighted depending on their effects on the SAIDI metric, which includes the number of customers and the fluted section's MTTR. The weighted effect of an interrupted load i on the SAIDI metric is calculated as follows:

$$L_{SAIDI}^i = MTTR^f * N^i \quad (3.4)$$

where L_{SAIDI}^i is the expected effects of load i , when interrupted, on system SAIDI (will be referred to as SAIDI weight), and N^i is the number of customers connected to load i .

For SAIFI, loads are weighted depending on their effects on the SAIFI metric, which represents the number of customers only. The weighted effect of an interrupted load i on the SAIFI metric is calculated as follows:

$$L_{SAIFI}^i = N^i \quad (3.5)$$

where L_{SAIFI}^i is the expected effect of an interrupted load i on the SAIFI metric and is referred to as the SAIFI weight.

3.3.3 Customers with Demand Side Management (DSM) Programs

The demand side management can be incorporated by modifying the values of $L_{ENS}^i(t)$, L_{SAIDI}^i , L_{SAIFI}^i depending on the factor DSM^i as follows:

$$\begin{aligned} L_{ENS}^{i,m}(t) &= L_{ENS}^i(t) * DSM^i \\ L_{SAIDI}^{i,m} &= L_{SAIDI}^i * DSM^i \\ L_{SAIFI}^{i,m} &= L_{SAIFI}^i * DSM^i \end{aligned} \quad (3.6)$$

where $L_{ENS}^{i,m}(t)$, $L_{SAIDI}^{i,m}$, and $L_{SAIFI}^{i,m}$ are the modified ENS, SAIDI, and SAIFI weights of load i , respectively. DSM^i is a factor that defines the Load Management Program (LMP) in which load i participates, as shown in Table 3.2:

Table 3.2 DSM programs and associated factors

LMP type	DSM^i
Paying for more reliable service	$DSM^i > 1$
Not participating	$DSM^i = 1$
Curtailed with reduced bills	$DSM^i < 1$

As shown in Table 3.2, if a load i is paying to obtain more improved service, its associated $L_{ENS}^i(t)$, L_{SAIDI}^i , and L_{SAIFI}^i weights increase as a result of being multiplied by a number greater than one. Thus, those loads receive higher weights and are prioritized in the restoration process. For example, if load i has $DSM^i=2$, then $L_{ENS}^i(t)$, L_{SAIDI}^i , and L_{SAIFI}^i are multiplied by 2 and load i is prioritized as if it had double the energy consumption, double the number of customers, and double the outage duration. This customer therefore enjoys a higher priority, a strategic advantage over other customers. In contrast, loads may arrange reduced billing costs in exchange for a DSM^i value of less than one, resulting in a lowered priority weight. Finally, non-participatory loads retain DSM^i equal to one, which does not alter their priority weights.

The specific values of the DSM^i factors depend on the utility programs and the contracts arranged between the utility and the participating customer. Additionally, the utility must consider all customers in the system when assigning DSM factors to avoid over-prioritizing or under-prioritizing participating loads. Therefore, this factor must be carefully tested before assignment to participating customers.

3.3.4 Estimated Cost of interruption.

The cost of interruption is estimated based on the values surveyed in the aforementioned official report submitted to the State Public Utility Commissions in the U.S. [40]. The study includes the cost of interruption for different types of loads at different times of the year. Additionally, it includes the cost of interruption depending on the duration of the fault which is represented by $MTTR^f$ and will be used as follows:

$$L_{cost}^i(t) = Cost^i(t, MTTR^f) \quad (3.7)$$

where $L_{cost}^i(t)$ is the expected cost of interruption for load i , when interrupted, at hour t (will be referred to as cost weight), $Cost^i(t, MTTR^f)$ is the surveyed cost of interruption for load i when experiencing an outage of duration $MTTR^f$ at hour t .

At this point, all prioritization weights associated with each load in the system have been defined; they are $L_{critic}^i(t)$, $L_{ENS}^{i,m}(t)$, $L_{SAIDI}^{i,m}$, $L_{SAIFI}^{i,m}$, and $L_{cost}^i(t)$. They can now be normalized, except for $L_{critic}^i(t)$, as follows based on the maximum load weight of each prioritization part:

$$L_{ENS}^{i,m}(t) = \frac{L_{ENS}^{i,m}(t)}{L_{ENS}^{max}(t)} \quad (3.8)$$

$$L_{SAIDI}^{i,m} = \frac{L_{SAIDI}^{i,m}}{L_{SAIDI}^{max}} \quad (3.9)$$

$$L_{SAIFI}^{i,m} = \frac{L_{SAIFI}^{i,m}}{L_{SAIFI}^{max}} \quad (3.10)$$

$$L_{cost}^i(t) = \frac{L_{cost}^i(t)}{L_{cost}^{max}(t)} \quad (3.11)$$

where $L_{ENS}^{max}(t)$, L_{SAIDI}^{max} , L_{SAIFI}^{max} , and $L_{cost}^{max}(t)$ are the maximum value between all loads in the system that is related to ENS, SAIDI, SAIFI and cost weights, respectively.

Then, the final weights associated for each load can be calculated as follows:

$$PL^i(t) = L_{critic}^i(t) + w_{ENS} * L_{ENS}^{i,m}(t) + w_{SAIDI} * L_{SAIDI}^{i,m} + w_{SAIFI} * L_{SAIFI}^{i,m} + w_{cost} * L_{cost}^i(t) \quad (3.12)$$

$$w_{ENS} + w_{SAIDI} + w_{SAIFI} + w_{cost} = 1 \quad (3.13)$$

where $PL^i(t)$: is the total priority weight of load i at hour t , w_{ENS} is the ENS weight w_{SAIDI} is the SAIDI weight, w_{SAIFI} is the SAIFI weight, and w_{cost} is the weight of cost importance.

The parameters w_{ENS} , w_{SAIDI} , w_{SAIFI} , and w_{cost} (referred to as importance weights) are assigned by the utility immediately when a fault occurs. The utility then evaluates the fault influence on the system total reliability indices and the total customer cost of interruption. By comparing these values with the utility's historical reliability indices and total cost of interruptions, the weights can be determined. For example, if the utility suffers from low historical ENS, the weight associated with ENS importance (w_{ENS}) is increased to prioritize those loads that will improve system ENS. The same strategy holds for SAIDI, SAIFI, and cost.

Finally, by arranging all loads in an ascending manner based on $PL^i(t)$ value, the final priority list is generated with an associated weight for each load in the system. A flow chart illustrating the complete prioritization methodology is shown in Figure 3.1.

3.4 Prioritizing RBTS Bus 4 Customers

The system used to apply the prioritizing method in this research is the RBTS Bus 4 [27]. The single line diagram for the system is shown in Figure 3.2. The number of components and customers in this system are shown in Table 3.3. Table 3.4 specifies the number of customers and load type for each load point in the system.

The system consist of a total of 38 load points with three types of loads, residential, commercial, and industrial. Detailed load information, including number of customers, and average and peak values, as well as system components reliability data of the system, that were used to extract the MTTR for each load, are illustrated in [27]. Load MTTR represents the average outage duration experienced by a certain load within a year. It can be viewed as the MTTR of all sections in the system that, when faulted, could cause an interruption to that particular load. Thereby, in order to provide a general priority list for RBTS Bus 4 system, and to avoid simulating random failures, the MTTR for each load will be used instead of the MTTR of the faulted section.

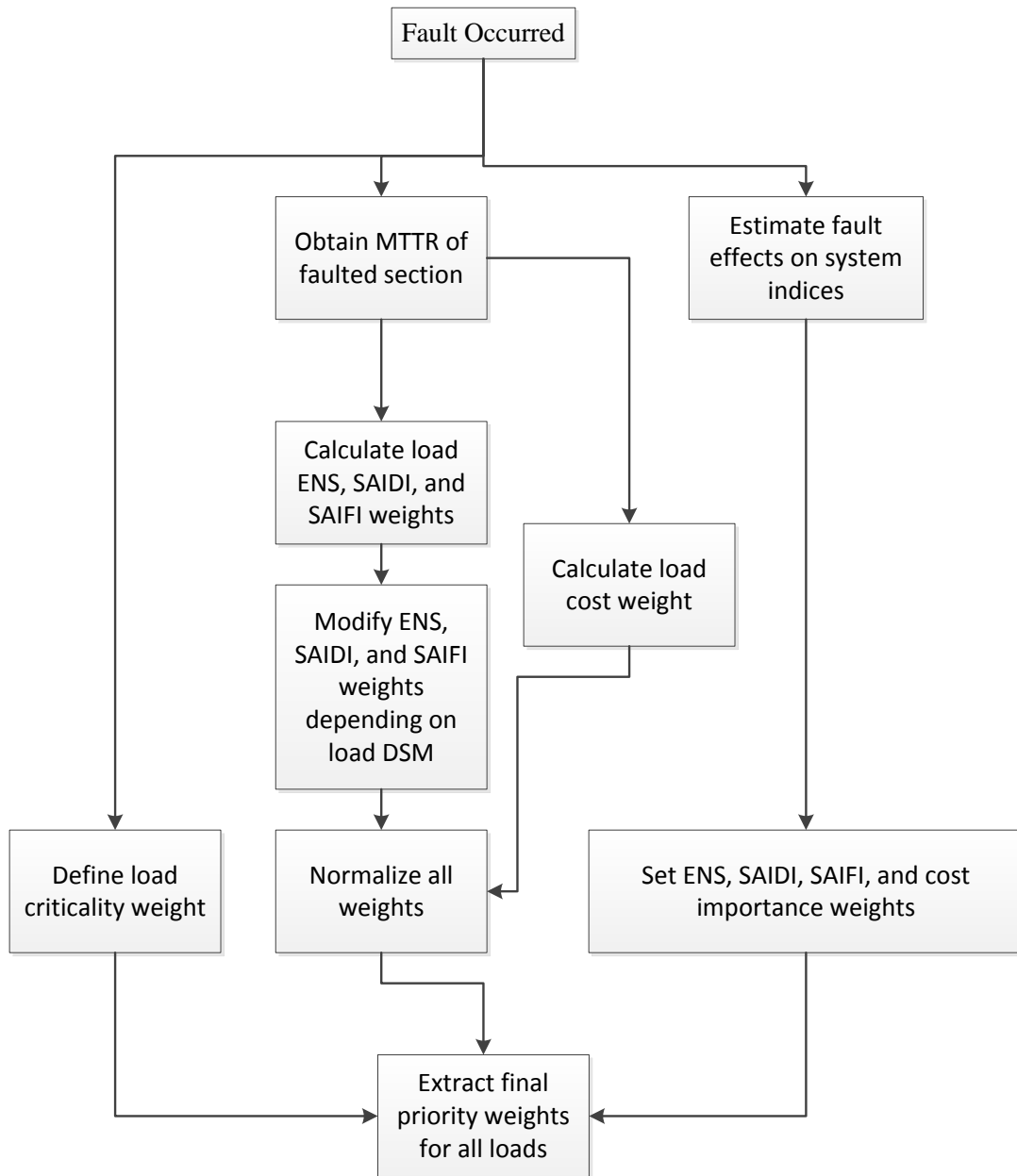


Figure 3.1 Flow chart of the prioritizing method

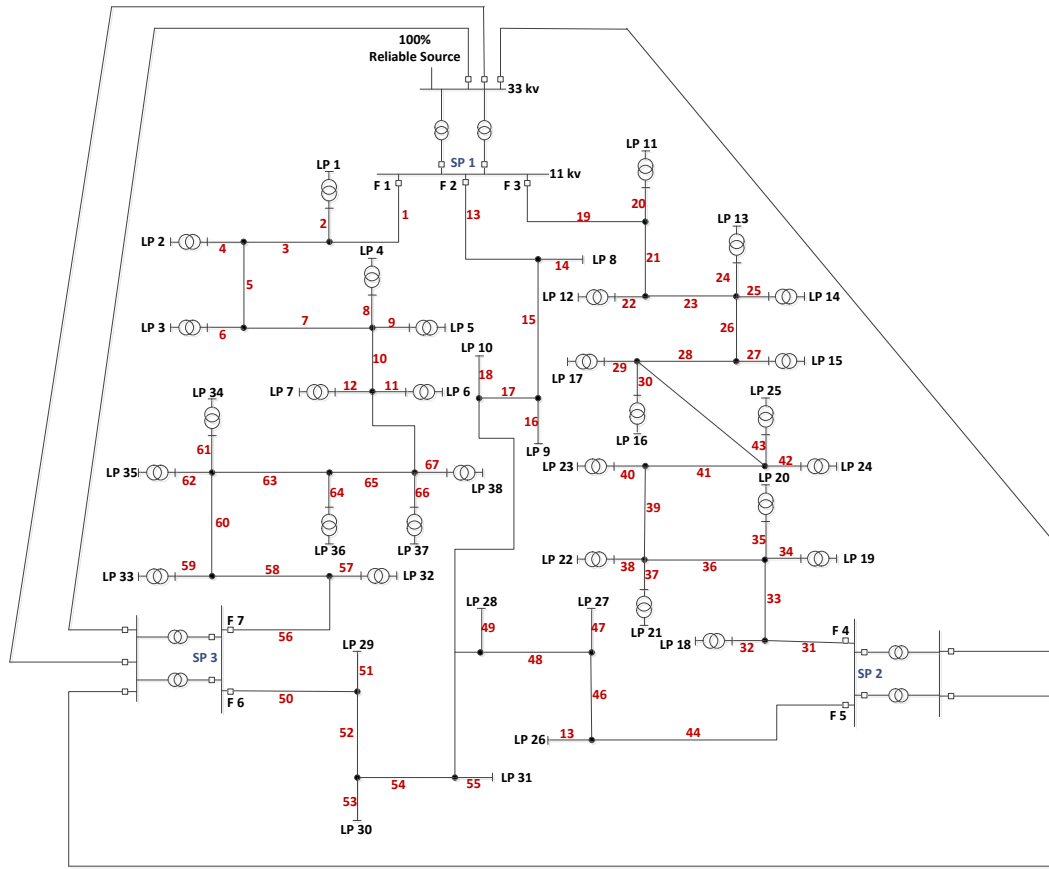


Figure 3.2 Single line diagram of RBTS Bus 4 distribution system [27]

Table 3.3 Number of components and customers for RBTS Bus 4

	11 kV subsystem	33 kV subsystem	Total
Feeders	67	4	71
Transformers	29	6	35
Busbars	3	3	6
Total number of components	99	13	112
Main feeders	7	-	7
Load points	38	-	38
Customers	4779	-	4779

Table 3.4 Number of customers and load type for all LPs in RBTS Bus-4 system

Load Point	Number of Customers/LP	Load Type
1-5, 11-15, 18-23, 32-37	200-210	Residential
6, 7, 16, 17, 24, 25, 38	10	Commercial
8-10, 26-31	1	Industrial

Several case studies are considered to test the proposed prioritization methodology.

In all cases, the values of w_{ENS} , w_{SAIDI} , w_{SAIFI} , and w_{cost} are taken to be 0.25 to generalize the study by assigning equal importance weights for each list of the four metrics: ENS, SAIDI, SAIFI, and cost. As mentioned previously, these factors should be specified depending on assessment of system history and the desired improvements in ENS, SAIDI, SAIFI, and cost of interruptions. The yearly load curves for each LP in the system were generated by a sequential method that is illustrated in section 2.2.1.

3.4.1 Case1: Original RBTS Bus 4 Data

In this case, the exact values of the RBTS-Bus 4 system have been used, including the loading amount, number of customers and MTTR for each load. Load prioritization was calculated at hour $t = 1:00$ a.m. on the first day of the year. The results of load prioritization are summarized in Figures 3.3 and 3.4. Figure 3.3 shows the normalized $L_{ENS}^{i,m}(t)$, $L_{SAIDI}^{i,m}$, $L_{SAIFI}^{i,m}$, and $L_{cost}^i(t)$ priority weights for each load. Figure 3.4 shows the total priority weights $PL^i(t)$ after combining $L_{ENS}^{i,m}(t)$, $L_{SAIDI}^{i,m}$, $L_{SAIFI}^{i,m}$, and $L_{cost}^i(t)$ for all loads and using 0.25 as the value for w_{ENS} , w_{SAIDI} , w_{SAIFI} , and w_{cost} . Note that all loads in this case are assumed to be non-critical with $L_{critic}^i(t) = 0$.

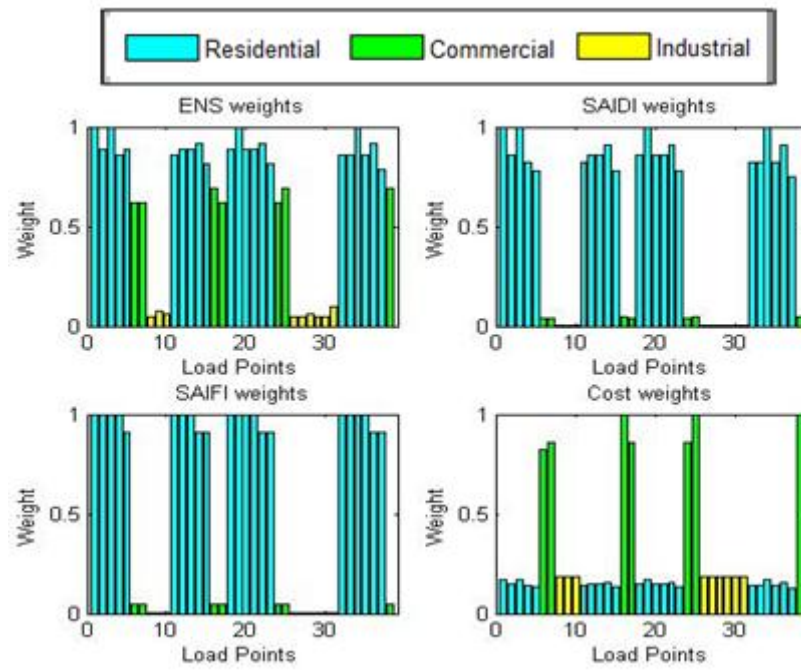


Figure 3.3 Case 1: load points ENS, SAIDI, SAIFI, and cost weights

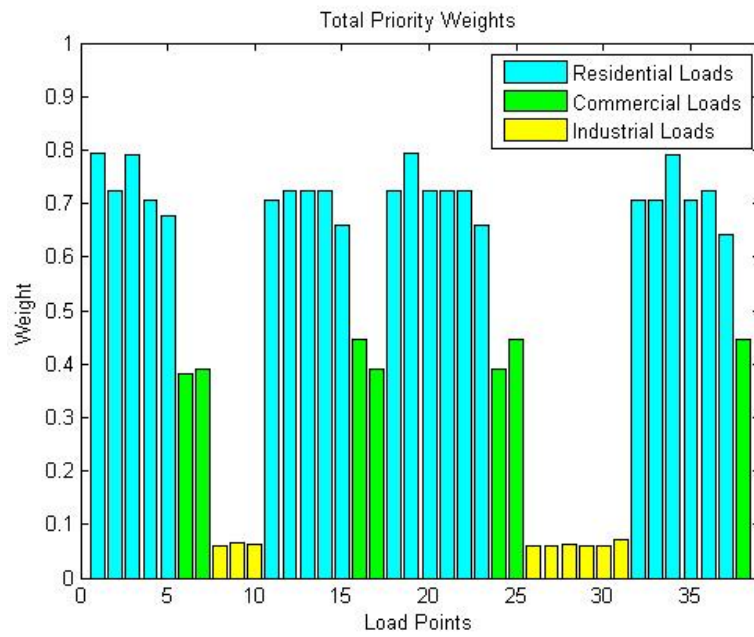


Figure 3.4 Case 1: load points total priority weights

As can be seen in Figure 3.3, the residential loads are dominant in SAIDI and SAIFI weights as a result of their high number of customers (refer to Table 3.4) which affects the SAIDI and SAIFI metrics. Additionally, commercial customers have the highest weights regarding cost of interruption as shown in Figure 3.3. Industrial customers, in contrast, have very low priority factors in all four sub-plots because of their relatively low MTTR (≈ 5 hrs). This is a result of the topology of the RBTS-Bus 4 system; because industrial customers are connected directly to the high voltage side, their transformers are considered customer property and are not included when calculating MTTR. In contrast, residential and commercial customers have a much higher MTTR (≈ 50 hrs).

This large difference between customer MTTR values affects the weighting and prioritization between the loads in the system. Additionally, the high MTTR of residential and commercial customers reduces the time sensitivity of prioritization.

3.4.2 Case 2: Simulating MG Loads

As stated previously, the use of MGs enhances the reliability of distribution systems, thereby reducing LP MTTR. However, it increases complexity by including customers with different levels of reliability requirements and DSM program participation. Therefore, to simulate the MG system and to test all factors in the proposed prioritization method, the following is assumed:

- Residential LPs 1-5 are paying for more reliable service with DSM factor = 2.
- Residential LPs 18-23 are benefiting from a reduced bill with lower reliability (DSM factor=1/2).
- LP 32 contains a school considered to have medium criticality with $L_{critic}^i = 1$.

- LP 38 is a hospital with a high level of criticality ($L_{critic}^i = 2$).
- The MTTR for all LPs is taken to be 3 hours to simulate the increased reliability of MGs.

Two cases are considered here by calculating the prioritization weights at two different hours on the first day of the year as follows:

A. Case 2.A: Prioritizing at 1:00a.m.

After including all assumption, the prioritization was calculated at 1:00a.m. of the first day of the simulated year. The results are shown in Figures 3.5 and 3.6.

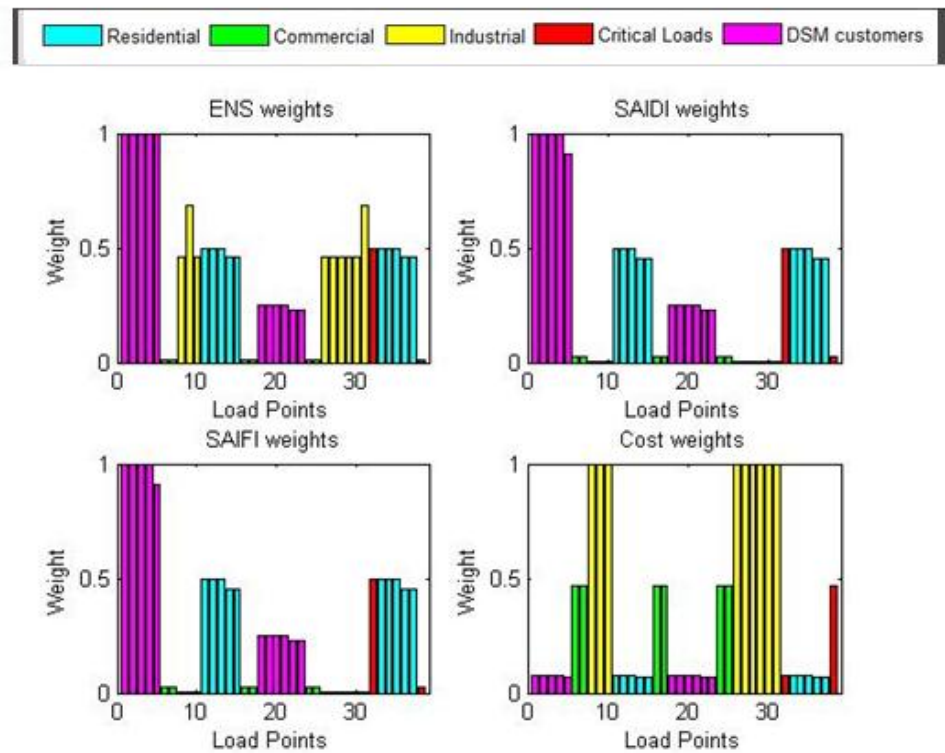


Figure 3.5 Case 2.A: load points ENS, SAIDI, SAIFI, and cost weights

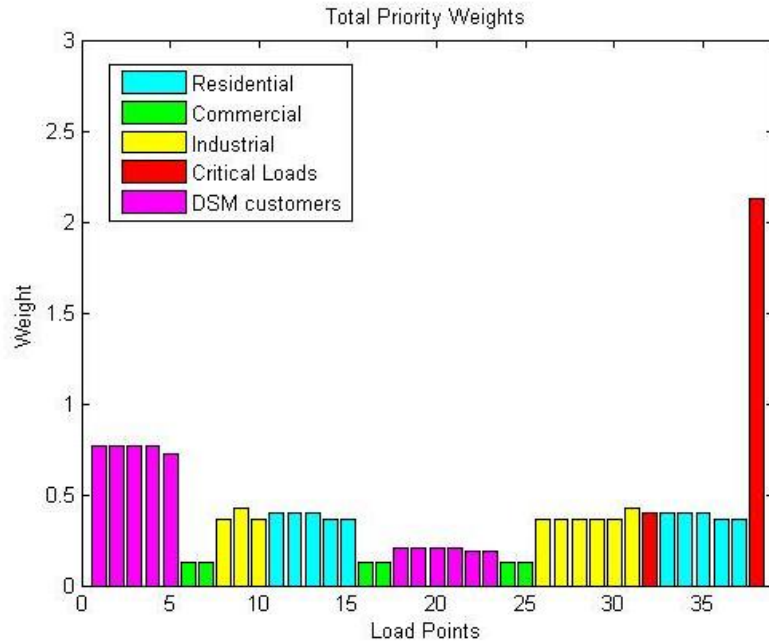


Figure 3.6 Case 2.A: load points total priority weights

B. Case 2.B: Prioritizing at 9:00 a.m.

The prioritization weight at 9:00a.m. of the first day of the simulated year are illustrated in Figures 3.7 and 3.8.

In both cases, residential customers have higher SAIDI and SAIFI weights because of their large number of customers. Additionally, prioritization differences can be observed for residential customers that are participating in different DSM programs: customers paying for higher reliability are now prioritized over both non-participating customers and customers participating with lower-reliability residential loads. Moreover, the hospital at LP 38, which is considered a highly critical load, has the largest total priority weight in both cases. In contrast, LP 32, which is assumed to include a school with medium criticality, has the second highest priority in the morning only (Case 2.B: 9:00 a.m.) because at 1:00 a.m. the school is not occupied and is not considered a critical load.

Furthermore, industrial and commercial customers consume larger amounts of energy at 9:00 a.m. than at 1:00 a.m., which increases their priority weights as seen clearly by comparing the ENS weight sub-plots in Figures 3.5 and 3.7.

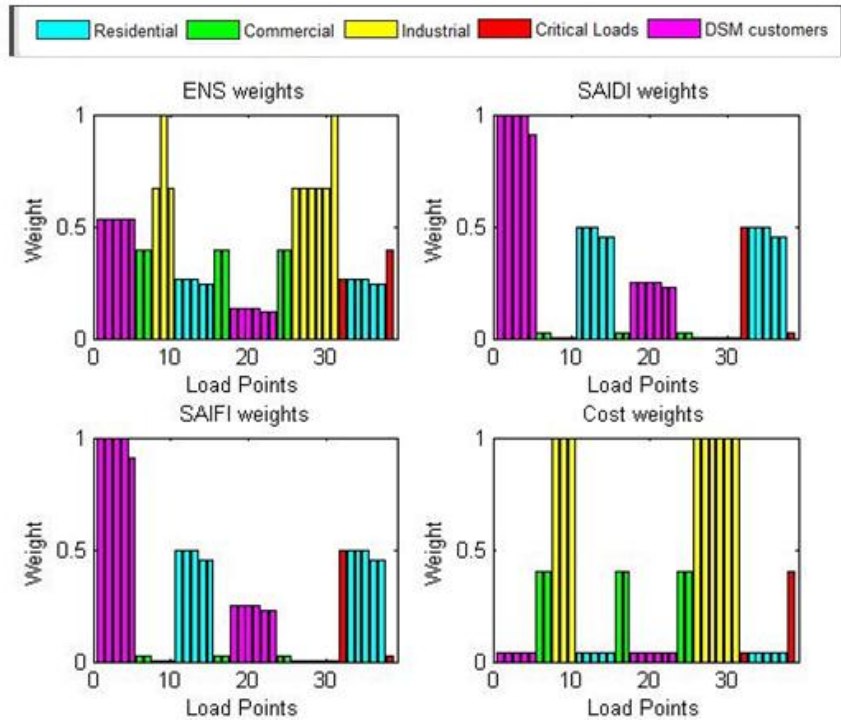


Figure 3.7 Case 2.B: load points ENS, SAIDI, SAIFI, and cost weights

3.5 Conclusions

A load prioritization method for MG systems is proposed in this chapter. The method prioritizes all loads in the system by assigning calculated weights that depend on two levels. The first level classifies critical loads and the second level specifies four prioritization criteria. These criteria consist of the load effect on system ENS, the load effect on the SAIDI metric, the load effect on the SAIFI metric, and the cost of load interruption. The RBTS Bus 4 distribution system was used as an implementation model

and was tested for two cases in which LPs were prioritized under different scenarios. The results demonstrate that the proposed load prioritization method is dynamic in time and takes into consideration the ENS, SAIDI, and SAIFI metrics and different load costs of interruption. Moreover, the methodology is capable of including customers participating in DSM programs as well as representing critical loads such as schools and hospitals.

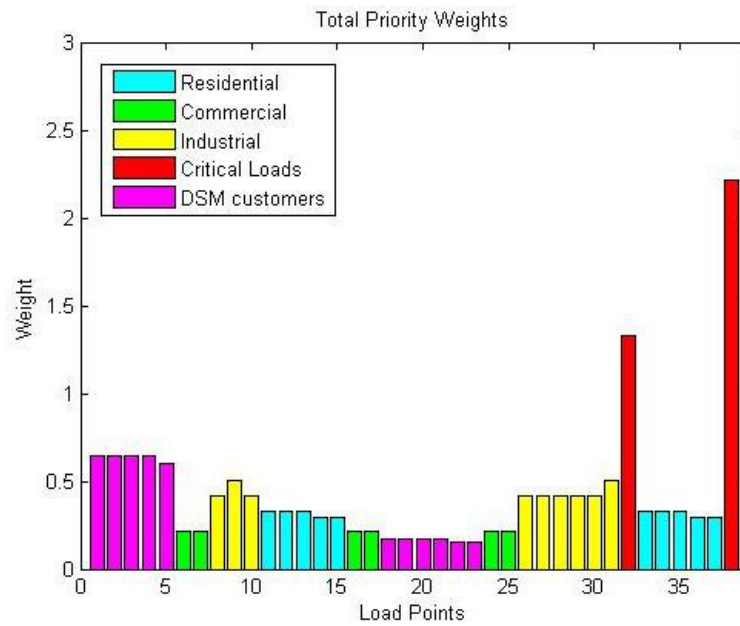


Figure 3.8 Case 2.B: load points total priority weights

CHAPTER 4

THE SMART SELF-HEALING OPTIMIZATION

TECNIQUE FOR MICROGRIDS

This chapter is considered the main contribution of this thesis where the system modeling and the mathematical formulation of the smart self-healing technique for electric microgrids is proposed. Also, the previously proposed priority weight in Chapter 3 is utilized in forming the optimization problem. As mentioned in the introduction of this document, the optimization of the proposed problem will be modeled and solved utilizing MILP reformulation.

In section 4.1, the chapter start with a detailed introduction about restoration optimization techniques proposed in the literature and comparing them to the mathematical approach which is considered in this thesis. The reader may notice that the introduction in this chapter is wide and expanded. This was intended in order to provide a structural background regarding the main contribution of the thesis.

Section 4.2 states the key parameters of the proposed model. It starts by discussing the main control variables that are included in the proposed optimization process. Then, the selected objective functions for the self-healing technique are introduced and explained in detail. Furthermore, other objective functions that are usually considered by researchers in restoration problems, and are not applied in this thesis, are mentioned. The reasons and

justifications for not considering such objectives will also be discussed. In the last part of section 4.2, the operational and managerial constraints of the problem are illustrated.

In section 4.3, the full mathematical formulation of the optimization problem is presented including modeling equations of all necessary components of the smart microgrid.

Finally, section 4.4 discuss the estimation of some technical parameters that are needed in the procedure of solving the MILP optimization problem.

4.1 Introduction

4.1.1 Restoration Optimization Techniques in the Literature

Mainly, the techniques that are used to solve the restoration optimization problem in the literature can be categorized into three types: heuristic or Expert Systems (ES), Soft Computing (SC) and Mathematical Programming (MP). The heuristic approach is considered a search strategy that utilizes the operators' knowledge and practical experience in order to find a final restoration configuration. For that reason, they are also referred to as expert systems. In [41], a heuristic reconfiguration algorithm was presented. It starts with all operable switches open, and at each step, the switch that result in least increase in the objective function is to be closed. The objective function is defined as incremental losses divided by incremental load served. A backtracking scheme is applied to suggest new switch locations that reduce the objective function. This method is efficient in the use of detailed feeder modeling and load flow solution. Also, it requires less computational efforts than sequential switching. The drawbacks, in the other hand, is that it does not consider priority listing, it only takes care of the practical losses. In addition, huge

computational processing is still required since load flow is calculated after each switching step. An early work done in [42] presents a restoration approach based on: (a) the collaboration between operating personals and system analysts, (b) access to available data from on-line computer facilities, and (c) the use of an interactive load flow program. Moreover, in [43], a heuristic search approach is developed for service restoration of a distribution system after locating and isolating faulted area. The developed method contains a set of heuristic rules that were gathered through interviews with experienced operators at Taiwan Power Company. The constructed plan and algorithms only considered faults on feeders. Faults on lateral or branching point was not investigated which is mostly the case in microgrids.

A practically real-time expert restoration guide for a dispatching center was introduced and evaluated in [44]. In order to get on/off –line information from the current state of the tested system, one of the work stations is connected to SCADA computer. The introduced restoration guide has two operation modes. The first one is an on-line guide mode which provides the operator with sufficient restoration plan and procedures based on expertise and heuristics restoration knowledge base. The other one is an off-line mode simulation which is utilized to verify the validity of acquired currently used knowledge. Implementation issues of this system such as system function, knowledge acquisition and representation, interface of SCADA system and man-machine interface are also discussed.

Nowadays, soft computing techniques are reaching out in solving restoration problems. They are considered learning methods that gradually increase their knowledge as more input is received. They can be used in a supervised or unsupervised manner to

learn, where in the supervised category, pairs of input and outputs are provided to these learning methods. The main advantage of learning methods is that they rapidly improve their knowledge and experience over time as more inputs are received [45]. A proposed scheme for solving restoration problems based on artificial neural networks (ANN) was proposed in [46]. The scheme was tested and examined on a 162-bus transmission system. The results indicates that this used approach is practical and feasible and should be implemented on real time applications. Furthermore, an approach based on conventional genetic algorithm to solve power restoration problems is developed in [47]. Priority customers were taken under consideration in the proposed algorithm. The method attempts to solve the restoration problem using remotely controlled switches which, therefore, speeded up the restoration process for interrupted areas. Although, soft computing is considered attractive for many researches, but they suffer from three main disadvantages. Many external parameters must be set for the optimization, they still do not guarantee global optimality, and finally, soft computing may require huge computational time for simple problems.

In the mathematical programming approach, the restoration problem is usually formed as a Mix Integer Programming (MIP) problem which can then be solved using any MIP solving technique. In [48], a two-stage algorithm for solving service restoration problems for distribution systems was introduced. The restoration problem was decomposed into two sub-problems (the maximization of available power to the de-energized area, and the minimization of the amount of unserved energy) which was then solved by a mixed integer programing technique. The minimization of restorative operation cost was considered in order to facilitate the optimization process. However, the reactive

power and system losses were both neglected which raise a huge issue especially at the microgrids scale due to the high R/X ratio. Another power restoration strategy was presented in [49] which incorporates optimization algorithm and interactive graphics. The process of selecting the control variable was formulated to a mathematical problem which was then solved by nonlinear programming. The problem with nonlinear programming is that existing commercial solvers still suffer from the huge nonlinear-computational time and the global optimality may not be reached. Paper [50] presents a combined power restoration method by a joint usage of an expert system (ES) and a Mathematical Programming (MP) approach. The optimal target for the system was formulated as a MIP problem which was decomposed into sub-problems based on ES knowledge. This paper also neglected the reactive power and the line losses.

In the past few decades, mathematical programming was rarely used in modeling and solving restoration problems due to the large computational time that might be required. However, with the improved high speed processors and the availability of efficient solvers, mathematical programming nowadays is gaining attention in modeling different practical optimization problems. Note that these efficient solvers are mainly specialized in linear mathematical programming where non-linear programming is still considered complex and not efficient computational wise.

4.1.2 Pure and Mixed Linear Integer Programming

Linear Programming (LP) is one of the most famous optimization techniques currently used in the literature. In this type of optimization problem, values of the variables are restricted to linear (in)-equalities. If, in some cases, variables are limited to be integers,

the problem is called pure Integer Programming (IP). Otherwise, if the model consist of both real and integer variables, it is called Mixed Integer Programming (MIP) and if the objective and all constraint are linear, it is called Mixed Integer Linear Programming (MILP). Simple MILP problems can usually be solved graphically, but complex ones containing thousands of variables and constrains need more sophisticated solution techniques and algorithms (solvers) to be implemented. Such techniques is the simplex algorithm where the linear problem is converted into the standard form which converts inequality constrains to equation by adding the slack variable. Many powerful software for solving LP models exist (e.g. CPLEX ILOG 2007 and XPRESS-MP Dash Optimization Ltd 2007) [51]. These softwares differ in terms of cost, speed and simplicity in operation.

MILP models have been widely used in many practical optimization problems in the literature such as hydro and wind unit commitment [52, 53], generation and transmission expansion planning [54, 55], AC optimal power flow in distribution systems [56] and in solving power restoration problems mathematically in order to find the optimal reconfiguration for interrupted networks[57-59]. In such restoration problems, the objective function of the MIP is usually to minimize the unserved energy and the cost of switching, and the constrains are typically: power capacity limitation in the substations, balance between supply and demand, branch capacity constraints, and radial configuration. However, [57-59] also did not consider reactive power in their linear model.

In this chapter, a self-healing restoration optimization problem is formulated linearly as a MILP problem. In addition to considering reactive power and line losses in

the formulation, the formulation will also take into account different specification of the future microgrids.

4.2 The Proposed Self-Healing Technique Model

For explanation purposes and before proceeding to the detailed mathematical formulation of the problem, it is important to clearly state in words the model of the self-healing technique including the control variables, objectives, and constraints. Since the focus of this thesis is on the restoration of smart microgrids, different parameters must be considered that do not usually appear in modeling restoration problems of traditional distribution systems.

4.2.1 Control Variables

There are basically three parameters that can be controlled in the services restoration within a microgrid and will be considered as control variables in the proposed technique. They are listed as follows:

- 1) Branch Switch Status y_{km}

By controlling the switches status in the microgrid, the topology of the network can be altered and by that, achieving different routes for the power to flow and to feed disconnected loads. This control variable is considered the most basic one among all other control variables that will be considered in this thesis. Although it is usually assumed that all switches in a microgrid are remotely controllable, however, the problem formulation in this thesis will account for switches that cannot be immediately controlled by removing them from the control variables.

2) DGs Real DG_k^P and Reactive DG_k^Q Power Output

A microgrid may include several DGs units that can be controlled in terms of both, their active and reactive power output. DGs can contribute significantly in the restoration process from different aspects. One, is by serving the substation in supplying loads during an interruption or even through operating in islanded mode. Second, is by improving the voltage profile of the system by injecting reactive power. It is worth mentioning that the formulation of the problem in this thesis will account for DGs that are not controllable such as renewable energy based DGs.

3) Amount of Load Curtailment LC_k and Shedding Loads μ_k

It must be noted that there is a difference between the two practices, load curtailment and load shedding. In the former, those customers that are participating in DSM programs are assumed to have controllable loads where the utility can partially reduce their loads up to a certain limit. In the latter, customers that are not participating in any kind of DSM, the utility has the choice to either serve their loads completely, or to totally shed their power. However, both procedures are considered in the problem formulation in this thesis.

4.2.2 Objective Functions

The services restoration problem is known to be a multi-objective optimization problem especially when including different control variables such as the ones mentioned previously. The different objective functions that will be considered in this thesis will be linearly weighted and combined to form one general objective function. Three objective

functions are modeled in the restoration formulation and are divided in two parts as follows:

1) To Maximize the Supplied Customers based on their Priorities

At the instant of a fault or prior to it, each customer in the system will be assigned a priority weight based on the prioritization method proposed in chapter 3. The first objective of restoration will be to restore customers as much as possible based on their priority weights. This specific objective can be seen as a multi-objective problem by its own where four different factors were included in the prioritizing model and the calculation of priority weights. In this thesis, these factors are assumed to be set by the utility depending on their historical reliability indices and the recorded loss of economic activities due to past interruptions. The investigation of optimizing these factors is listed among future work topics.

2) To Minimize the Cost Associated with the Restoration Process

It becomes necessary for a robust efficient restoration technique to minimize the associated operational cost. Two source of operational cost are considered in this thesis and are listed as follows:

a. DGs Operational Cost

All DGs in the system will be assumed to have an estimated operational cost that is linearly related to their supplied real power. The objective function, is of course, to minimize the DGs total operational cost.

b. Cost of Load Curtailment

Based on the agreement between the utility and customers that are participating in special kind of DSM programs, the utility may provide financial compensations to curtailed customers. The compensation cost will be assumed in this thesis to have a linear relation with the amount of curtailed load. Although researchers in the literature have been conservative in such objective function, but with the increased competition between number of electric power suppliers and the AMI provided in a future microgrid, this practice between the utility and the customer is highly expected which may serve as an insurance procedures.

Other objective functions where considered in the literature such as minimizing the power loss in the new system configuration and to minimize the number of switching [60, 61]. These two objectives can be neglected for two reasons:

- 1) The restoration process is considered an emergency case where the power loss is not as much important as retrieving lost loads. Some may argue that system losses could affect the operational cost, but this was already included in the previously mentioned objective function where by setting minimizing cost of DGs output as one of the objectives, the optimization method will be indirectly forced to find the route with minimal losses. Moreover, system configuration can be changed to minimize the losses after the restoration procedure is completed.
- 2) It is usually considered that all switches in a microgrid are remotely controlled and their cost of operation is negligible where no manpower is

needed. However, those switches that are not remotely controlled will not be considered as control variables as mentioned previously. This can be justified in the sense that the restoration optimization is supposed to give results and operate within seconds to minutes which is far less than the time required to operate a manually controlled switch. Furthermore, switches in a microgrid are expected to operate with zero switching time. Thereby, and because of the preceding reasons, setting minimization of switching as an objective function can be ignored.

4.2.3 Problem Constraint

The constraint to be considered in the proposed restoration optimization problem can be categorized into two main categories as follows:

1) Technical Constraints

In any type of restoration, certain technical constraints must be taken into account which guarantee maintaining system performance within acceptable limits. The technical constraint that are modeled in this thesis are as follows:

- a. Bus voltages must lie within specified acceptable limits.
- b. Branch current flow must not exceed the rating of the line.
- c. DGs must be operating under their rating apparent power.
- d. Radially Constraint.

Although smart microgrids are expected to be designed and operated as meshed or weakly meshed aspect, however, for the purpose of generality, the radially constraint will be modeled and considered in special case studies.

2) Management Constraint

The other type of constraint is basically related to the load curtailment practice and the agreement built between the utility and customers participating in load curtailment DSM programs.

a. Load curtailment should not exceed the allowable limit

It must be noted that there are other types of constraints in the optimization problem that are related to MILP formulation and approximation of non-linear equation in the power flow. These constraint will be specified together with all problem constraint in the MILP model in the following section.

4.3 The MILP Mathematical formulation of the Optimization Problem

The MILP model that is used in this thesis in formulating the service restoration problem is adapted from the flexible MILP approach to the AC optimal power flow presented by Refael S. Ferreira [62]. Several modifications were added to the original formulation in order for the model to be utilized in optimizing service restoration problems including load prioritizing and also, to capture the features of smart microgrids such as DSM customers and DG units. Moreover, different approaches were used in the approximation process that will yield to significant improvement in term of the

computational time. This is necessary since the restoration optimization is considered an emergency case and convenient results must be obtained as fast as possible.

Since the proposed self-healing technique model is based on MILP, different linearization and reformulation methods must be utilized. Appendix A.2 provides an overview of the reformulation methods that are used in this section in order to model the restoration optimization problem. Four methods are discussed and will be referred to as reformulation methods 1 to 4.

One of the key characteristics of Ferreira's formulation is that it express complex variables in rectangular coordinates instead of polar coordinates. Also, Kirchhoff's laws are modeled based on voltages and currents instead of voltages and power quantities as will be seen in the following formulation details. This formulation of Kirchhoff's law gives a great advantages in the sense that the relations are linear by nature which can be directly modeled in the MILP.

For organization and illustration purposes, problem constraint will be modeled first in this section followed by the objective functions.

4.3.1 Formulating Problem Constraint

4.3.1.1 Kirchhoff's Laws Formulation

1) Node Injection

$$I_{d,k}^{re} + \sum_{m \in \Gamma_k} I_{km}^{re} = I_{g,k}^{re} + \sum_{m \in \Gamma_k} I_{mk}^{re} \quad \forall k \in \Gamma_N \quad (4.1)$$

$$I_{d,k}^{im} + \sum_{m \in \Gamma_k} I_{km}^{im} = I_{g,k}^{im} + \sum_{m \in \Gamma_k} I_{mk}^{im} \quad \forall k \in \Gamma_N \quad (4.2)$$

2) Branch Flow

$$V_k^{re} - V_m^{re} = I_{km}^{re} \cdot R_{km} - I_{km}^{im} \cdot X_{km} \quad \forall km \in \{\Gamma_B \setminus \Gamma_{sw}\} \quad (4.3)$$

$$V_k^{im} - V_m^{im} = I_{km}^{re} \cdot X_{km} + I_{km}^{im} \cdot R_{km} \quad \forall km \in \{\Gamma_B \setminus \Gamma_{sw}\} \quad (4.4)$$

Note that equations (4.3) and (4.4) are only used for the set of un-switchable branches. If a branch is assumed to be switchable, these constraints must be changed in order to include the case if the branch was switched off where these two equations do not hold any more. This can be modeled using reformulation method 1 (Disjunctive Constraints) illustrated in appendix A.2 as follows:

$$-M_{km}^{V,re} \cdot (1 - y_{km}) \leq V_k^{re} - V_m^{re} - I_{km}^{re} \cdot R_{km} + I_{km}^{im} \cdot X_{km} \leq M_{km}^{V,re} \cdot (1 - y_{km}) \quad \forall km \in \Gamma_{sw} \quad (4.5)$$

$$-M_{km}^{V,im} \cdot (1 - y_{km}) \leq V_k^{im} - V_m^{im} - I_{km}^{re} \cdot X_{km} - I_{km}^{im} \cdot R_{km} \leq M_{km}^{V,im} \cdot (1 - y_{km}) \quad \forall km \in \Gamma_{sw} \quad (4.6)$$

where

$M_{km}^{V,re}$ is a disjunctive constant that is assured to be always greater than

$$|V_k^{re} - V_m^{re} - I_{km}^{re} \cdot R_{km} + I_{km}^{im} \cdot X_{km}|$$

$M_{km}^{V,im}$ is a disjunctive constant that is assured to be always greater than

$$|V_k^{im} - V_m^{im} - I_{km}^{re} \cdot X_{km} - I_{km}^{im} \cdot R_{km}|$$

The reader will notice from equations (4.5) and (4.6) that these constraints are only considered when the switch $y_{km} = 1$. Another important constraint to be added is that I_{km}^{re} and I_{km}^{im} must be set equal to zero if $y_{km} = 0$. This can be achieved similarly by introducing a disjunctive constant as follows:

$$-M_{km}^{I,re} \cdot y_{km} \leq I_{km}^{re} \leq M_{km}^{I,re} \cdot y_{km} \quad \forall km \in \Gamma_{sw} \quad (4.7)$$

$$-M_{km}^{I,im} \cdot y_{km} \leq I_{km}^{im} \leq M_{km}^{I,im} \cdot y_{km} \quad \forall km \in \Gamma_{sw} \quad (4.8)$$

where

$M_{km}^{I,re}$ is a disjunctive constant that is assured to be always greater than $|I_{km}^{re}|$

$M_{km}^{I,im}$ is a disjunctive constant that is assured to be always greater than $|I_{km}^{im}|$

4.3.1.2 DGs Power Output

Since the formulation in this thesis is based on currents and voltages in rectangular form, the integration of the substations and DGs power output to the MILP model can be obtained as follows:

$$I_{DG,k}^{re} = \frac{V_k^{re}}{(V_k^{re2} + V_k^{im2})} \cdot DG_k^P + \frac{V_k^{im}}{(V_k^{re2} + V_k^{im2})} \cdot DG_k^Q \quad \forall k \in \Gamma_{DG} \quad (4.9)$$

$$I_{DG,k}^{im} = \frac{V_k^{im}}{(V_k^{re2} + V_k^{im2})} \cdot DG_k^P - \frac{V_k^{re}}{(V_k^{re2} + V_k^{im2})} \cdot DG_k^Q \quad \forall k \in \Gamma_{DG} \quad (4.10)$$

It is obvious that these equations are non-linear and need to be reformulated. In [62], this problem was tackled by using reformulation method 4 (piecewise approximation

with SOS2 sets) for the non-linear terms $\frac{V_k^{re}}{(V_k^{re2}+V_k^{im2})}$ and $\frac{V_k^{im}}{(V_k^{re2}+V_k^{im2})}$. Then, by using reformulation method 2 (MacCromick's Envelopes) for the bilinear product between the DG power output and the piecewise voltages terms, the equations are finally linearized.

Using piecewise approximation approach in MILP modeling was found to require superior computational time, as will be shown in the case studies, due to the increased integer constraint that are needed to form an SOS2 set (refer to equations (A.27-A.32) in the appendices) which will amplify the branch and bound process in the solution. Since the purpose of this thesis is to propose an efficient robust restoration technique which must require minimal computational time as possible, a different approach was considered which heavily rely on McCromick's envelopes. In the following steps, the linearization and reformulation of equations (4.9) and (4.10) is achieved.

Step 1: Rearrange equations (4.9) and (4.10) to be in the form:

$$I_{DG,k}^{re} \cdot V_k^{re} \cdot V_k^{re} + I_{DG,k}^{re} \cdot V_k^{im} \cdot V_k^{im} = V_k^{re} \cdot DG_k^P + V_k^{im} \cdot DG_k^Q \quad \forall k \in \Gamma_{DG} \quad (4.11)$$

$$I_{DG,k}^{im} \cdot V_k^{re} \cdot V_k^{re} + I_{DG,k}^{im} \cdot V_k^{im} \cdot V_k^{im} = V_k^{im} \cdot DG_k^P - V_k^{re} \cdot DG_k^Q \quad \forall k \in \Gamma_{DG} \quad (4.12)$$

Step 2: Approximate the bilinear products $(V_k^{re} \cdot V_k^{re})$ and $(V_k^{im} \cdot V_k^{im})$ to ζ_k and η_k , respectively, by McCromick's envelopes using the following sets of constraints:

$$2 \cdot V_k^{re,min} \cdot V_k^{re} - V_k^{re,min}^2 \leq \zeta_k \quad \forall k \in \Gamma_N \quad (4.13)$$

$$2 \cdot V_k^{re,max} \cdot V_k^{re} - V_k^{re,max}^2 \leq \zeta_k \quad \forall k \in \Gamma_N \quad (4.14)$$

$$(V_k^{re,min} + V_k^{re,max}) \cdot V_k^{re} - V_k^{re,min} \cdot V_k^{re,max} \geq \zeta_k \quad \forall k \in \Gamma_N \quad (4.15)$$

$$2. V_k^{im,min} \cdot V_k^{im} - V_k^{im,min^2} \leq \eta_k \quad \forall k \in \Gamma_N \quad (4.16)$$

$$2. V_k^{im,max} \cdot V_k^{im} - V_k^{im,max^2} \leq \eta_k \quad \forall k \in \Gamma_N \quad (4.17)$$

$$(V_k^{im,min} + V_k^{im,max}) \cdot V_k^{im} - V_k^{im,min} \cdot V_k^{im,max} \geq \eta_k \quad \forall k \in \Gamma_N \quad (4.18)$$

Note that only three constraints instead of four were needed for each approximation due to the similarity of the two components in the bilinear product. Also, observe these constraints are applied for the set of all nodes in the system as the values of ζ_k and η_k will be used later in other constraints.

These equations are linear and can be integrated to the MILP formulation directly as the case for all McCormick's envelopes that will be used later. Equations (4.9) and (4.10) can now be replaced with:

$$I_{DG,k}^{re} \cdot \zeta_k + I_{DG,k}^{re} \cdot \eta_k = V_k^{re} \cdot DG_k^P + V_k^{im} \cdot DG_k^Q \quad \forall k \in \Gamma_{DG} \quad (4.19)$$

$$I_{DG,k}^{im} \cdot \zeta_k + I_{DG,k}^{im} \cdot \eta_k = V_k^{im} \cdot DG_k^P - V_k^{re} \cdot DG_k^Q \quad \forall k \in \Gamma_{DG} \quad (4.20)$$

Step 3: Apply McCormick's envelopes to all bilinear products in equations (4.19) and (4.20):

$$1) I_{DG,k}^{re} \cdot \zeta_k \approx g_k^{P,Vre}$$

$$I_{DG,k}^{re,min} \cdot \zeta_k + \zeta_k^{min} \cdot I_{DG,k}^{re} - I_{DG,k}^{re,min} \cdot \zeta_k^{min} \leq g_k^{P,Vre} \quad \forall k \in \Gamma_{DG} \quad (4.21)$$

$$I_{DG,k}^{re,max} \cdot \zeta_k + \zeta_k^{max} \cdot I_{DG,k}^{re} - I_{DG,k}^{re,max} \cdot \zeta_k^{max} \leq g_k^{P,Vre} \quad \forall k \in \Gamma_{DG} \quad (4.22)$$

$$I_{DG,k}^{re,min} \cdot \zeta_k + \zeta_k^{max} \cdot I_{DG,k}^{re} - I_{DG,k}^{re,min} \cdot \zeta_k^{max} \geq g_k^{P,Vre} \quad \forall k \in \Gamma_{DG} \quad (4.23)$$

$$I_{DG,k}^{re,max} \cdot \zeta_k + \zeta_k^{min} \cdot I_{DG,k}^{re} - I_{DG,k}^{re,max} \cdot \zeta_k^{min} \geq g_k^{P,Vre} \quad \forall k \in \Gamma_{DG} \quad (4.24)$$

$$2) I_{DG,k}^{re} \cdot \eta_k \approx g_k^{P,Vim}$$

$$I_{DG,k}^{re,min} \cdot \eta_k + \eta_k^{min} \cdot I_{DG,k}^{re} - I_{DG,k}^{re,min} \cdot \eta_k^{min} \leq g_k^{P,Vim} \quad \forall k \in \Gamma_{DG} \quad (4.25)$$

$$I_{DG,k}^{re,max} \cdot \eta_k + \eta_k^{max} \cdot I_{DG,k}^{re} - I_{DG,k}^{re,max} \cdot \eta_k^{max} \leq g_k^{P,Vim} \quad \forall k \in \Gamma_{DG} \quad (4.26)$$

$$I_{DG,k}^{re,min} \cdot \eta_k + \eta_k^{max} \cdot I_{DG,k}^{re} - I_{DG,k}^{re,min} \cdot \eta_k^{max} \geq g_k^{P,Vim} \quad \forall k \in \Gamma_{DG} \quad (4.27)$$

$$I_{DG,k}^{re,max} \cdot \eta_k + \eta_k^{min} \cdot I_{DG,k}^{re} - I_{DG,k}^{re,max} \cdot \eta_k^{min} \geq g_k^{P,Vim} \quad \forall k \in \Gamma_{DG} \quad (4.28)$$

$$3) I_{DG,k}^{im} \cdot \zeta_k \approx g_k^{Q,Vre}$$

$$I_{DG,k}^{im,min} \cdot \zeta_k + \zeta_k^{min} \cdot I_{DG,k}^{im} - I_{DG,k}^{im,min} \cdot \zeta_k^{min} \leq g_k^{Q,Vre} \quad \forall k \in \Gamma_{DG} \quad (4.29)$$

$$I_{DG,k}^{im,max} \cdot \zeta_k + \zeta_k^{max} \cdot I_{DG,k}^{im} - I_{DG,k}^{im,max} \cdot \zeta_k^{max} \leq g_k^{Q,Vre} \quad \forall k \in \Gamma_{DG} \quad (4.30)$$

$$I_{DG,k}^{im,min} \cdot \zeta_k + \zeta_k^{max} \cdot I_{DG,k}^{im} - I_{DG,k}^{im,min} \cdot \zeta_k^{max} \geq g_k^{Q,Vre} \quad \forall k \in \Gamma_{DG} \quad (4.31)$$

$$I_{DG,k}^{im,max} \cdot \zeta_k + \zeta_k^{min} \cdot I_{DG,k}^{im} - I_{DG,k}^{im,max} \cdot \zeta_k^{min} \geq g_k^{Q,Vre} \quad \forall k \in \Gamma_{DG} \quad (4.32)$$

$$4) I_{DG,k}^{im} \cdot \eta_k \approx g_k^{Q,Vim}$$

$$I_{DG,k}^{im,min} \cdot \eta_k + \eta_k^{min} \cdot I_{DG,k}^{im} - I_{DG,k}^{im,min} \cdot \eta_k^{min} \leq g_k^{Q,Vim} \quad \forall k \in \Gamma_{DG} \quad (4.33)$$

$$I_{DG,k}^{im,max} \cdot \eta_k + \eta_k^{max} \cdot I_{DG,k}^{im} - I_{DG,k}^{im,max} \cdot \eta_k^{max} \leq g_k^{Q,Vim} \quad \forall k \in \Gamma_{DG} \quad (4.34)$$

$$I_{DG,k}^{im,min} \cdot \eta_k + \eta_k^{max} \cdot I_{DG,k}^{im} - I_{DG,k}^{im,min} \cdot \eta_k^{max} \geq g_k^{Q,Vim} \quad \forall k \in \Gamma_{DG} \quad (4.35)$$

$$I_{DG,k}^{im,max} \cdot \eta_k + \eta_k^{min} \cdot I_{DG,k}^{im} - I_{DG,k}^{im,max} \cdot \eta_k^{min} \geq g_k^{Q,Vim} \quad \forall k \in \Gamma_{DG} \quad (4.36)$$

$$5) V_k^{re} \cdot DG_k^P \approx h_k^{P,Vre}$$

$$V_k^{re,min} \cdot DG_k^P + DG_k^{P,min} \cdot V_k^{re} - V_k^{re,min} \cdot DG_k^{P,min} \leq h_k^{P,Vre} \quad \forall k \in \Gamma_{CDG} \quad (4.37)$$

$$V_k^{re,max} \cdot DG_k^P + DG_k^{P,max} \cdot V_k^{re} - V_k^{re,max} \cdot DG_k^{P,max} \leq h_k^{P,Vre} \quad \forall k \in \Gamma_{CDG} \quad (4.38)$$

$$V_k^{re,min} \cdot DG_k^P + DG_k^{P,max} \cdot V_k^{re} - V_k^{re,min} \cdot DG_k^{P,max} \geq h_k^{P,Vre} \quad \forall k \in \Gamma_{CDG} \quad (4.39)$$

$$V_k^{re,max} \cdot DG_k^P + DG_k^{P,min} \cdot V_k^{re} - V_k^{re,max} \cdot DG_k^{P,min} \geq h_k^{P,Vre} \quad \forall k \in \Gamma_{CDG} \quad (4.40)$$

Note that equations (4.37-4.40) are only applied for the set of controllable DGs where in non-controllable DGs, the value DG_k^P is considered as a known parameter and no approximation is needed for the product $V_k^{re} \cdot DG_k^P$ since it is already linear. The same applies in the following parts 6, 7, and 8.

$$6) V_k^{im} \cdot DG_k^Q \approx h_k^{Q,Vim}$$

$$V_k^{im,min} \cdot DG_k^Q + DG_k^{Q,min} \cdot V_k^{re} - V_k^{im,min} \cdot DG_k^{Q,min} \leq h_k^{Q,Vim} \quad \forall k \in \Gamma_{CDG} \quad (4.41)$$

$$V_k^{im,max} \cdot DG_k^Q + DG_k^{Q,max} \cdot V_k^{re} - V_k^{im,max} \cdot DG_k^{Q,max} \leq h_k^{Q,Vim} \quad \forall k \in \Gamma_{CDG} \quad (4.42)$$

$$V_k^{im,min} \cdot DG_k^Q + DG_k^{Q,max} \cdot V_k^{re} - V_k^{im,min} \cdot DG_k^{Q,max} \geq h_k^{Q,Vim} \quad \forall k \in \Gamma_{CDG} \quad (4.43)$$

$$V_k^{im,max} \cdot DG_k^Q + DG_k^{Q,min} \cdot V_k^{re} - V_k^{im,max} \cdot DG_k^{Q,min} \geq h_k^{Q,Vim} \quad \forall k \in \Gamma_{CDG} \quad (4.44)$$

$$7) V_k^{im} \cdot DG_k^P \approx h_k^{P,Vim}$$

$$V_k^{im,min} \cdot DG_k^P + DG_k^{P,min} \cdot V_k^{re} - V_k^{im,min} \cdot DG_k^{P,min} \leq h_k^{P,Vim} \quad \forall k \in \Gamma_{CDG} \quad (4.45)$$

$$V_k^{im,max} \cdot DG_k^P + DG_k^{P,max} \cdot V_k^{re} - V_k^{im,max} \cdot DG_k^{P,max} \leq h_k^{P,Vim} \quad \forall k \in \Gamma_{CDG} \quad (4.46)$$

$$V_k^{im,min} \cdot DG_k^P + DG_k^{P,max} \cdot V_k^{re} - V_k^{im,min} \cdot DG_k^{P,max} \geq h_k^{P,Vim} \quad \forall k \in \Gamma_{CDG} \quad (4.47)$$

$$V_k^{im,max} \cdot DG_k^P + DG_k^{P,min} \cdot V_k^{re} - V_k^{im,max} \cdot DG_k^{P,min} \geq h_k^{P,Vim} \quad \forall k \in \Gamma_{CDG} \quad (4.48)$$

$$8) V_k^{re} \cdot DG_k^Q \approx h_k^{Q,Vre}$$

$$V_k^{re,min} \cdot DG_k^Q + DG_k^{Q,min} \cdot V_k^{re} - V_k^{re,min} \cdot DG_k^{Q,min} \leq h_k^{Q,Vre} \quad \forall k \in \Gamma_{CDG} \quad (4.49)$$

$$V_k^{re,max} \cdot DG_k^Q + DG_k^{Q,max} \cdot V_k^{re} - V_k^{re,max} \cdot DG_k^{Q,max} \leq h_k^{Q,Vre} \quad \forall k \in \Gamma_{CDG} \quad (4.50)$$

$$V_k^{re,min} \cdot DG_k^Q + DG_k^{Q,max} \cdot V_k^{re} - V_k^{re,min} \cdot DG_k^{Q,max} \geq h_k^{Q,Vre} \quad \forall k \in \Gamma_{CDG} \quad (4.51)$$

$$V_k^{re,max} \cdot DG_k^Q + DG_k^{Q,min} \cdot V_k^{re} - V_k^{re,max} \cdot DG_k^{Q,min} \geq h_k^{Q,Vre} \quad \forall k \in \Gamma_{CDG} \quad (4.52)$$

Step 4: Finally, equations (4.19) and (4.20) can be re-written linearly as:

For non-controllable DGs:

$$g_k^{P,Vre} + g_k^{P,Vim} = V_k^{re} \cdot DG_k^P + V_k^{im} \cdot DG_k^Q \quad \forall k \in \{\Gamma_{DG} \setminus \Gamma_{CDG}\} \quad (4.53)$$

$$g_k^{Q,Vre} + g_k^{Q,Vim} = V_k^{im} \cdot DG_k^P - V_k^{re} \cdot DG_k^Q \quad \forall k \in \{\Gamma_{DG} \setminus \Gamma_{CDG}\} \quad (4.54)$$

For controllable DGs:

$$g_k^{P,Vre} + g_k^{P,Vim} = h_k^{P,Vre} + h_k^{Q,Vim} \quad \forall k \in \Gamma_{CDG} \quad (4.55)$$

$$g_k^{Q,Vre} + g_k^{Q,Vim} = h_k^{P,Vim} - h_k^{Q,Vre} \quad \forall k \in \Gamma_{CDG} \quad (4.56)$$

The specific maximum and minimal bounds used in the previously listed McCromick's Envelopes will be discussed and examined in detail in section 4.4. It is worth mentioning at this stage that the generated output power from a substation is modeled exactly as the generated output of a controllable DG. The only difference will appear when

considering the cost of generated output in the objective function, where the substation power is usually seen as free of charge and its associated cost is set to zero.

4.3.1.3 Formulating Loads

The mathematical formulation of loads are very similar to that of DGs where loads participating in load curtailment programs can be seen as controllable DGs and those customers not participating can be seen as non-controllable DGs. The main difference in load modeling is the introduction of the decision binary variable μ_k . If $\mu_k = 1$, the load k is supplied, and if $\mu_k = 0$, the load k is totally out of service.

Starting from the fact that:

$$I_{L,k}^{re} = \frac{V_k^{re}}{(V_k^{re2} + V_k^{im2})} \cdot L_k^P + \frac{V_k^{im}}{(V_k^{re2} + V_k^{im2})} \cdot L_k^Q \quad \forall k \in \Gamma_L \quad (4.57)$$

$$I_{L,k}^{im} = \frac{V_k^{im}}{(V_k^{re2} + V_k^{im2})} \cdot L_k^P - \frac{V_k^{re}}{(V_k^{re2} + V_k^{im2})} \cdot L_k^Q \quad \forall k \in \Gamma_L \quad (4.58)$$

The formulation steps can be shown as follows:

Step 1: Rearrange equations (4.57) and (4.58) and substitute the values of ζ_k and η_k

yields the following:

$$I_{L,k}^{re} \cdot \zeta_k + I_{L,k}^{re} \cdot \eta_k = V_k^{re} \cdot L_k^P + V_k^{im} \cdot L_k^Q \quad \forall k \in \Gamma_L \quad (4.59)$$

$$I_{L,k}^{im} \cdot \zeta_k + I_{L,k}^{im} \cdot \eta_k = V_k^{im} \cdot L_k^P - V_k^{re} \cdot L_k^Q \quad \forall k \in \Gamma_L \quad (4.60)$$

Step 2: Apply McCormick's envelopes to all bilinear products in equations (4.59)

and (4.60):

$$1) I_{L,k}^{re} \cdot \zeta_k \approx l_k^{P,Vre}$$

$$I_{L,k}^{re,min} \cdot \zeta_k + \zeta_k^{min} \cdot I_{L,k}^{re} - I_{L,k}^{re,min} \cdot \zeta_k^{min} \leq l_k^{P,Vre} \quad \forall k \in \Gamma_L \quad (4.61)$$

$$I_{L,k}^{re,max} \cdot \zeta_k + \zeta_k^{max} \cdot I_{L,k}^{re} - I_{L,k}^{re,max} \cdot \zeta_k^{max} \leq l_k^{P,Vre} \quad \forall k \in \Gamma_L \quad (4.62)$$

$$I_{L,k}^{re,min} \cdot \zeta_k + \zeta_k^{max} \cdot I_{L,k}^{re} - I_{L,k}^{re,min} \cdot \zeta_k^{max} \geq l_k^{P,Vre} \quad \forall k \in \Gamma_L \quad (4.63)$$

$$I_{L,k}^{re,max} \cdot \zeta_k + \zeta_k^{min} \cdot I_{L,k}^{re} - I_{L,k}^{re,max} \cdot \zeta_k^{min} \geq l_k^{P,Vre} \quad \forall k \in \Gamma_L \quad (4.64)$$

$$2) I_{L,k}^{re} \cdot \eta_k \approx l_k^{P,Vim}$$

$$I_{L,k}^{re,min} \cdot \eta_k + \eta_k^{min} \cdot I_{L,k}^{re} - I_{L,k}^{re,min} \cdot \eta_k^{min} \leq l_k^{P,Vim} \quad \forall k \in \Gamma_L \quad (4.65)$$

$$I_{L,k}^{re,max} \cdot \eta_k + \eta_k^{max} \cdot I_{L,k}^{re} - I_{L,k}^{re,max} \cdot \eta_k^{max} \leq l_k^{P,Vim} \quad \forall k \in \Gamma_L \quad (4.66)$$

$$I_{L,k}^{re,min} \cdot \eta_k + \eta_k^{max} \cdot I_{L,k}^{re} - I_{L,k}^{re,min} \cdot \eta_k^{max} \geq l_k^{P,Vim} \quad \forall k \in \Gamma_L \quad (4.67)$$

$$I_{L,k}^{re,max} \cdot \eta_k + \eta_k^{min} \cdot I_{L,k}^{re} - I_{L,k}^{re,max} \cdot \eta_k^{min} \geq l_k^{P,Vim} \quad \forall k \in \Gamma_L \quad (4.68)$$

$$3) I_{L,k}^{im} \cdot \zeta_k \approx l_k^{Q,Vre}$$

$$I_{L,k}^{im,min} \cdot \zeta_k + \zeta_k^{min} \cdot I_{L,k}^{im} - I_{L,k}^{im,min} \cdot \zeta_k^{min} \leq l_k^{Q,Vre} \quad \forall k \in \Gamma_L \quad (4.69)$$

$$I_{L,k}^{im,max} \cdot \zeta_k + \zeta_k^{max} \cdot I_{L,k}^{im} - I_{L,k}^{im,max} \cdot \zeta_k^{max} \leq l_k^{Q,Vre} \quad \forall k \in \Gamma_L \quad (4.70)$$

$$I_{L,k}^{im,min} \cdot \zeta_k + \zeta_k^{max} \cdot I_{L,k}^{im} - I_{L,k}^{im,min} \cdot \zeta_k^{max} \geq l_k^{Q,Vre} \quad \forall k \in \Gamma_L \quad (4.71)$$

$$I_{L,k}^{im,max} \cdot \zeta_k + \zeta_k^{min} \cdot I_{L,k}^{im} - I_{L,k}^{im,max} \cdot \zeta_k^{min} \geq l_k^{Q,Vre} \quad \forall k \in \Gamma_L \quad (4.72)$$

$$4) I_{L,k}^{im} \cdot \eta_k \approx I_k^{Q,Vim}$$

$$I_{L,k}^{im,min} \cdot \eta_k + \eta_k^{min} \cdot I_{L,k}^{im} - I_{L,k}^{im,min} \cdot \eta_k^{min} \leq I_k^{Q,Vim} \quad \forall k \in \Gamma_L \quad (4.73)$$

$$I_{L,k}^{im,max} \cdot \eta_k + \eta_k^{max} \cdot I_{L,k}^{im} - I_{L,k}^{im,max} \cdot \eta_k^{max} \leq I_k^{Q,Vim} \quad \forall k \in \Gamma_L \quad (4.74)$$

$$I_{L,k}^{im,min} \cdot \eta_k + \eta_k^{max} \cdot I_{L,k}^{im} - I_{L,k}^{im,min} \cdot \eta_k^{max} \geq I_k^{Q,Vim} \quad \forall k \in \Gamma_L \quad (4.75)$$

$$I_{L,k}^{im,max} \cdot \eta_k + \eta_k^{min} \cdot I_{L,k}^{im} - I_{L,k}^{im,max} \cdot \eta_k^{min} \geq I_k^{Q,Vim} \quad \forall k \in \Gamma_L \quad (4.76)$$

$$5) V_k^{re} \cdot L_k^P \approx m_k^{P,Vre}$$

$$V_k^{re,min} \cdot L_k^P + L_k^{P,min} \cdot V_k^{re} - V_k^{re,min} \cdot L_k^{P,min} \leq m_k^{P,Vre} \quad \forall k \in \Gamma_{CL} \quad (4.77)$$

$$V_k^{re,max} \cdot L_k^P + L_k^{P,max} \cdot V_k^{re} - V_k^{re,max} \cdot L_k^{P,max} \leq m_k^{P,Vre} \quad \forall k \in \Gamma_{CL} \quad (4.78)$$

$$V_k^{re,min} \cdot L_k^P + L_k^{P,max} \cdot V_k^{re} - V_k^{re,min} \cdot L_k^{P,max} \geq m_k^{P,Vre} \quad \forall k \in \Gamma_{CL} \quad (4.79)$$

$$V_k^{re,max} \cdot L_k^P + L_k^{P,min} \cdot V_k^{re} - V_k^{re,max} \cdot L_k^{P,min} \geq m_k^{P,Vre} \quad \forall k \in \Gamma_{CL} \quad (4.80)$$

Note that equations (4.77-4.80) are only applied for the set of curtailable loads where in non-curtailable loads, the value L_k^P is considered as a constant parameter and no approximation is needed for the product $V_k^{re} \cdot L_k^P$ since it is already linear. The same applies in the following parts 6, 7, and 8.

$$6) V_k^{im} \cdot L_k^Q \approx m_k^{Q,Vim}$$

$$V_k^{im,min} \cdot L_k^Q + L_k^{Q,min} \cdot V_k^{re} - V_k^{im,min} \cdot L_k^{Q,min} \leq m_k^{Q,Vim} \quad \forall k \in \Gamma_{CL} \quad (4.81)$$

$$V_k^{im,max} \cdot L_k^Q + L_k^{Q,max} \cdot V_k^{re} - V_k^{im,max} \cdot L_k^{Q,max} \leq m_k^{Q,Vim} \quad \forall k \in \Gamma_{CL} \quad (4.82)$$

$$V_k^{im,min} \cdot L_k^Q + L_k^{Q,max} \cdot V_k^{re} - V_k^{im,min} \cdot L_k^{Q,max} \geq m_k^{Q,Vim} \quad \forall k \in \Gamma_{CL} \quad (4.83)$$

$$V_k^{im,max} \cdot L_k^Q + L_k^{Q,min} \cdot V_k^{re} - V_k^{im,max} \cdot L_k^{Q,min} \geq m_k^{Q,Vim} \quad \forall k \in \Gamma_{CL} \quad (4.84)$$

$$7) V_k^{im} \cdot L_k^P \approx m_k^{P,Vim}$$

$$V_k^{im,min} \cdot L_k^P + L_k^{P,min} \cdot V_k^{re} - V_k^{im,min} \cdot L_k^{P,min} \leq m_k^{P,Vim} \quad \forall k \in \Gamma_{CL} \quad (4.85)$$

$$V_k^{im,max} \cdot L_k^P + L_k^{P,max} \cdot V_k^{re} - V_k^{im,max} \cdot L_k^{P,max} \leq m_k^{P,Vim} \quad \forall k \in \Gamma_{CL} \quad (4.86)$$

$$V_k^{im,min} \cdot L_k^P + L_k^{P,max} \cdot V_k^{re} - V_k^{im,min} \cdot L_k^{P,max} \geq m_k^{P,Vim} \quad \forall k \in \Gamma_{CL} \quad (4.87)$$

$$V_k^{im,max} \cdot L_k^P + L_k^{P,min} \cdot V_k^{re} - V_k^{im,max} \cdot L_k^{P,min} \geq m_k^{P,Vim} \quad \forall k \in \Gamma_{CL} \quad (4.88)$$

$$8) V_k^{re} \cdot L_k^Q \approx m_k^{Q,Vre}$$

$$V_k^{re,min} \cdot L_k^Q + L_k^{Q,min} \cdot V_k^{re} - V_k^{re,min} \cdot L_k^{Q,min} \leq m_k^{Q,Vre} \quad \forall k \in \Gamma_{CL} \quad (4.89)$$

$$V_k^{re,max} \cdot L_k^Q + L_k^{Q,max} \cdot V_k^{re} - V_k^{re,max} \cdot L_k^{Q,max} \leq m_k^{Q,Vre} \quad \forall k \in \Gamma_{CL} \quad (4.90)$$

$$V_k^{re,min} \cdot L_k^Q + L_k^{Q,max} \cdot V_k^{re} - V_k^{re,min} \cdot L_k^{Q,max} \geq m_k^{Q,Vre} \quad \forall k \in \Gamma_{CL} \quad (4.91)$$

$$V_k^{re,max} \cdot L_k^Q + L_k^{Q,min} \cdot V_k^{re} - V_k^{re,max} \cdot L_k^{Q,min} \geq m_k^{Q,Vre} \quad \forall k \in \Gamma_{CL} \quad (4.92)$$

Step 3: Finally, equations (4.59) and (4.60) can be re-written linearly with the inclusion of the binary decision variable μ_k as:

For non-curtailable loads:

$$-M_k^{L,re} \cdot (1 - \mu_k) \leq l_k^{P,Vre} + l_k^{P,Vim} - V_k^{re} \cdot L_k^P - V_k^{im} \cdot L_k^Q \leq M_k^{L,re} \cdot (1 - \mu_k)$$

$$\forall k \in \{\Gamma_L \setminus \Gamma_{CL}\} \quad (4.93)$$

$$-M_k^{L,im} \cdot (1 - \mu_k) \leq l_k^{Q,Vre} + l_k^{Q,Vim} - V_k^{im} \cdot L_k^P + V_k^{re} \cdot L_k^Q \leq M_k^{L,im} \cdot (1 - \mu_k)$$

$$\forall k \in \{\Gamma_L \setminus \Gamma_{CL}\} \quad (4.94)$$

where

$M_k^{L,re}$ is a disjunctive constant that is assured to be always greater than

$$\left| l_k^{P,Vre} + l_k^{P,Vim} - V_k^{re} \cdot L_k^P - V_k^{im} \cdot L_k^Q \right|$$

$M_k^{L,im}$ is a disjunctive constant that is assured to be always greater than

$$\left| l_k^{Q,Vre} + l_k^{Q,Vim} - V_k^{im} \cdot L_k^P + V_k^{re} \cdot L_k^Q \right|$$

For curtailable loads:

$$-M_k^{CL,im} \cdot (1 - \mu_k) \leq l_k^{P,Vre} + l_k^{P,Vim} - m_k^{P,Vre} - m_k^{Q,Vim} \leq M_k^{CL,re} \cdot (1 - \mu_k)$$

$$\forall k \in \Gamma_{CL} \quad (4.95)$$

$$-M_k^{CL,im} \cdot (1 - \mu_k) \leq l_k^{Q,Vre} + l_k^{Q,Vim} - m_k^{P,Vim} + m_k^{Q,Vre} \leq M_k^{CL,re} \cdot (1 - \mu_k)$$

$$\forall k \in \Gamma_{CL} \quad (4.96)$$

where

$M_k^{CL,re}$ is a disjunctive constant that is assured to be always greater than

$$\left| l_k^{P,Vre} + l_k^{P,Vim} - m_k^{P,Vre} - m_k^{Q,Vim} \right|$$

$M_k^{CL,im}$ is a disjunctive constant that is assured to be always greater than

$$\left| l_k^{Q,Vre} + l_k^{Q,Vim} - m_k^{P,Vim} + m_k^{Q,Vre} \right|$$

If a load is completely shed ($\mu_k = 0$) the real and imaginary load current must be equal to zero. This can be achieved as follows:

$$-M_k^{LL,re} \cdot \mu_k \leq I_{L,k}^{re} \leq M_k^{LL,re} \cdot \mu_k \quad \forall k \in \Gamma_L \quad (4.97)$$

$$-M_k^{LL,im} \cdot \mu_k \leq I_{L,k}^{im} \leq M_k^{LL,im} \cdot \mu_k \quad \forall k \in \Gamma_L \quad (4.98)$$

where

$M_k^{LL,re}$ is a disjunctive constant that is assured to be always greater than $|I_{L,k}^{re}|$

$M_k^{LL,im}$ is a disjunctive constant that is assured to be always greater than $|I_{L,k}^{im}|$

It must be noted that if the load current was equated to zero using equations (4.97) and (4.98), the set of envelope constraints containing the variables $I_{L,k}^{re}$ or $I_{L,k}^{im}$ (4.61-4.76) must be relaxed since the value zero of these control variables might not be within the ranges $(I_{L,k}^{re,min}, I_{L,k}^{re,max})$, $(I_{L,k}^{im,min}, I_{L,k}^{im,max})$ that are used in building McCormick's envelopes. The relaxation can be easily achieved using reformulation method 1 with a disjunctive constant that depends on the control decision variable μ_k . The specific ranges of McCormick's envelopes will be illustrated in section 4.4.

4.3.1.4 Load Curtailment Constraints

First, a control variable representing the amount of load curtailed is defined in order to be used in the objective function as will be illustrated in section 4.3.2.

$$LC_k = L_k^{P,max} - L_k^P \quad \forall k \in \Gamma_{CL} \quad (4.99)$$

Note that the value of LC_k depends only on real power demand where in this thesis, the curtailment decision is based on real load and the imaginary load is related as follows:

$$\frac{L_k^Q}{L_k^{Q,max}} = \frac{L_k^P}{L_k^{P,max}} \quad \forall k \in \Gamma_{CL} \quad (4.100)$$

Constraint (4.100) will always guarantee that the percentage of curtailed real power is equal to the percentage of curtailed imaginary power keeping the load power factor constant.

Finally, each curtailed load has a defined maximum limit that cannot be exceeded and it is modeled as follows:

$$LC_k \leq LC_k^{max} \quad \forall k \in \Gamma_{CL} \quad (4.101)$$

4.3.1.5 Operational Constraints

1) Node voltage limits

Since the values of V_k^{re2} and V_k^{im2} where already approximated to ζ_k and η_k , respectively, they can be used directly in modeling the voltage limits constraint as follows:

$$V_k^{min2} \leq \zeta_k + \eta_k \leq V_k^{max2} \quad \forall k \in \Gamma_N \quad (4.102)$$

2) Branch current limits

$$I_{km}^{re2} + I_{km}^{im2} \leq I_{km}^{max2} \quad \forall km \in \Gamma_B \quad (4.103)$$

Reformulation method 4 (polygonal inner-approximation) is used to model the non-linear constraint of the current limits as follows:

$$\overline{I_{km}^{re}}^p \cdot I_{km}^{re} + \overline{I_{km}^{im}}^p \cdot I_{km}^{im} \leq I_{km}^{max2} \quad \forall p \in \{1,2, \dots, E\}, \quad \forall km \in \Gamma_B \quad (4.104)$$

where the coefficients $\overline{I_{km}^{re}}^p$ and $\overline{I_{km}^{im}}^p$ can be found as:

$$\overline{I_{km}^e}^p = I_{km}^{max} \cdot \cos \left[(p - 0.5) \cdot \frac{2\pi}{E} \right] \quad \forall p \in \{1, 2, \dots, E\}, \quad \forall km \in \Gamma_B \quad (4.105)$$

$$\overline{I_{km}^i}^p = I_{km}^{max} \cdot \sin \left[(p - 0.5) \cdot \frac{2\pi}{E} \right] \quad \forall p \in \{1, 2, \dots, E\}, \quad \forall km \in \Gamma_B \quad (4.106)$$

The number of polygonal edges will be taken as $E = 36$ yielding 36 linear constraint. It was examined that with this number of edges, the approximation is highly sufficient (refer to Figure A.2 in the appendices).

3) DGs Power output limit

DGs are limited depending on their maximum apparent power DG_k^{max} as follows:

$$DG_k^{P^2} + DG_k^{Q^2} \leq DG_k^{S,max^2} \quad \forall k \in \Gamma_{CDG} \quad (4.107)$$

Similar to branch current limit, formulation method 4 (polygonal inner-approximation) is used to model the non-linear constraint of the DG power output limits. The difference is that only the right half of the circle need to be approximated since the real generated power is always positive. The formulation is achieved as follows:

$$\overline{DG_k^P}^p \cdot DG_k^P + \overline{DG_k^Q}^p \cdot DG_k^Q \leq DG_k^{S,max^2} \quad \forall p \in \left\{ 1, 2, \dots, \frac{E}{2} \right\}, \quad \forall k \in \Gamma_{CDG} \quad (4.108)$$

If E was chosen to be an odd number, $(E + 1)/2$ is used instead of $E/2$.

The coefficients $\overline{DG_k^P}^p$ and $\overline{DG_k^Q}^p$ can be found as:

$$\overline{DG_k^P}^p = DG_k^{S,max} \cdot \cos \left[\left(p - \frac{E + 4}{4} \right) \cdot \frac{2\pi}{E} \right] \quad \forall p \in \left\{ 1, 2, \dots, \frac{E}{2} \right\},$$

$$\forall k \in \Gamma_{CDG} \quad (4.109)$$

$$\overline{DG_k^Q}^p = DG_k^{S,max} \cdot \sin \left[\left(p - \frac{E+4}{4} \right) \cdot \frac{2\pi}{E} \right] \quad \forall p \in \left\{ 1, 2, \dots, \frac{E}{2} \right\},$$

$$\forall k \in \Gamma_{CDG} \quad (4.110)$$

The number of polygonal edges here will also be taken as $E = 36$ yielding 18 linear constraint.

4.3.1.6 Radiality Constraints

Two approaches to formulate the radiality constraint in the MILP problem are discussed in this section.

1) Radiality constraint approach I

The first approach to model the radiality constraint proposed by [57] has a great advantage in the sense that it does not require any integer or binary variables. It is based on a depth-first search (DFS) strategy to detect all loops in the system. After finding all possible loops, the radiality constraints can be simply modeled as follows:

$$\sum_{km=1}^{N_{loop,i}} y_{km} \leq N_{loop,i} - 1 \quad \forall km \in loop_i, \quad \forall i \in \Gamma_{loop} \quad (4.111)$$

Where

$N_{loop,i}$ is the number of branches in loop i

2) Radiality constraint approach II

Reference [63] proposed a formulation for radiality by constraining that each node in the system, except the root node which is usually a substation, has only one parent node.

This formulation is obtained using binary decision variables and can be modeled as follows:

$$\gamma_{km}^k + \gamma_{km}^m = 1 \quad \forall km \in \{\Gamma_B/\Gamma_{sw}\} \quad (4.112)$$

$$\gamma_{km}^k + \gamma_{km}^m = y_{km} \quad \forall km \in \Gamma_{sw} \quad (4.113)$$

$$\gamma_{km}^k = 0 \quad \forall km \in \{\Gamma_B|k \in \Gamma_{sub}\} \quad (4.114)$$

$$\gamma_{km}^m = 0 \quad \forall km \in \{\Gamma_B|m \in \Gamma_{sub}\} \quad (4.115)$$

where:

γ_{km}^k is a binary decision variables that takes the value 1 if node k is the parent of node m , and zero otherwise.

γ_{km}^m is a binary decision variables that takes the value 1 if node m is the parent of node k , and zero otherwise.

Although this method has been adopted from many MILP radiality formulation in the literature, it has a disadvantage in the since that it requires binary constraints, which as discussed previously, may affect the computational time due to the increased branch and bound process. In the other hand, it guarantees the radiality constraint more practically since no loop searching is required, and for large system, this could be a difficult matter. Thereby, this approach will be considered when setting the radiality constraint in this thesis.

4.3.2 Formulating Objective Functions of the Problem

As stated previously, the restoration optimization technique proposed in this thesis is a multi-objective problem. The objectives that are considered are listed as follows:

4.3.2.1 To Maximize the Supplied Customers based on their Priorities

$$Max \sum_{k \in \Gamma_L} PL_k \cdot \mu_k \quad (4.116)$$

where

PL_k is the priority weight for load k

4.3.2.2 To Minimize the Cost Associated with the Restoration Process

1) DGs Operational Cost

$$Min \sum_{k \in \Gamma_{CDG}} C_k^{DG} \cdot DG_k^P \quad (4.117)$$

where

C_k^{DG} is the cost related to the real power output of the k^{th} DG in the microgrid

2) Cost of Load Curtailment

$$Min \sum_{k \in \Gamma_{LC}} C_k^{LC} \cdot LC_k \quad (4.118)$$

where

C_k^{LC} is the cost related to the real power curtailed from load k

Note that the values in each objective function have different units and scales. The priority weight PL_k in the first objective is in per unit and ranging between zero to one for

each load. In the other hand, the values in the second objective are in \$/ (MW or KW) and may take any value depending on the assigned prices for each DG and each curtailable load. This raise an important issue and must be taken under consideration by normalizing each objective function based on the maximum value they may assume. Keeping in mind that the priority weights of each load are determined immediately after the outage and before the optimization, and that DGs maximum outputs and maximum allowed curtailment for each load are also known, we can define the following bases for each objective:

$$Base1 = \sum_{k \in \Gamma_L} PL_k \quad (4.119)$$

$$Base2 = \sum_{k \in \Gamma_{CDG}} C_k^{DG} \cdot DG_k^{P,max} \quad (4.120)$$

$$Base3 = \sum_{k \in \Gamma_{LC}} C_k^{LC} \cdot LC_k^{max} \quad (4.121)$$

Finally, the general multi-objective function of the proposed self-healing technique for electric microgrids will be in the form:

$$\begin{aligned} Min \quad & - \frac{\omega_{priority}^{Obj}}{Base1} \cdot \sum_{k \in \Gamma_N} PL_k \cdot \mu_k + \frac{\omega_{DG\ cost}^{Obj}}{Base2} \cdot \sum_{k \in \Gamma_{CDG}} C_k^{DG} \cdot DG_k^P \\ & + \frac{\omega_{LC\ cost}^{Obj}}{Base3} \cdot \sum_{k \in \Gamma_{LC}} C_k^{LC} \cdot LC_k \quad (4.122) \end{aligned}$$

where

$\omega_{priority}^{Obj}$ is the weight of the first objective function related to load priorities

$\omega_{DG\ cost}^{Obj}$ is the weight of the second objective function related to DGs operational cost

$\omega_{LC\ cost}^{Obj}$ is the weight of the third objective function related to LC cost

These weights are set depending on the user or the utilities decision and the comparison between the importance of restoring loads, DGs operational cost, and LC cost in the restoration process.

4.4 Set of Bounds for McCormick's Envelopes

Since the formulation of the DGs power output and the loads was highly dependent on McCormick's envelopes and the approximation of bilinear products, it becomes important to devote this section for defining the necessary parameters in the approximation process, mainly, the maximum and minimal bounds which are needed in McCormick's envelopes constraints. In most cases, these bounds depend on operational system behavior such as, voltage magnitudes and angles range, DGs generation limits, and amount of loading. The reader should keep in mind at this section that these operational behaviors of the system differ significantly during the case of an outage and at the process of restoration. For example, nominal voltage limits are usually relaxed up to a certain level during restoration in order to allow restoring as much loads as possible.

It becomes convenient at this stage to recall the equations that were approximated using McCormick's envelopes. These equation are listed as follows:

- 1) The square of real and imaginary node voltages

$$V_k^{re} \cdot V_k^{re} \approx \zeta_k \quad \forall k \in \Gamma_N \quad (4.123)$$

$$V_k^{im} \cdot V_k^{im} \approx \eta_k \quad \forall k \in \Gamma_N \quad (4.124)$$

2) The bilinear products in DG's generation constraints

$$I_{DG,k}^{re} \cdot \zeta_k + I_{DG,k}^{re} \cdot \eta_k = V_k^{re} \cdot DG_k^P + V_k^{im} \cdot DG_k^Q \quad \forall k \in \Gamma_{CDG} \quad (4.125)$$

$$I_{DG,k}^{im} \cdot \zeta_k + I_{DG,k}^{im} \cdot \eta_k = V_k^{im} \cdot DG_k^P - V_k^{re} \cdot DG_k^Q \quad \forall k \in \Gamma_{CDG} \quad (4.126)$$

3) The bilinear products in Load demand constraints

$$I_{L,k}^{re} \cdot \zeta_k + I_{L,k}^{re} \cdot \eta_k = V_k^{re} \cdot L_k^P + V_k^{im} \cdot L_k^Q \quad \forall k \in \Gamma_{CL} \quad (4.127)$$

$$I_{L,k}^{im} \cdot \zeta_k + I_{L,k}^{im} \cdot \eta_k = V_k^{im} \cdot L_k^P - V_k^{re} \cdot L_k^Q \quad \forall k \in \Gamma_{CL} \quad (4.128)$$

The main goal of this section is to set overestimate and underestimate bounds for each variable included in a bilinear product in equations (4.123 - 4.128). Note that the notation of a maximum and minimum bound will be \blacksquare^{max} and \blacksquare^{min} , respectively.

1) Real and imaginary voltage limits

The real and imaginary node voltages can be represented in polar form as follows:

$$V_k^{re} = V_k \cdot \cos\theta_k \quad \forall k \in \Gamma_N \quad (4.129)$$

$$V_k^{im} = V_k \cdot \sin\theta_k \quad \forall k \in \Gamma_N \quad (4.130)$$

where

V_k is the voltage magnitude of bus k in the system in per unit

θ_k is the phase voltage angle of bus k in the system in degrees

In order to set bounds for equations (4.129 & 4.130), bounds for voltage magnitude

$V_k^{min} \leq V_k \leq V_k^{max}$ and phase angle $\theta_k^{min} \leq \theta_k \leq \theta_k^{max}$ must be assumed. In order to ensure

efficient reliable performance of a network, voltage magnitudes are usually constrained to be within the range of $0.95 \leq V_k \leq 1.05$ but in the case of emergency, however, these limits might be relaxed to be $0.90 \leq V_k \leq 1.10$. Moreover, voltage phase angles in distribution system typically range within a narrow interval apart from the reference value. These intervals can be measured by running several power flow analysis, under different scenarios, on the microgrid to be analyzed. Tighter intervals will result better accuracy. Considering a reference phase of zero degrees, most distribution systems in the literature incorporate a bus phase voltage interval in the range of $-5^\circ \leq \theta_k \leq 5^\circ$ [56].

After defining magnitude and phase voltage bounds, one can write the following for overestimate and underestimate bounds of real and imaginary voltage variables:

$$V_k^{re,max} = V_k^{max} \quad \forall k \in \Gamma_N \quad (4.131)$$

$$V_k^{re,min} = V_k^{min} \cdot \cos(\max\{|\theta_k^{max}|, |\theta_k^{min}|\}) \quad \forall k \in \Gamma_N \quad (4.132)$$

$$V_k^{im,max} = V_k^{re,max} \cdot \sin\theta_k^{max} \quad \forall k \in \Gamma_N \quad (4.133)$$

$$V_k^{im,min} = V_k^{re,max} \cdot \sin\theta_k^{min} \quad \forall k \in \Gamma_N \quad (4.134)$$

Hence, bounds for ζ_k and η_k , which represent V_k^{re2} and V_k^{im2} , respectively, can be found as follows:

$$\zeta_k^{max} = V_k^{max2} \quad \forall k \in \Gamma_N \quad (4.135)$$

$$\zeta_k^{min} = [V_k^{min} \cdot \cos(\max\{|\theta_k^{max}|, |\theta_k^{min}|\})]^2 \quad \forall k \in \Gamma_N \quad (4.136)$$

$$\eta_k^{max} = [V_k^{re,max} \cdot \sin\theta_k^{max}]^2 \quad \forall k \in \Gamma_N \quad (4.137)$$

$$\eta_k^{min} = 0 \quad \forall k \in \Gamma_N \quad (4.138)$$

2) DGs power and current generation

a. Active and reactive DGS power output

The values of the active and reactive power outputs of DG related to the apparent power can be calculated as follows:

$$DG_k^P = DG_k^S \cdot \cos\phi_k^{DG} \quad \forall k \in \Gamma_{DG} \quad (4.139)$$

$$DG_k^Q = DG_k^S \cdot \sin\phi_k^{DG} \quad \forall k \in \Gamma_{DG} \quad (4.140)$$

where

DG_k^S is the apparent power of the DG at node k

ϕ_k^{DG} is the power angle of the DG at node k

Bounds for DG_k^S and ϕ_k^{DG} should be determined in order to set bounds for DG_k^P and DG_k^Q . Before doing that, we should carefully study the system operational behavior during an interruption. It is well known that during an occurrence of an outage, the voltage profile of the system decrease substantially. Thereby, controlled DG units connected to the network are expected to supply reactive power rather than absorbing it in order to enhance system voltage level to be within acceptable ranges. If this can be generalized to all DG's in the microgrid, it would result in setting tighter bounds for DGs reactive power output since it would only accept positive values (supplying reactive power). The issue is that there exists induction dependent DGs that always require reactive power from the grid to operate unless they are self-excited using capacitor banks. However, to generalize the study, the set of DGs will be divided into two categories when determining their bounds.

One relating to DGs that supply reactive power, and the other to those absorbing reactive power.

The maximum limit DG_k^S can take is by default defined as the rated apparent power of the DG, $DG_k^{S,max}$, and the minimum bound is of course set to zero. Regarding the power angle, DG units are usually designed to operate with a power factor within the range of (0.8 leading, 0.8 lagging,) resulting the limits for the power angle as $-36.87^\circ \leq \phi_k^{DG} \leq 36.87^\circ$. Thereby, we can write the following for active and reactive bounds:

$$DG_k^{P,max} = DG_k^{S,max} \quad \forall k \in \Gamma_{CDG} \quad (4.141)$$

$$DG_k^{P,min} = 0 \quad \forall k \in \Gamma_{CDG} \quad (4.142)$$

$$DG_k^{Q,max} = 0 \quad \forall k \in \Gamma_{DG,absorb Q} \quad (4.143)$$

$$DG_k^{Q,min} = DG_k^{S,max} \cdot \sin \phi_k^{DG,min} \quad \forall k \in \Gamma_{DG,absorb Q} \quad (4.144)$$

$$DG_k^{Q,max} = DG_k^{S,max} \cdot \sin \phi_k^{DG,max} \quad \forall k \in \Gamma_{DG,supply Q} \quad (4.145)$$

$$DG_k^{Q,min} = 0 \quad \forall k \in \Gamma_{DG,supply Q} \quad (4.146)$$

Where

$\Gamma_{DG,absorb Q}$ is the set of DGs that absorb reactive power

$\Gamma_{DG,supply Q}$ is the set of DGs that supply reactive power

Note that due to the assumed ϕ_k^{DG} bounds, the values in equations (4.141 & 4.145) will always be positive. In the other hand, and the value in equation (4.144) will be negative.

b. Real and imaginary DGs generated currents

The derivation in this part was taken directly from [62]. By using polar form to represent the voltages and substituting $DG_k^P = DG_k^S \cdot \cos\phi_k^{DG}$ and $DG_k^Q = DG_k^S \cdot \sin\phi_k^{DG}$ in equations (4.9 & 4.10), yield:

$$I_{DG,k}^{re} = \frac{V_k \cdot \cos\theta_k \cdot DG_k^S \cdot \cos\phi_k^{DG} + V_k \cdot \sin\theta_k \cdot DG_k^S \cdot \sin\phi_k^{DG}}{V_k^2} \quad \forall k \in \Gamma_{CDG} \quad (4.147)$$

$$I_{DG,k}^{im} = \frac{V_k \cdot \sin\theta_k \cdot DG_k^S \cdot \cos\phi_k^{DG} - V_k \cdot \cos\theta_k \cdot DG_k^S \cdot \sin\phi_k^{DG}}{V_k^2} \quad \forall k \in \Gamma_{CDG} \quad (4.148)$$

Taking voltage magnitude and the apparent power as common factors results in:

$$I_{DG,k}^{re} = \frac{DG_k^S}{V_k} \cdot (\cos\theta_k \cdot \cos\phi_k^{DG} + \sin\theta_k \cdot \sin\phi_k^{DG}) \quad \forall k \in \Gamma_{CDG} \quad (4.149)$$

$$I_{DG,k}^{im} = \frac{DG_k^S}{V_k} \cdot (\sin\theta_k \cdot \cos\phi_k^{DG} - \cos\theta_k \cdot \sin\phi_k^{DG}) \quad \forall k \in \Gamma_{CDG} \quad (4.150)$$

By using trigonometric identities to reform the expressions inside the parentheses outcomes the following:

$$I_{DG,k}^{re} = \frac{DG_k^S}{V_k} \cdot \cos(\theta_k - \phi_k^{DG}) \quad \forall k \in \Gamma_{CDG} \quad (4.151)$$

$$I_{DG,k}^{im} = \frac{DG_k^S}{V_k} \cdot \sin(\theta_k - \phi_k^{DG}) \quad \forall k \in \Gamma_{CDG} \quad (4.152)$$

The bounds for the currents can now be easily determined considering the previously mentioned limits of the node voltage magnitude, phase angle, apparent power

of the DG, and the power angle limits. Real and imaginary generated current bounds for McCormicks envelopes are found as:

$$I_{DG,k}^{re,max} = \frac{DG_k^{S,max}}{V_k^{min}} \quad \forall k \in \Gamma_{DG} \quad (4.153)$$

$$I_{DG,k}^{re,min} = 0 \quad \forall k \in \Gamma_{DG} \quad (4.154)$$

$$I_{DG,k}^{im,max} = \frac{DG_k^{S,max}}{V_k^{min}} \cdot \sin(\theta_k^{max} - \phi_k^{DG,min}) \quad \forall k \in \Gamma_{DG,absorb Q} \quad (4.155)$$

$$I_{DG,k}^{im,min} = 0 \quad \forall k \in \Gamma_{DG,absorb Q} \quad (4.156)$$

$$I_{DG,k}^{im,max} = 0 \quad \forall k \in \Gamma_{DG,supply Q} \quad (4.157)$$

$$I_{DG,k}^{im,min} = \frac{DG_k^{S,max}}{V_k^{min}} \cdot \sin(\theta_k^{min} - \phi_k^{DG,max}) \quad \forall k \in \Gamma_{DG,supply Q} \quad (4.158)$$

Note that these bounds only hold due to the assumed limits for the phase and power angles, as $\theta_k^{DG,min} - \phi_k^{DG,max} < 90^\circ$. Otherwise, for instance, the minimum bound for the real current in equation (4.154) may take negative values rather than being zero (refer to the cosine in equation (4.151)).

For the power and current output of a substation, similar procedure is used utilizing the rated values of the substation itself or the feeder connected to it, whichever is less, in finding their limits.

3) Loads power and current demands

First let us define the following:

$$L_k^S = \sqrt{L_k^{P^2} + L_k^{Q^2}} \quad \forall k \in \Gamma_L \quad (4.159)$$

$$\phi_k^L = \tan^{-1} \frac{L_k^Q}{L_k^P} \quad \forall k \in \Gamma_L \quad (4.160)$$

The maximum real $L_k^{P,max}$ and reactive $L_k^{Q,max}$ demands are set directly as the load nominal value. In the proposed modeling of the general problem, loads were divided into curtailable and non-curtailable loads. Only curtailable loads are addressed when setting the bounds, where, as mentioned previously, non-curtailable loads are considered constant and seen as input parameters for the problem. Recall from constraint (4.101) that each curtailable load has a maximum amount of allowed curtailment. Using this limit, and the relation defined in constraint (4.100), we can write the following for the minimal real and reactive demand bounds:

$$L_k^{P,min} = L_k^{P,max} - LC_k^{max} \quad \forall k \in \Gamma_{CL} \quad (4.161)$$

$$L_k^{Q,min} = \frac{L_k^{Q,max}}{L_k^{P,max}} \cdot (1 - LC_k^{max}) \quad \forall k \in \Gamma_{CL} \quad (4.162)$$

where

$L_k^{P,max}$ is the nominal active demand of load k

$L_k^{Q,max}$ is the nominal reactive demand of load k

In order to define bounds for demand currents, we apply similar derivation used when defining DGs current output bounds. Hence, we can immediately write the following for load currents:

$$I_{L,k}^{re} = \frac{L_k^S}{V_k} \cdot \cos(\theta_k - \phi_k^L) \quad \forall k \in \Gamma_L \quad (4.163)$$

$$I_{L,k}^{im} = \frac{L_k^S}{V_k} \cdot \sin(\theta_k - \phi_k^L) \quad \forall k \in \Gamma_L \quad (4.164)$$

The limits for L_k^S , V_k , and θ_k were already specified. Regarding the load power angle ϕ_k^L , it can be measured easily since the nominal real and reactive demands are considered inputs and that the power factor is kept constant even for curtailable loads. However, usually, typical power factor range within (0.8 leading, 0.8 lagging) which result in setting ranges for the load power angle as $-36.87^\circ \leq \phi_k^L \leq 36.87^\circ$. Considering ϕ_k^L as know value, the ranges of real and imaginary load current can be found from:

$$I_{L,k}^{re,max} = \frac{L_k^{S,max}}{V_k^{min}} \cdot \max_{\theta_k^{min} \leq \theta_k \leq \theta_k^{max}} \left\{ \cos(\theta_k - \phi_k^L) \right\} \quad \forall k \in \Gamma_{CL} \quad (4.165)$$

$$I_{L,k}^{re,min} = \frac{L_k^{S,min}}{V_k^{max}} \cdot \min_{\theta_k^{min} \leq \theta_k \leq \theta_k^{max}} \left\{ \cos(\theta_k - \phi_k^L) \right\} \quad \forall k \in \Gamma_{CL} \quad (4.166)$$

$$I_{L,k}^{im,max} = \max_{\substack{\theta_k^{min} \leq \theta_k \leq \theta_k^{max} \\ L_k^{S,min} \leq L_k^S \leq L_k^{S,max} \\ V_k^{min} \leq V_k \leq V_k^{min}}} \left\{ \frac{L_k^S}{V_k} \cdot \sin(\theta_k - \phi_k^L) \right\} \quad \forall k \in \Gamma_{CL} \quad (4.167)$$

$$I_{L,k}^{im,min} = \min_{\substack{\theta_k^{min} \leq \theta_k \leq \theta_k^{max} \\ L_k^{S,min} \leq L_k^S \leq L_k^{S,max} \\ V_k^{min} \leq V_k \leq V_k^{min}}} \left\{ \frac{L_k^S}{V_k} \cdot \sin(\theta_k - \phi_k^L) \right\} \quad \forall k \in \Gamma_{CL} \quad (4.168)$$

Where $L_k^{S,max}$ and $L_k^{S,min}$ can be simply found as:

$$L_k^{S,max} = \sqrt{L_k^{P,max^2} + L_k^{Q,max^2}} \quad \forall k \in \Gamma_{CL} \quad (4.169)$$

$$L_k^{S,min} = \sqrt{L_k^{P,min^2} + L_k^{Q,min^2}} \quad \forall k \in \Gamma_{CL} \quad (4.170)$$

Note that these limits are only set for McCormick's envelopes and not for the general problem since the real currents may be equated to zero if the load is completely shed.

It is important to emphasize that all previously numerical specified bounds were set depending on typical distribution system values and can be altered depending on the system to be analyzed. They are basically considered as input variable to the problem. The user is recommended to examine the analyzed system carefully in order to set bounds as tight as possible which will enhance the accuracy.

CHAPTER 5

MICROGRIDS SELF-HEALING OPTIMIZATION – CASE

STUDIES AND DISCUSSION

The objective of this chapter is to verify and examine the proposed self-healing strategy. The chapter is divided into 5 sections as follows:

- Section 5.1 deals with the verification of the MILP formulation proposed in Chapter 4. This will be achieved by optimizing the configuration of the studied system and comparing the output results with results taken from the literature.
- In section 5.2, a comparison between the proposed formulation and the formulation presented in [68] will be drawn. The comparison will be based on the computational time and the accuracy of the solution in each method.
- In section 5.3, the integration of the proposed prioritizing method into the MILP formulation will be achieved. Several case studies will be presented demonstrating the effects on system reliability when utilizing the proposed prioritizing scheme in the optimization of service restoration.
- In section 5.4, several case studies simulating the self-healing strategy of smart microgrids will be presented with the inclusion of DGs and DSM customers in the system. The restoration of a smart microgrid will be

compared with the restoration of a conventional distribution system that do not include DGs or DSM customers.

- Finally, in section 5.5, sensitivity analysis of the multi-objective function are presented by interchanging the priority, DGs cost, and LC cost weights.

All case studies are solved using MATLAB MILP solver on an Intel Core i7 1.73 GHz computer. The system that will be utilized to demonstrate the study is the IEEE 3 feeder 16 bus distribution system. The online diagram of the system is shown in Figure 5.1 and bus and line data are shown in Tables 5.1 and 5.2, respectively. This system was chosen because it has been widely used in the literature in network reconfiguration and optimization problems [64-69]. The system consist of three main feeders and 13 load buses with a total of 28.7 MW and 17.3 MVAR demand. Also, 7 capacitor banks are installed is different locations as illustrated in Table 5.1. The nominal voltage of the system is 23KV and the apparent power base is taken to be 100MVA. All branches in the system are assumed to be switchable, yielding 2^{16} possible configuration, and the original configuration of the system is achieved by opening switches $S_{5,11}$, $S_{10,14}$, and $S_{7,16}$ as in Figure 5.1.

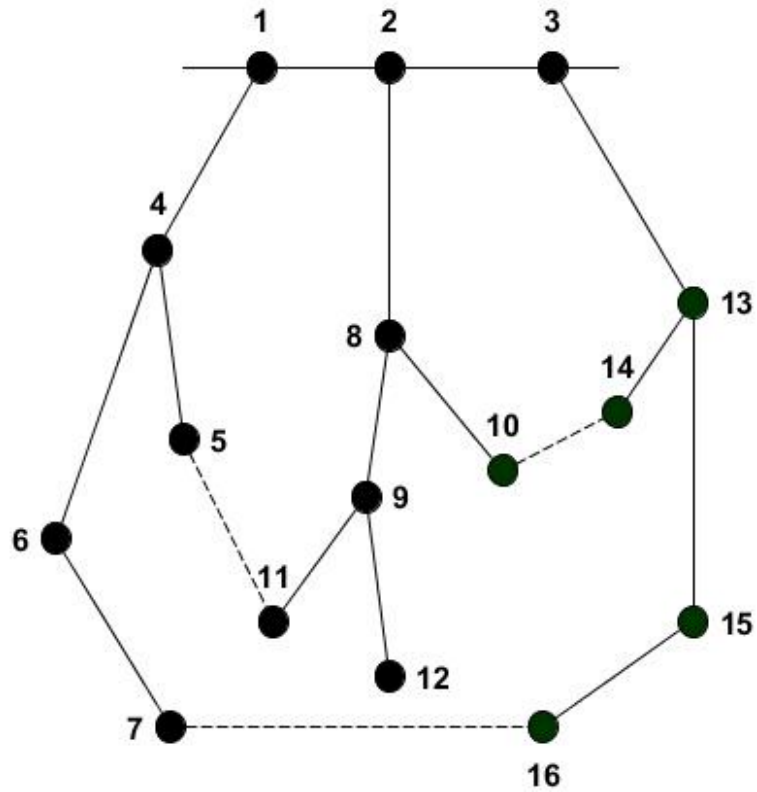


Figure 5.1 IEEE 16 bus test system

Table 5.1 IEEE three feeder 16 bus system node data

Load Point	Load P (MW)	Load Q (MVAR)	Capacitor (MVAR)
4	2	1.6	-
5	3	1.5	1.1
6	2	0.8	1.2
7	1.5	1.2	-
8	4	2.7	-
9	5	3	1.2
10	1	0.9	-
11	0.6	0.1	0.6
12	4.5	2	3.7
13	1	0.9	-
14	1	0.7	1.8
15	1	0.9	-
16	2.1	1	1.8

Table 5.2 IEEE 3 feeder 16 bus system line data

From	To	Resistance (p.u.)	Reactance (p.u.)	Rated I_{km}^{max} (p.u.)
1	4	0.075	0.1	0.2
4	5	0.08	0.11	0.2
4	6	0.09	0.18	0.2
6	7	0.04	0.04	0.2
2	8	0.11	0.11	0.2
8	9	0.08	0.11	0.2
8	10	0.11	0.11	0.2
9	11	0.11	0.11	0.2
9	12	0.08	0.11	0.2
3	13	0.11	0.11	0.2
13	14	0.09	0.12	0.2
13	15	0.08	0.11	0.2
15	16	0.04	0.04	0.2
5	11	0.04	0.04	0.2
10	14	0.04	0.04	0.2
7	16	0.09	0.12	0.2

Before starting the case studies, it is recommended to analyze the system, at its original configuration, in order to provide the reader with a more depth knowledge about the system behavior. After running the load flow of the system, the total losses was found to be 511.5 KW and the voltage magnitude and phase angles of all buses are shown in Figures 5.2 and 5.3 respectively. Note that nodes 1, 2, and 3 were taken as slack buses with voltage magnitude of 1 p.u. and zero phase angle.

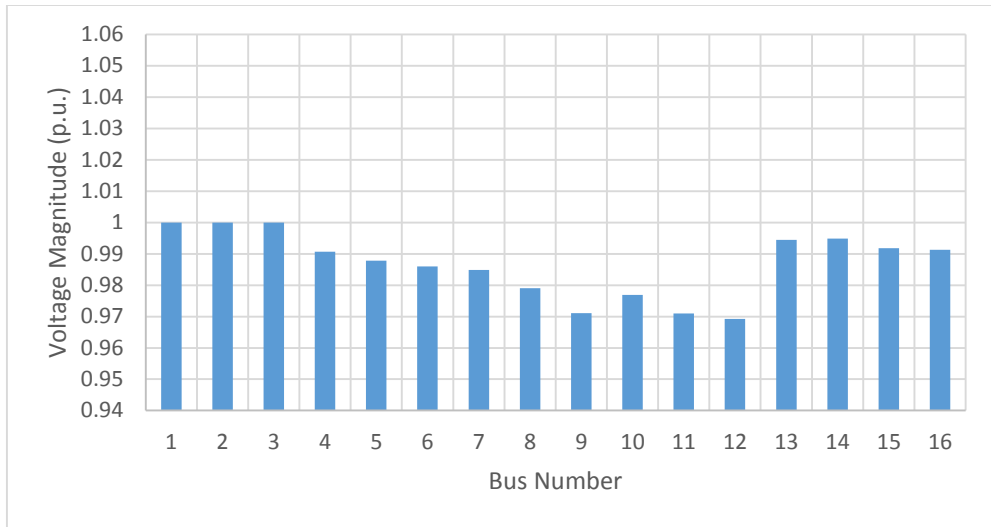


Figure 5.2 IEEE 16 bus voltage magnitudes – original configuration

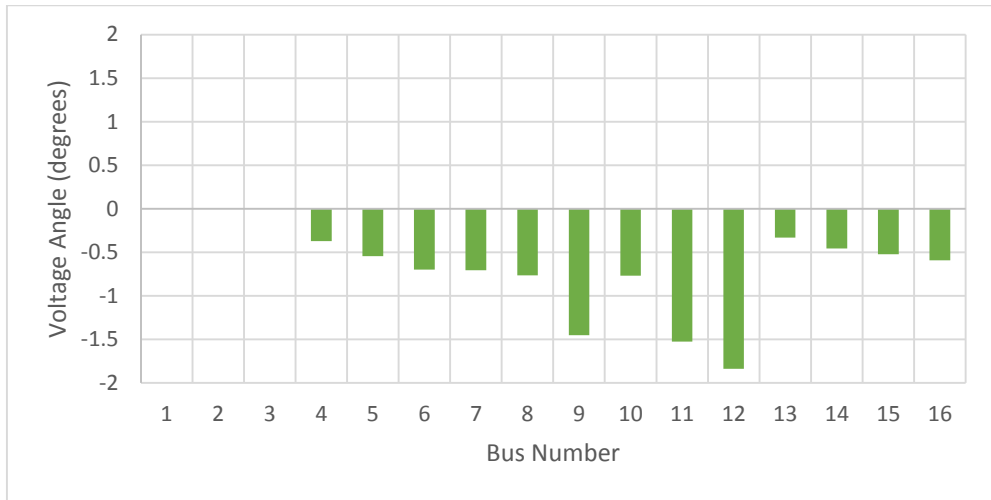


Figure 5.3 IEEE 16 bus voltage phase angles – original configuration

5.1 Verification of the Proposed Formulation

The verification of the proposed formulation will be achieved in this section. Most of the reconfiguration optimization problems in the literature are based on system loss minimization. Thereby, the verification was chosen to be accomplished by optimizing the

power loss reduction in the IEEE 3 feeder 16 bus system. Then, the results will be compared with references found in the literature solving the same problem.

Although the proposed MILP formulation in this thesis was constructed for the goal of optimizing service restoration, however, by applying few modification on the formulation, it can be then used for optimizing other technical problems such as loss minimization. The modification to obtain loss minimization optimization using the proposed method are as follows:

- 1) The objective function is changed to be in the form:

$$\text{Min} \sum_{k \in \Gamma_{sub}} DG_k^P - \sum_{k \in \Gamma_L} L_k^P \quad (5.1)$$

Where

Γ_{sub} is the set of substations in the system

Γ_L is the set of loads in the system

Be reminded that the subscript DG_k^P is used for any real power generation in the system including substations and distributed generators, if any.

- 2) One constraint is added, which is to fully supply all loads in the system and can be formulated as follows:

$$\mu_k = 1 \quad \forall k \in \Gamma_L \quad (5.2)$$

Figure 5.4 shows the configuration the system after optimization which was achieved by opening switches $S_{9,11}$, $S_{8,10}$, and $S_{7,16}$ and closing all other switches. A result comparison is drawn in Table 5.3. Note that the radiality constraint hold in this specific

problem. The voltage profile of the system at optimal configuration is shown in Figures 5.5 and 5.6.

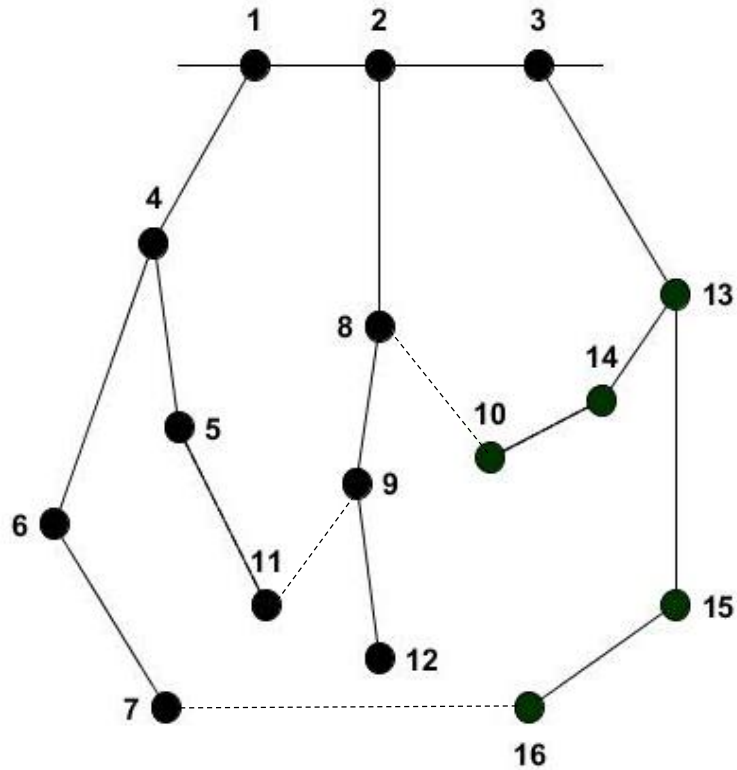


Figure 5.4 Optimal configuration for loss reduction of the IEEE 3 feeder 16 bus system

The improvement in voltage level were mainly observed in buses 10 and 11. This is because in the original configuration, these loads were supplied from feeder 2-8 which happens to also supply high demand loads 8, 9, and 12. Then, in the optimal configuration, loads 10 and 11 were switched to be supplied from feeders 3-13 and 1-4, respectively which yield the recorder voltage improvement.

Table 5.3 IEEE 3 feeder 16 bus system - loss minimization results and coparison

	Original Configuration	Method of Optimization		
		Simulated Annealing [74]	Differential Evolution [75]	Proposed MILP
Tie Switches	$S_{5,11}, S_{10,14}, S_{7,16}$	$S_{9,11}, S_{8,10}, S_{7,16}$	$S_{9,11}, S_{8,10}, S_{7,16}$	$S_{9,11}, S_{8,10}, S_{7,16}$
Power Loss (KW)	511.5	466.1	466.1	466.1
Loss Reduction	-	8.88%	8.88%	8.88%

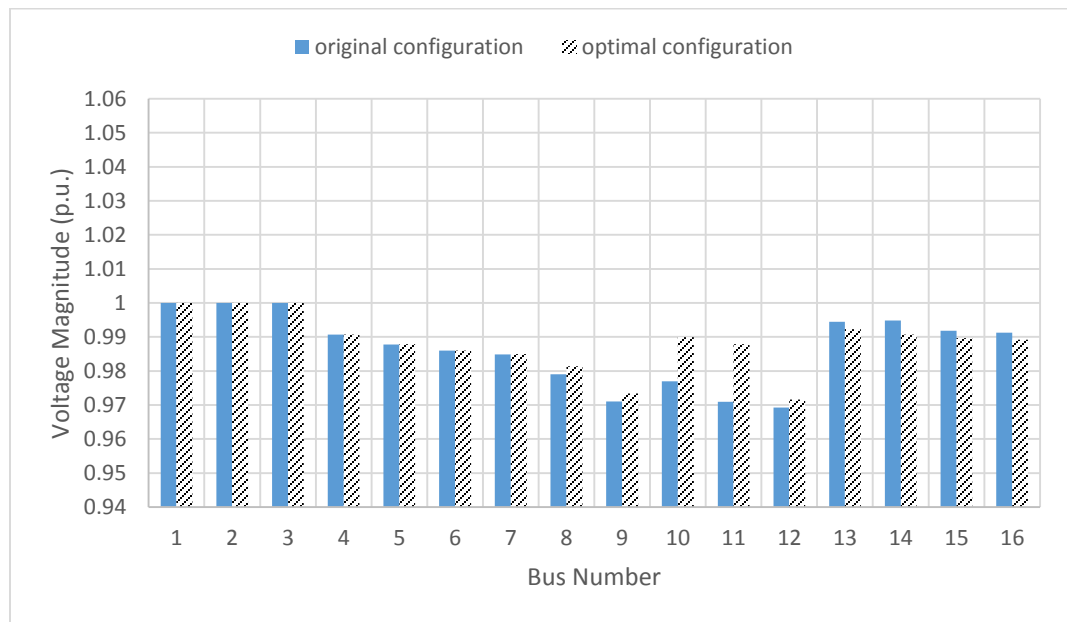


Figure 5.5 Voltage magnitudes – optimal configuration

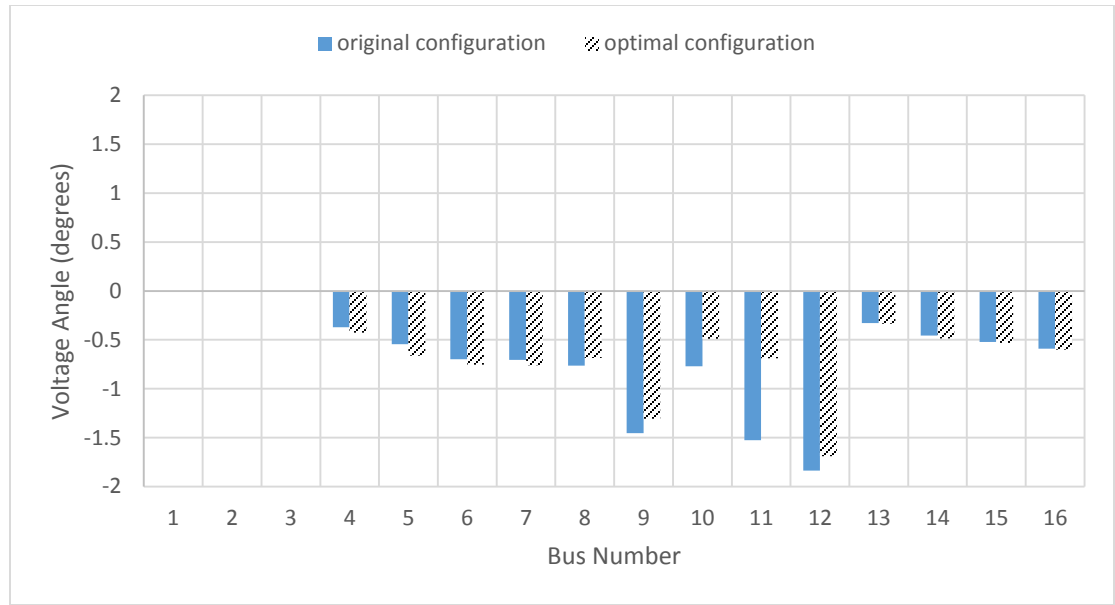


Figure 5.6 Phase angles – optimal configuration

By that, and from Table 5.3 comparing with results from the literature, the formulation is verified. In the next section, a comparison is drawn between the proposed formulation and the one found in [68].

5.2 Comparison Based Study

As have been illustrated in chapter 4, the proposed MILP formulation was dependent on McCormick’s envelopes for load and generation currents. However, in [68], the formulation for load and generation currents was achieved using piece-wise approximations and sets of type SOS2 which was explained in section 4.3.4. Due to the fact that SOS2 sets require extra integer constraint, the computational time was found to be large compared to the proposed McCormick’s envelopes formulation that require no integer constraint. It is always preferable to reduce the integer constraint as much as possible in order to decrease the branch and bound process in solving the MILP problem.

This will surely enhance the computational time of finding the optimal solution which is necessary especially when applied to a service restoration problem.

From this section onwards, all capacitor banks in the IEEE 16 bus system are assumed to be removed in order to lower the voltage enhancement. This will demonstrate the results of the restoration strategy more effectively since now, more loads are expected to be unserved during an interruption due to the absence of reactive generation from these capacitor banks. The effects of removing the capacitor banks in the voltage profile is shown in Figure 5.7. Moreover, the pre-fault system configuration of all upcoming case studies is taken to be the optimal configuration shown in Figure 5.4. Note that the optimal configuration found in the previous section was also found to be the optimal configuration even after the removal the capacitor banks.

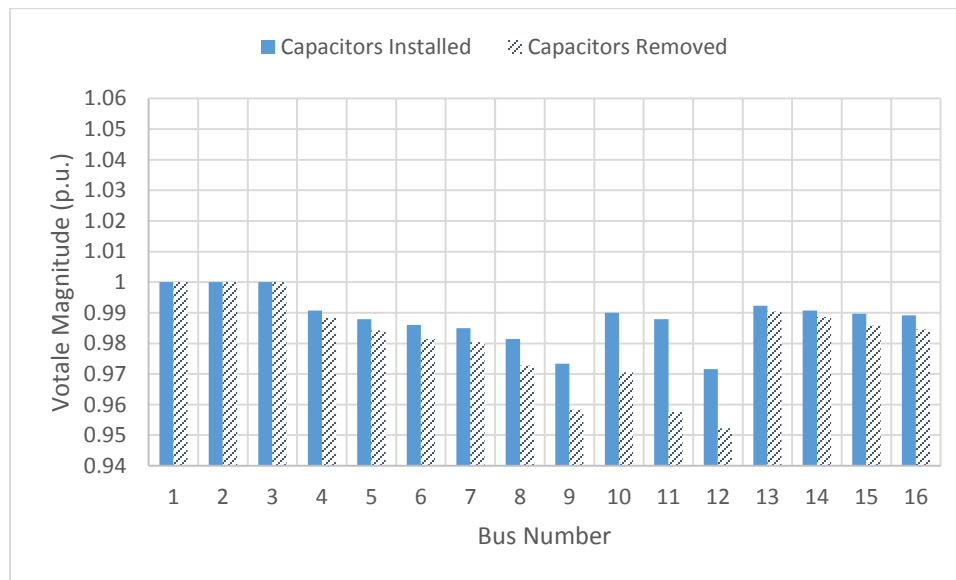


Figure 5.7 Effects of removing the capacitor banks on voltage profile

After running the load flow for the system at optimal configuration, it was found that feeder 2-8 is the most loaded feeder among the three. Thereby, it is assumed that a

sustained fault occurred at this particular feeder in order to test the system under high loaded emergency case as shown in Figure 5.8. The nodes within the dashed circle are the loads that are facing an interruption if no restoration is applied. Table 5.4 summarizes the fault incident.

Table 5.4 Fault at feeder 2-8

Fault Location	Disconnected Busses	Total Interrupted Load (MW)
Feeder 2-8	8, 9, 12	13.5

The process of finding the optimal system configuration for maximizing total restored load was then applied using the two formulation, the formulation in [68], and the proposed formulation. The final optimal configuration achieved from both formulations was similar and shown in Figure 5.9 where loads that are shed during service restoration are circled.

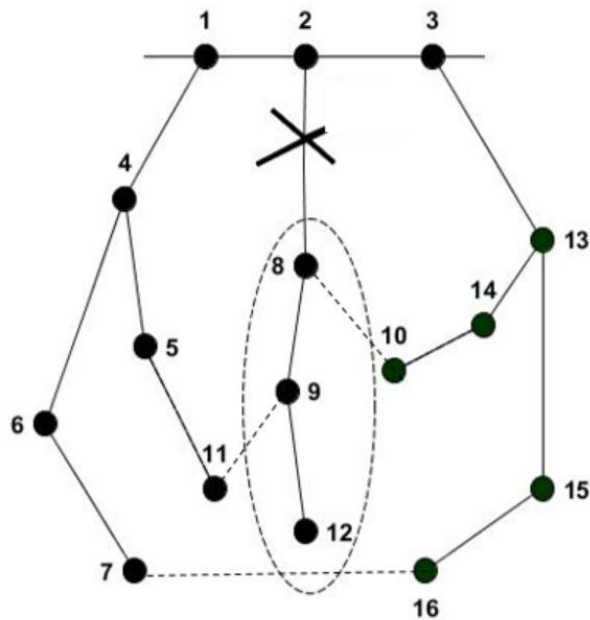


Figure 5.8 Fault incident at feeder 2-8

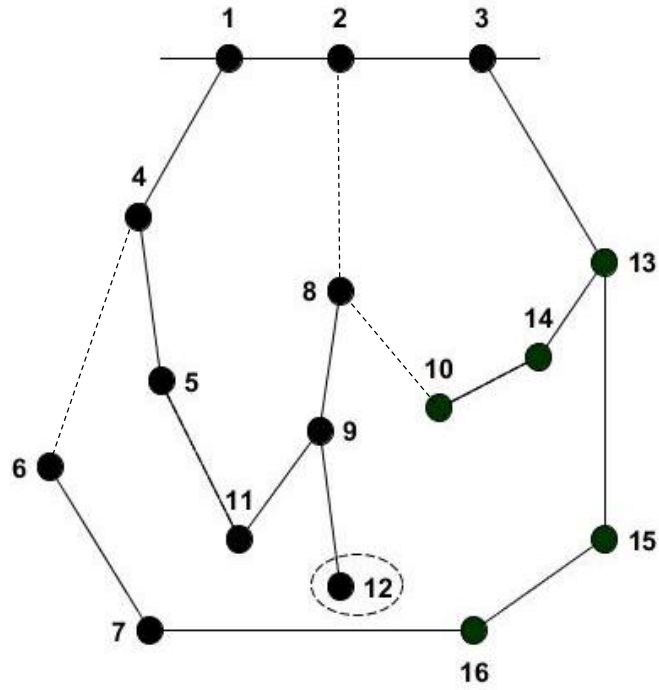


Figure 5.9 Optimal system configuration after service restoration

The summary of the restoration process is shown in Table 5.5. Figures 5.10 and 5.11 shows the voltage magnitudes and angles, respectively, obtained from both methods as well as the real value from load flow analysis after obtaining system configuration.

Table 5.5 Restoration process for fault at feeder 2-8

Switches to be open	Switches to be closed	Total restored load (MW)	Total interrupted load (MW)	Busses that are shed
$S_{4,6}$	$S_{7,16}$ $S_{9,11}$	9	4.5	12

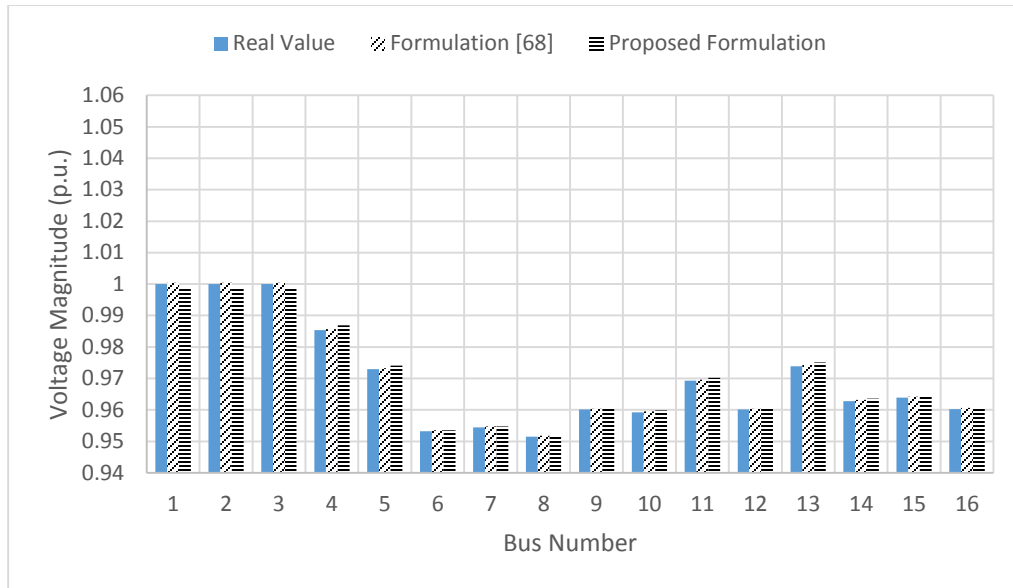


Figure 5.10 Comparison in voltage magnitude between method [68] and the proposed method

It can be seen from Figure 5.10 that the formulation in [68] is slightly more accurate than the proposed formulation, however, the computational time, in the other hand, improved substantially in the case of the proposed formulation as illustrated in Table 5.6.

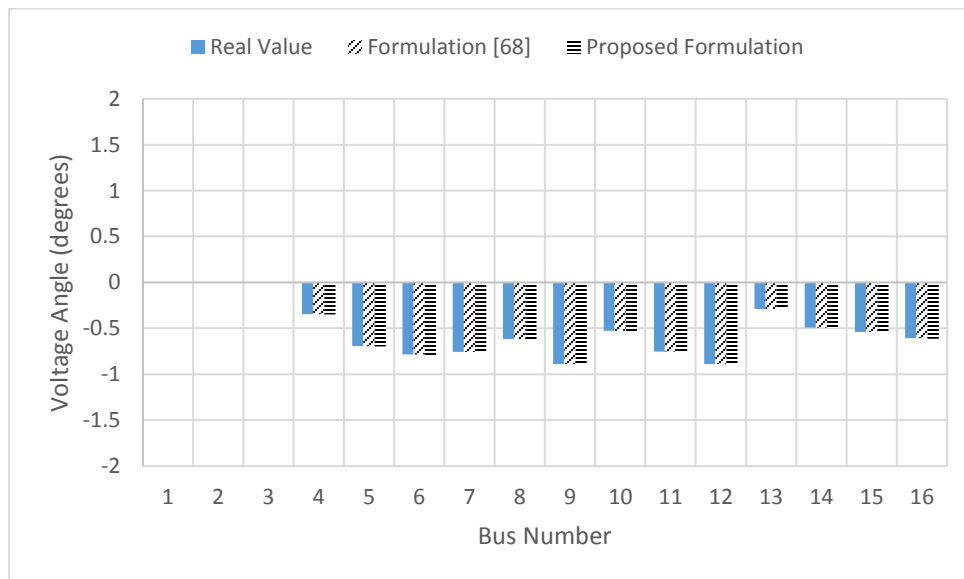


Figure 5.11 Comparison in voltage angle between method [68] and the proposed method

Table 5.6 Computational time comparison

Formulation [68] (sec)	Proposed formulation (sec)	Computational time reduction (%)
45.10	4.25	90.6

This difference in computational time was caused by the branch and bound process in the solution of the MILP problem. Figure 5.12 shows the process of finding the optimal solution when using the formulation in [68]. It can be seen the number of nodes explored in order to find the solution is huge ≈ 9100 compared to the proposed formulation ≈ 75 shown in Figure 5.13. The best objective (-0.242) shown in Figures 5.12 and 5.13 are related to the total supplied load after reconfiguration which is equal to 24.2 MW.

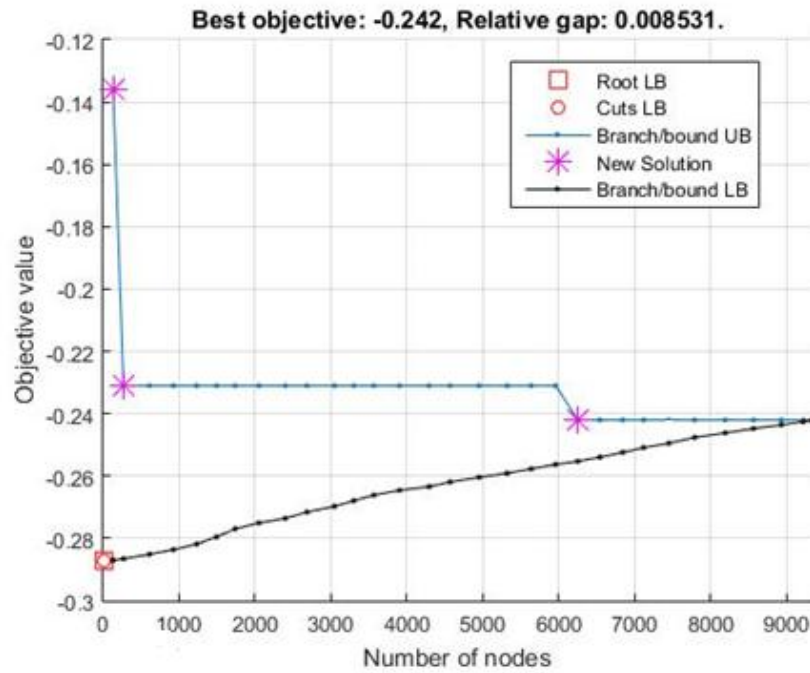


Figure 5.12 Solution process using formulation [68]

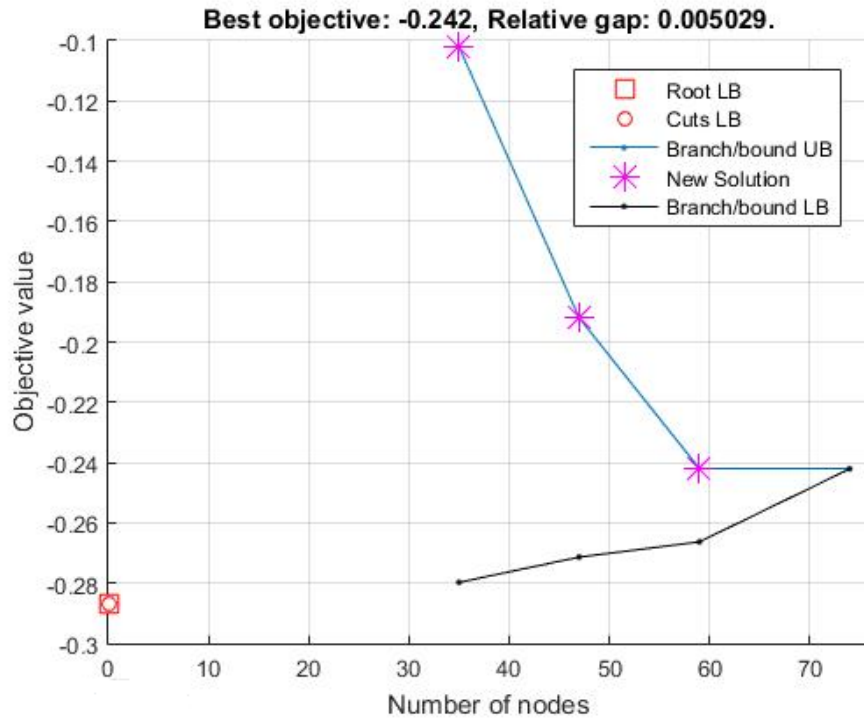


Figure 5.13 Solution process of the proposed formulation

It can be stated that, since the formulation in [68] results in slightly more accurate solutions, it is recommended to be used in system planning optimization problems where fast computational time is not as important as gaining an accurate solution. In the other hand, in operational optimization problems, such as the service restoration problem, the computational time is highly crucial and approximation in the results are considered accepted up to a certain limit. Thereby, it can be concluded that the proposed formulation is more suitable for the purpose of the thesis.

5.3 Testing the Prioritizing Methodology

The objective of this section is to analyze the proposed customer prioritizing method. Before illustrating the procedure of testing, it becomes convenient for the reader to recall the main equation of the proposed prioritizing methodology as follows:

$$PL^i(t) = L_{critic}^i(t) + w_{ENS} * L_{ENS}^{i,m}(t) + w_{SAIDI} * L_{SAIDI}^{i,m} + w_{SAIFI} * L_{SAIFI}^{i,m} + w_{cost} * L_{cost}^i(t) \quad (5.3)$$

$$w_{ENS} + w_{SAIDI} + w_{SAIFI} + w_{cost} = 1 \quad (5.4)$$

$PL^i(t)$: is the total priority weight of load i at hour t .

$L_{critic}^i(t)$, $L_{ENS}^{i,m}(t)$, $L_{SAIDI}^{i,m}$, $L_{SAIFI}^{i,m}$, and $L_{cost}^i(t)$ are weights associated with each load in the system.

w_{ENS} : is weight of ENS importance

w_{SAIDI} : is weight of SAIDI importance

w_{SAIFI} : is weight of SAIFI importance

w_{cost} : is weight of cost importance

Be reminded that the importance weights are set depending of the utilities decision and evaluation. For instance, if the recorder total energy not supplied (ENS) of the utility is very high, utilities will pay more attention when restoring the services to the expected ENS, thereby, give more weight to w_{ENS} . The same applies for all other weights. Hence,

by proving that these weights can be controlled by the utility to improve system reliability, the methodology is justified. This is the main goal of this section. Also, a comparison will be provided by studying a base case where the restoration is not depending on the presented prioritizing method. The prioritizing in this case will be depending only on the load amount of each customer where the objective of restoration is to maximum the restored load regardless to other factors. This case represents a traditional restoration procedure.

The case studies that will be presented are based on an entire year microgrid simulation. The following steps illustrates the process:

- 1) Assume a load type for each load in the IEEE 3 feeder 16 bus system (i.e residential, commercial, industrial).

Note that each load type has an assumed number of customers taken from [27] and an assumed cost of interruption taken from [40]. Loads information are shown in Table 5.7. All loads are assumed to be non-critical and not participating in DSM programs.

- 2) Produce hourly load curves for all loads depending on their type as presented in section 2.2.1.

This is achieved by multiplying the nominal demand for each load by the per unit load types yearly curves. Figure 5.14 shows the load curves for the first day of the year. These curves simulates the behavior of each load type.

- 3) Set values for the importance weights that are appearing in equation (5.4).
- 4) Simulate fail and repair incidents as illustrated in section 2.2.5.

Similar fail and repair times produced previously are used here and are shown in Table 5.8. At each incident, the fault locations is assumed to be at two feeders simultaneously in order to causes severe damage to the system. This will definitely show the impact of prioritizing more effectively since more loads are expected to be disconnected.

- 5) Optimize the restoration of the system using the proposed MILP formulation with the integration of the prioritizing method.

This step is done immediately after each fault incident.

- 6) Calculate system total ENS, SAIDI, SAIFI, and interruptions cost caused from all failure incidents in the simulated year.

Table 5.7 Load points information

Load Point	Load Type*	Number of Customers	Cost of Interruption per customer (\$/hr)	Criticality L_{critic}^i
4	1	210	3	0
5	2	10	750	0
6	1	210	3	0
7	1	210	3	0
8	2	10	750	0
9	2	10	750	0
10	3	1	15000	0
11	1	210	3	0
12	2	10	750	0
13	2	10	750	0
14	3	1	15000	0
15	3	1	15000	0
16	3	1	15000	0

*1: residential 2: commercial 3: Industrial

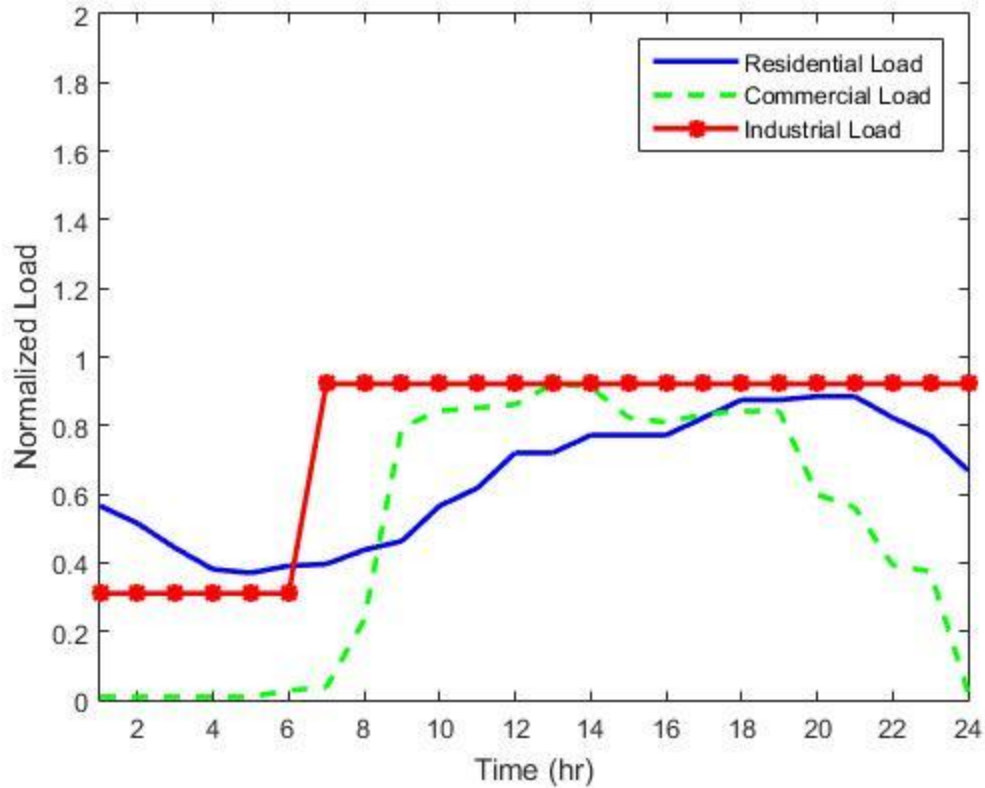


Figure 5.14 Load curves for each load type

Table 5.8 Intruption information

Fault No.	Date	From	To	Faulted Feeders
1	June 15	06:00 a.m.	10:00 a.m.	1-4,2-8
2	July 9	03:00 a.m.	10:00 a.m.	1-4,10-13
3	August 25	03:00 p.m.	08:00 p.m.	2-8,10-13
4	October 15	10:00 a.m.	03:00 p.m.	1-4,2-8
5	October 30	09:00 a.m.	12:00 p.m.	1-4,10-13
6	November 8	09:00 a.m.	03:00 p.m.	2-8,10-13

The case studies considered in this section are summarized in Table 5.9. Case 1 represents the base case, case 2-6 were obtained using the proposed method. Note that each case of cases 3, 4, 5, and 6 will have one dominant importance weight among the four in

order to clearly observe the effect of each weight separately. In other words, in each one of cases 3-6, the objective is set to minimize only one measure among ENS, SAIDI, SAIFI, and cost of interruption.

Table 5.9 Case studies

Case No.	Method of restoration prioritizing	w_{ENS}	w_{SAIDI}	w_{SAIFI}	w_{cost}
1	Base Case	N/A	N/A	N/A	N/A
2	Proposed Method	0.25	0.25	0.25	0.25
3		1	0	0	0
4		0	1	0	0
5		0	0	1	0
6		0	0	0	1

All previously mentioned faults in Table 5.8 are studied and applied at each case in Table 5.9 yielding a total of 36 restoration simulation. Note that the pre-fault system configuration was taken to be the optimal for loss reduction obtained in section 5.1. Also, the radiality constraint holds in all restoration process. The comparison between all cases will be based on system total ENS, SAIDI, SAIFI, and interruptions cost for the simulated year. The restoration optimization result for each case are shown in Tables 5.10-5.15 including the switching configuration and the recorded ENS, SAIDI, SAIFI and Cost of interruption for each fault incident. Moreover, Figures 5.15-5.18 show a comparison between all cases in terms of total ENS, SAIDI, SAIFI, and cost of interruption. These values are tabulated in Table 5.16 with the indication of maximum improvement achieved by using the proposed method.

Table 5.10 Case 1 simulation results

Fault No.	Switches to be open after restoration	Lost load points	ENS (MWh)	SAIDI (hrs)	SAIFI	COST (\$)	cpu time
1	$S_{1,4}, S_{2,8}, S_{5,11}$	4,6,8,10,12	29.3	1.973	0.493	125,040	7.23
2	$S_{1,4}, S_{3,13}, S_{7,16}$	4,6,7,11,15	21.87	6.585	0.941	122,640	3.63
3	$S_{2,8}, S_{3,13}, S_{10,14}$	8,11,12	35.95	1.286	0.257	78,150	5.48
4	$S_{1,4}, S_{2,8}, S_{9,11}$	4,6,8,11,12	52.44	3.635	0.727	84,450	9.23
5	$S_{1,4}, S_{4,6}, S_{3,13}$	5,6,7,11,13,15	26.11	2.185	0.728	95,670	5.42
6	$S_{2,8}, S_{3,13}, S_{13,15}$	8,10,12,13,14	70.87	0.215	0.036	315,000	4.5
Total	-	29	236.5	15.88	3.182	820,950	35.5

Table 5.11 Case 2 simulation results

Fault No.	Switches to be open after restoration	Lost Load Points	ENS (MWh)	SAIDI (hrs)	SAIFI	COST (\$)	cpu time
1	$S_{1,4}, S_{2,8}, S_{4,5}$	5,9,12	24.84	0.134	0.034	90,000	4.11
2	$S_{1,4}, S_{3,13}, S_{7,16}$	9,12	17.48	0.157	0.022	105,000	3.25
3	$S_{2,8}, S_{3,13}, S_{13,14}$	8,9	36.04	0.112	0.022	75,000	2.64
4	$S_{1,4}, S_{2,8}, S_{9,11}$	5,8,9	53.74	0.168	0.034	112,500	1.81
5	$S_{1,4}, S_{6,7}, S_{3,13}$	5,12,13,16	36.54	0.104	0.035	112,500	3.45
6	$S_{2,8}, S_{3,13}, S_{13,14}$	8,9,12	81.9	0.201	0.034	135,000	3.95
Total	-	17	250.5	0.876	0.18	630,000	19.2

Table 5.12 Case 3 simulation results

Fault No.	Switches to be open after restoration	Lost Load Points	ENS (MWh)	SAIDI (hrs)	SAIFI	COST (\$)	cpu time
1	$S_{1,4}, S_{2,8}, S_{8,9}$	5,9,12	24.84	0.134	0.034	90,000	5.69
2	$S_{1,4}, S_{3,13}, S_{6,7}$	5,13,15	12.04	0.164	0.023	210,000	3.08
3	$S_{2,8}, S_{3,13}, S_{10,14}$	8,11,12	35.95	1.286	0.257	78,150	5.2
4	$S_{1,4}, S_{2,8}, S_{9,11}$	4,6,8,11,12	52.44	3.635	0.727	84,450	3.19
5	$S_{1,4}, S_{7,16}, S_{3,13}$	4,5,7,11,13,15	26.11	2.185	0.728	95,670	5.17
6	$S_{2,8}, S_{3,13}, S_{8,9}$	7,8,12,13,14	70.37	1.617	0.27	228,780	11
Total	-	25	221.8	9.022	2.039	787,050	33.4

Table 5.13 Case 4 simulation results

Fault No.	Switches to be open after restoration	Lost Load Points	ENS (MWh)	SAIDI (hrs)	SAIFI	COST (\$)	cpu time
1	$S_{1,4}, S_{2,8}, S_{5,11}$	9,10,12,14,15,16	40.11	0.107	0.027	300,000	5.61
2	$S_{1,4}, S_{3,13}, S_{6,7}$	9,16	19.04	0.086	0.012	157,500	3.09
3	$S_{2,8}, S_{3,13}, S_{13,14}$	8,9	36.04	0.112	0.022	75,000	3.31
4	$S_{1,4}, S_{2,8}, S_{5,11}$	5,9,12	55.98	0.168	0.034	112,500	4.36
5	$S_{1,4}, S_{4,6}, S_{3,13}$	9,10,14,15,16	36.04	0.047	0.016	202,500	2.09
6	$S_{2,8}, S_{3,13}, S_{13,14}$	9,10,12,14	70.87	0.148	0.025	270,000	2.81
Total	-	22	258.1	0.67	0.135	1,117,500	21.3

Table 5.14 Case 5 simulation results

Fault No.	Switches to be open after restoration	Lost Load Points	ENS (MWh)	SAIDI (hrs)	SAIFI	COST (\$)	cpu time
1	$S_{1,4}, S_{2,8}, S_{5,11}$	9,10,12,14,15,16	40.11	0.107	0.027	300,000	6.05
2	$S_{1,4}, S_{3,13}, S_{6,7}$	9,16	19.04	0.086	0.012	157,500	2.67
3	$S_{2,8}, S_{3,13}, S_{13,14}$	8,9	36.04	0.112	0.022	750,00	3.41
4	$S_{1,4}, S_{2,8}, S_{5,11}$	5,9,12	55.98	0.168	0.034	112,500	4.19
5	$S_{1,4}, S_{4,6}, S_{3,13}$	9,10,14,15,16	36.04	0.047	0.016	202,500	2.34
6	$S_{2,8}, S_{3,13}, S_{13,14}$	9,10,12,14	70.87	0.148	0.025	270,000	2.95
Total	-	22	258.1	0.668	0.135	1,117,500	21.6

Table 5.15 Case 6 simulation results

Fault No.	Switches to be open after restoration	Lost Load Points	ENS (MWh)	SAIDI (hrs)	SAIFI	COST (\$)	cpu time
1	$S_{1,4}, S_{2,8}, S_{9,11}$	4,6,7,9,12	30.21	2.908	0.727	67,560	5.17
2	$S_{1,4}, S_{3,13}, S_{7,16}$	9,12	17.48	0.157	0.022	105,000	3.8
3	$S_{2,8}, S_{3,13}, S_{10,14}$	9,12	38.04	0.112	0.022	75,000	3.61
4	$S_{1,4}, S_{2,8}, S_{5,11}$	4,6,9,12	55.05	2.461	0.492	81,300	2.86
5	$S_{1,4}, S_{15,16}, S_{3,13}$	4,5,6,7,9	38.85	2.181	0.727	50,670	2.58
6	$S_{2,8}, S_{3,13}, S_{13,14}$	8,9,12	81.9	0.201	0.034	135,000	2.97
Total	-	21	261.5	8.02	2.025	514,530	21

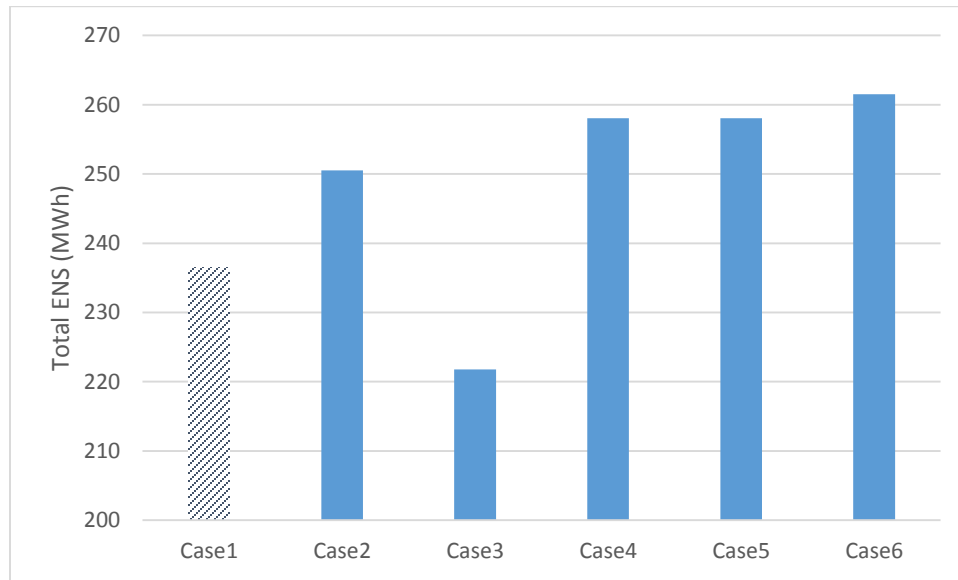


Figure 5.15 ENS comparison between all cases - dashed bar for base case - solid bar for proposed method

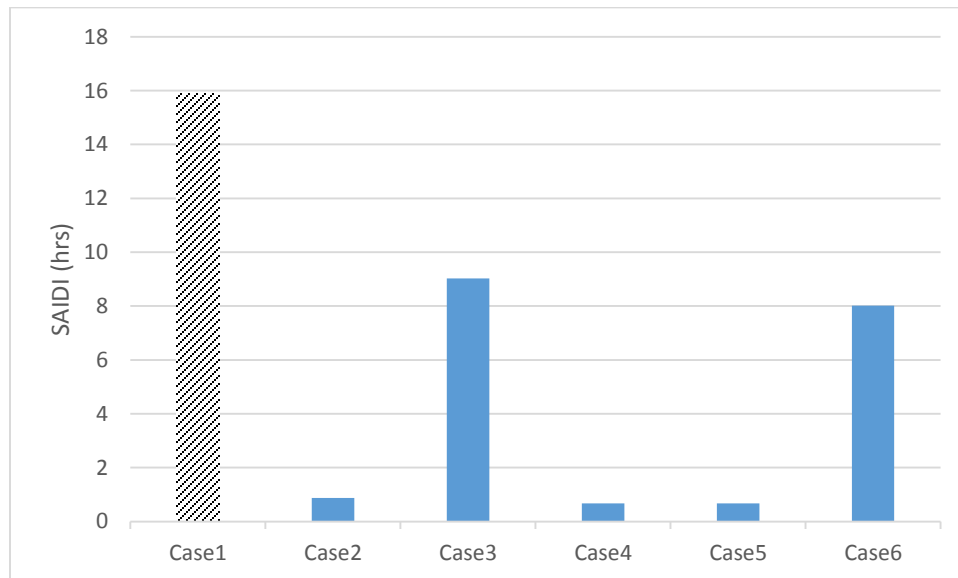


Figure 5.16 SAIDI comparison between all cases - dashed bar for base case - solid bar for proposed method

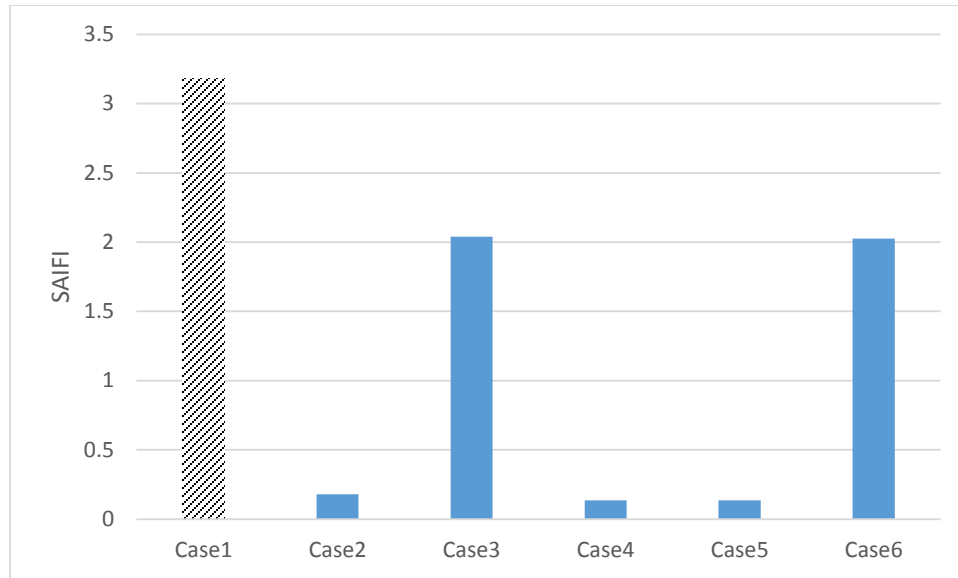


Figure 5.17 SAIIFI comparison between all cases - dashed bar for base case - solid bar for proposed method

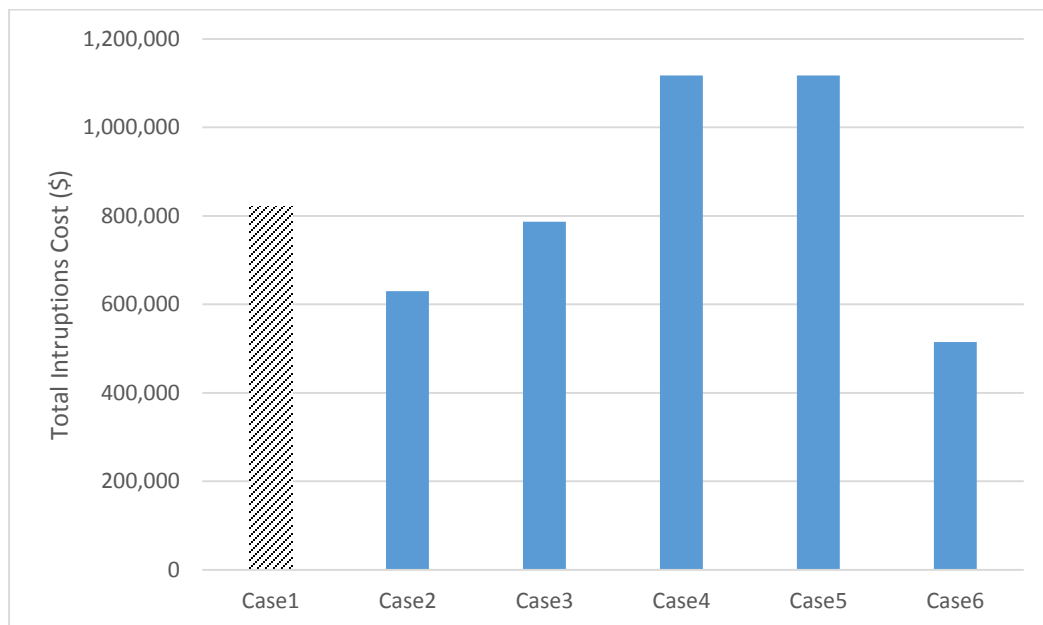


Figure 5.18 Interruption cost comparison between all cases - dashed bar for base case - solid bar for proposed method

Table 5.16 Summary of results

Method	Case No.	ENS (MWh)	SAIDI (hrs)	SAIFI	COST (\$)
Base Case	1	236.5	15.88	3.182	820,950
Proposed Method	2	250.5	0.876	0.18	630,000
	3	221.8	9.022	2.039	787,050
	4	258.1	0.668	0.135	1,117,500
	5	258.1	0.668	0.135	1,117,500
	6	261.5	8.02	2.025	514,530
Max. Reduction (%)	-	6.2%	95.8%	95.8%	37.3%

It can be seen from Table 5.16 that by using the proposed prioritizing method in restoration, an improvement was recorded in each one of the four measures, ENS, SAIDI, SAIFI, and COST. The largest reduction was achieved in SAIDI and SAIFI indices. This is due to the fact that the prioritizing in the base case was only depending on the load amount regardless to the number of customers. Also, note that the reduction in SAIDI is exactly the same as the reduction in SAIFI because they both depend on the number of customers. Thereby, minimizing SAIDI will automatically minimize SAIFI with the same ratio, and vice versa (refer to equations 3.1 and 3.2). Furthermore, it can be observed from comparing case 2 with the base case that by setting equal importance weights for ENS, SAIDI, SAIFI and COST, an improvement is achieved in all measures except a small increase in ENS. However, case 3 showed an improvement in all four evaluation measures.

It can be concluded that by using the proposed method and manipulating the importance weights, utilities can improve the figure of reliability in restoration. Also, utilities can decide and control specifically what measure to be improved in each restoration process. Although the proposed method was generally able to improve all measures, however, the percent of reduction and the importance weights to be set depend

on the system analyzed and the loads connected. Thereby, studies must be made for each system before applying the method in order to find the optimum weights and the corresponding improvement. This topic is listed among possible future work where it is required to set the best weights that will guarantee a certain reliability requirement for a utility or an individual system.

5.4 Comparing Conventional Distribution System with Smart Microgrid System

Two main case studies will be illustrated in this section. One considering a conventional distribution system and the other simulating the functioning of a smart microgrid. The studies will be applied on the IEEE 3 feeder 16 bus system. All simulated faults will be considered to occur during the nominal load value. Also, the MTTR for any faulted branch is assumed to be 5 hours. The calculated priority weights for each load are shown in Table 5.17. These priority weights were obtained considering equal importance weights for ENS, SAIDI, SAIFI, and interruption cost and using the load information previously shown in Table 5.7.

Three faults will be studied in each case simulating three levels of emergency as shown in Table 5.18. Note that at fault C, all feeders are disconnected and the system is left without any supplied power from the grid. The pre-fault configuration in all cases is taken to be the optimal for loss reduction shown in Figure 5.4. Also, the permissible voltage limit is taken to be $0.95 \leq V \leq 1.05$. In each fault incident, ENS, SAIDI, SAIFI and the interruption cost will be calculated and a comparison between the two main cases will be drawn at the end of this section.

Table 5.17 Load point priority weights

Load Point	Priority weight PL^i
4	0.6105
5	0.2988
6	0.6105
7	0.5855
8	0.3488
9	0.3988
10	0.3024
11	0.5405
12	0.3738
13	0.1988
14	0.3024
15	0.3024
16	0.3574

Table 5.18 Fault incidents

	Location	MTTR (hrs)
Fault A	Feeder 1-4	5
Fault B	Feeders 1-4 & 2-8	5
Fault C	Feeders 1-4, 2-8, & 3-13	5

5.4.1 Case 1 – Conventional Distribution System

In this case of study, the system is taken to be an ordinary distribution system where the following points are assumed:

- 1) No DG is connected.
- 2) All customers are not participating in any kind of DSM programs.
- 3) The radiality constraint holds where no loops are allowed.

Fault A: One feeder out of service

The configuration of the system after restoration from fault A is shown in Figure 5.19. The circled loads are those completely shed at the restoration process. Two loads were shed, these are load 5 and load 8. In total, 24.4% of the system load was interrupted. Although load 4 is further away from the source than the interrupted loads, however, it was restored due to its high priority weight compared to loads 5 and 8 (refer to Table 5.17).

Table 5.19 shows detailed results including the ENS, SAIDI, SAIFI, and total cost of interruption of the fault, as well as the optimization computational time. The results of voltage magnitudes and angles after restoration are shown in Figures 5.20 and 5.21, respectively including the MILP result and actual results from load flow analysis. All bus voltages were within the specified permissible limits after the process of restoration.

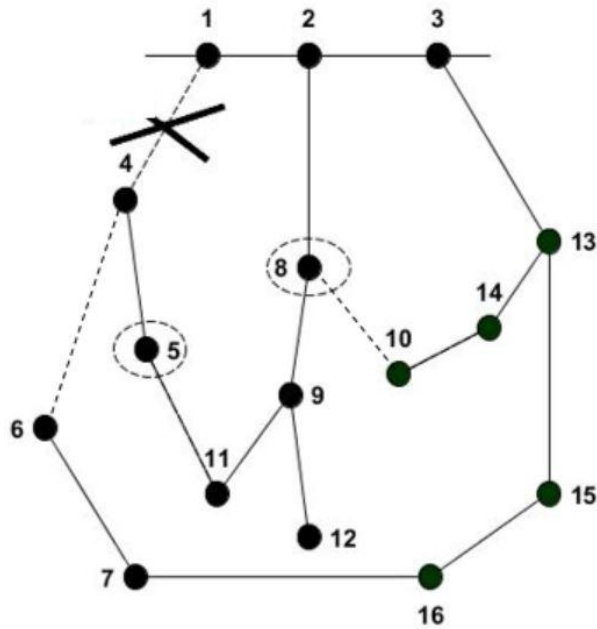


Figure 5.19 Restoration configuration result - case 1 - fault A

Table 5.19 Interruption results - case 1 - fault A

Fault	Lost Load Points	ENS (MWh)	SAIDI (hrs)	SAIFI	Interruption Cost (\$)	CPU time (sec)
-------	------------------	-----------	-------------	-------	------------------------	----------------

A	5,8	35	0.1118	0.0224	75,000	4.78
---	-----	----	--------	--------	--------	------

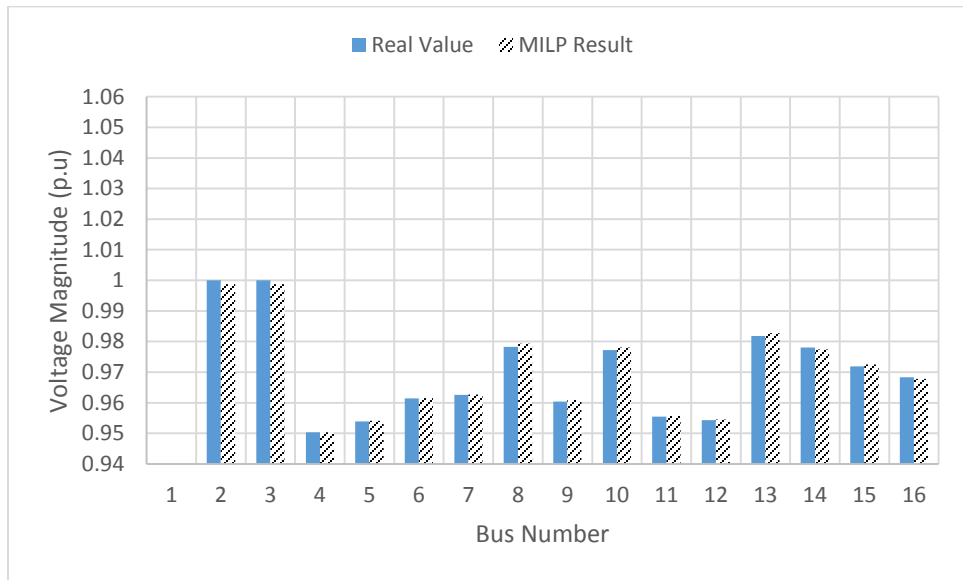


Figure 5.20 Voltage magnitudes - case 1 - fault A

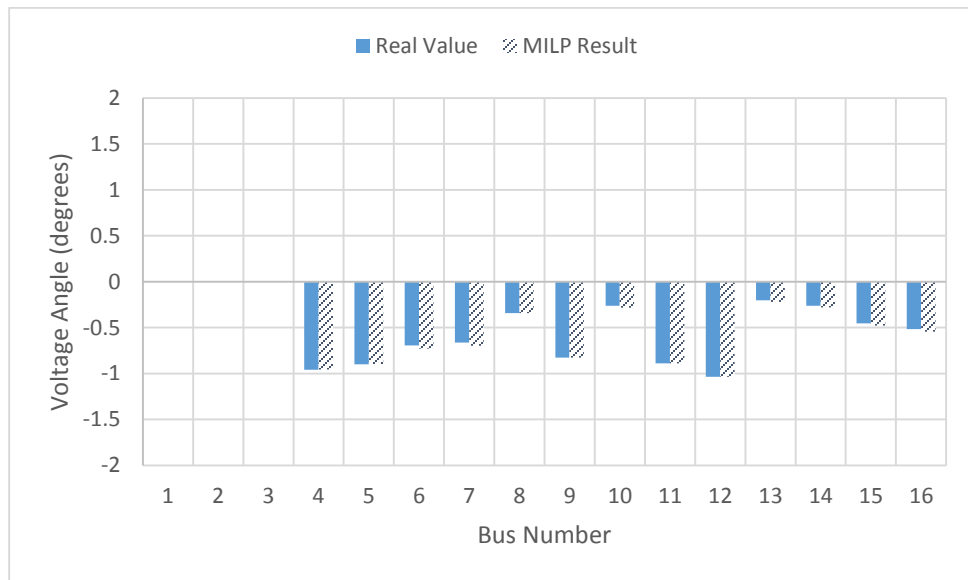


Figure 5.21 Voltage angles - case 1 - fault A

Fault B: Two feeders out of service

The conventional system in this case is at a higher emergency level than the previous one due to the loss of two feeders. The obtained configuration of the system after restoration using MILP formulation from fault B is shown in Figure 5.22. 40% of the total system load was restored where 5 loads were completely shed.

Table 5.20 shows detailed results including the ENS, SAIDI, SAIFI, and total cost of interruption of the fault, as well as the optimization computational time. The results of voltage magnitudes and angles after restoration are shown in Figures 5.23 and 5.24. All bus voltages were within the specified permissible limits after the process of restoration.

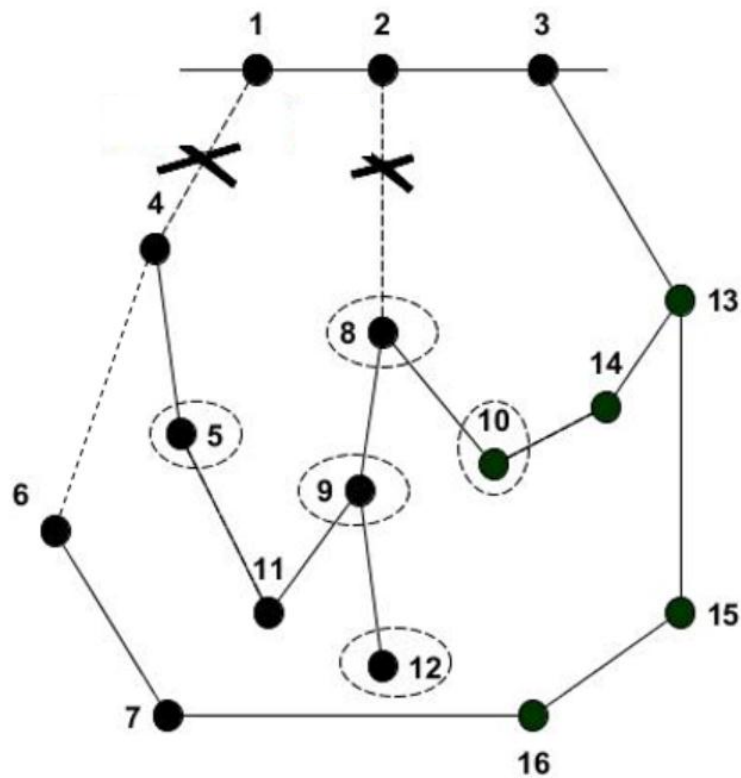


Figure 5.22 Restoration configuration result - case 1 – fault B

Table 5.20 Interruption results - case 1 - fault B

Fault	Lost Load Points	ENS (MWh)	SAIDI (hrs)	SAIFI	Interruption Cost (\$)	CPU time (sec)
B	5,8,9,10,12	87.5	0.2293	0.04586	225,000	8.38

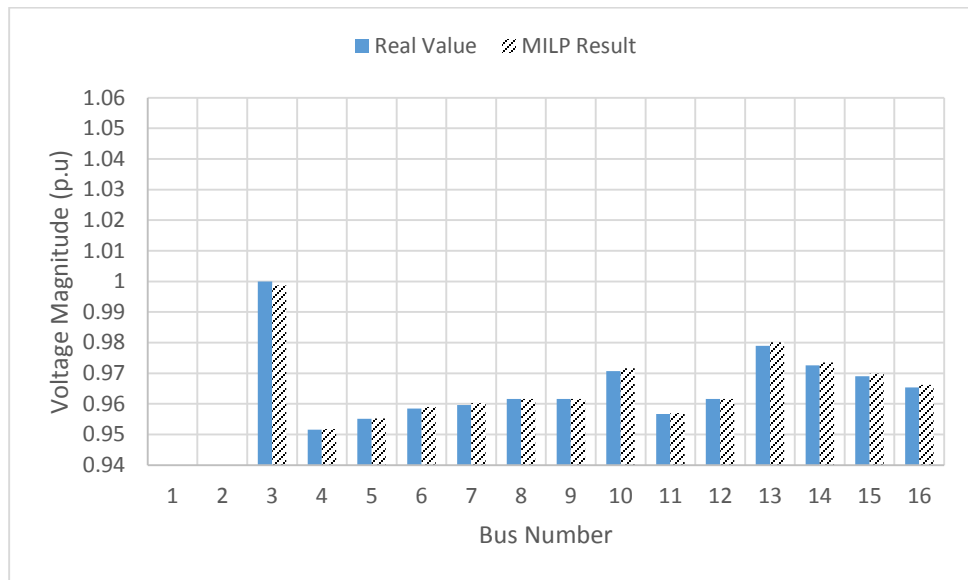


Figure 5.23 Voltage magnitudes - case 1 - fault B

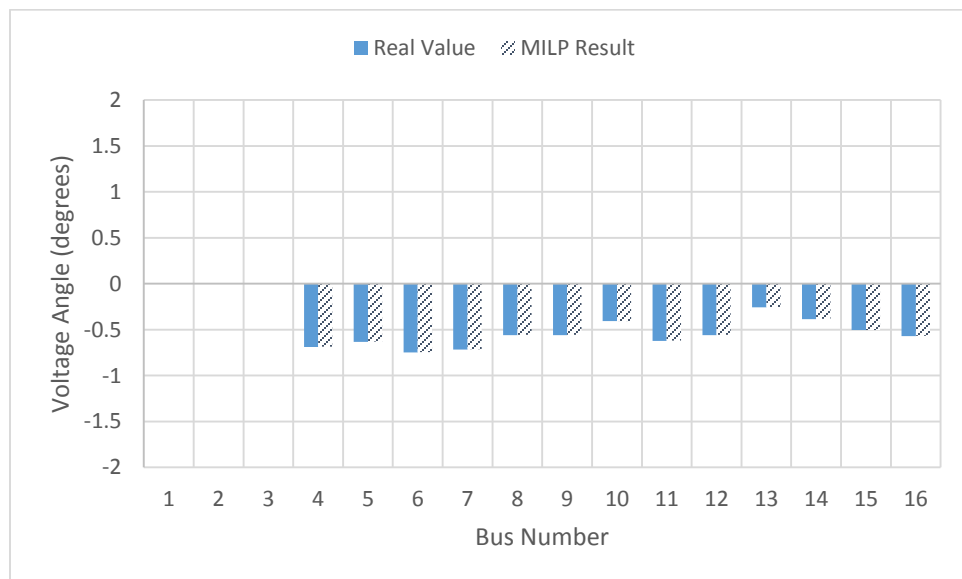


Figure 5.24 Voltage angles - case 1 - fault B

Fault C: Three feeders out of service

This case simulates a complete blackout, where all loads in the system are disconnected. Table 5.20 shows detailed results including the ENS, SAIDI, SAIFI, and total cost caused from the interruption.

Table 5.21 Interruption results - case 1 - fault C

Fault	Lost Load Points	ENS (MWh)	SAIDI (hrs)	SAIFI	Interruption Cost (\$)	CPU time (sec)
C	All Loads	143.5	5	1	500,100	-

This case was studied in order to be used in the comparison part between the conventional and the smart microgrid systems. It is desirable to observe how the smart microgrid that contains DGs, will operate under the situation of a blackout.

5.4.2 Case 2 – Microgrid Operation

In this case of study, the system is considered to be a smart microgrid where the following is assumed:

- 1) Two controllable DGs are connected to the system. Their assumed locations, ratings and cost of generation are shown in Table 5.22. Their total size is 38.5% of total system load.
- 2) Residential loads 4, 6, 7, and 11 are assumed to be participating in curtailment programs where, instead of totally shedding their loads, there loads can be controlled and reduced up to a certain limit as shown in Table 5.23. The curtailment is associated with an assumed cost per MWh of curtailment as shown in Table 5.23.
- 3) Meshed operation is allowed.

4) Islanding mode operation is allowed.

Table 5.22 Connected DGs data

DG	Location	Rated (MVA)	Cost of Operation C_k^{DG} (\$/MWh)
1	Node 9	7	150
2	Node 16	5	100

Table 5.23 Curtailed loads data

DSM Node	Max. Curtailment (%) of nominal load value	Cost of Curtailment C_k^{LC} (\$/MWh)
Node 4	25	200
Node 6	25	200
Node 7	25	200
Node 11	25	200

The same fault incidents shown in Table 5.18 are assumed in this case. Note that the weights of the objective function (4.153) related to the DGs and LC cost were assigned to be equal and very low compared to the weight of the other objective function that is related to load priorities ($\omega_{DG,cost}^{Obj} = \omega_{LC,cost}^{Obj} \ll \omega_{priority}^{Obj}$). Assigning the exact weights will depend on the user decision and how important is restoring loads compared to the cost of operation. However, since the main purpose of this thesis is self-healing, and restoring customers is highly crucial, this approach was considered. This will guarantee the restoration of as much customers as possible. The cost of DGs and LC is by that, considered as a second level of optimization.

Fault A: One feeder out of service

The configuration of the microgrid system after restoration from fault A is shown in Figure 5.25. All loads were completely restored without the need of curtailment or DGs active power output. As can be seen from Table 5.24, the DGs were used only to supply reactive power and to enhance the voltage profile of the microgrid to be within the permissible limits. Thereby, the operational cost of the DGs is equal to zero since their cost is assumed to be dependent on only active power output. As indicated in Table 5.25, zero ENS, SAIDI, SAIFI, and interruption cost was recorded since all loads were completely restored. Both bus voltage magnitudes and angles after restoration are shown in Figures 5.26 and 5.27, respectively.

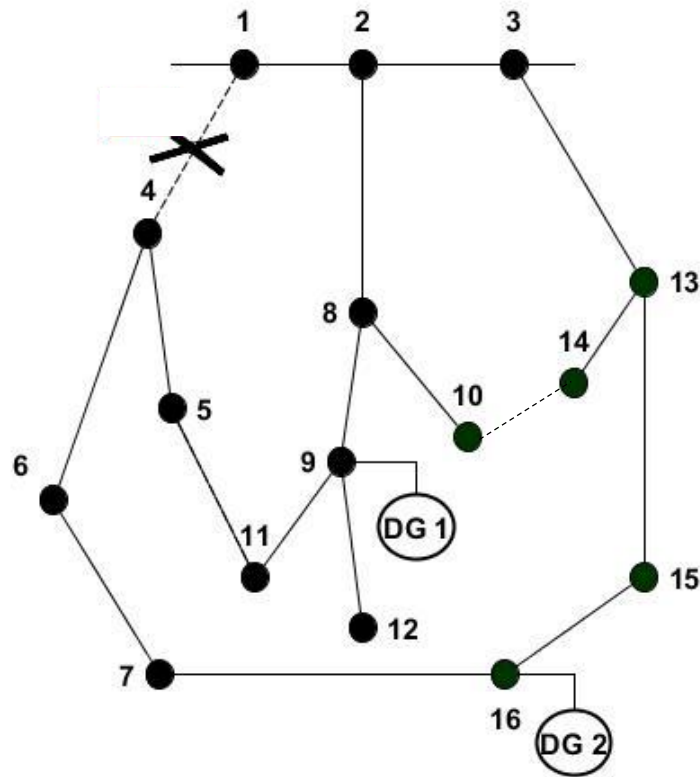


Figure 5.25 Restoration configuration result - Case 2 – Fault A

Table 5.24 DG outputs – case 2 – fault A

	DG Active Power Output (MW)	DG Reactive Power Output (MVAR)	DG Apparent Power Output (MVA)	Total DGs Operational Cost across MTTR (\$)
DG 1	0	3.7	3.7	0
DG 2	0	3.2	3.2	0
Total	0	6.9	6.9	0

Table 5.25 Interruption results - case 2 - fault A

Fault	Lost Load Points	ENS (MWh)	SAIDI (hrs)	SAIFI	Interruption Cost (\$)	Operational Cost (\$)	CPU time (sec)
A	None	0	0	0	0	0	3.02

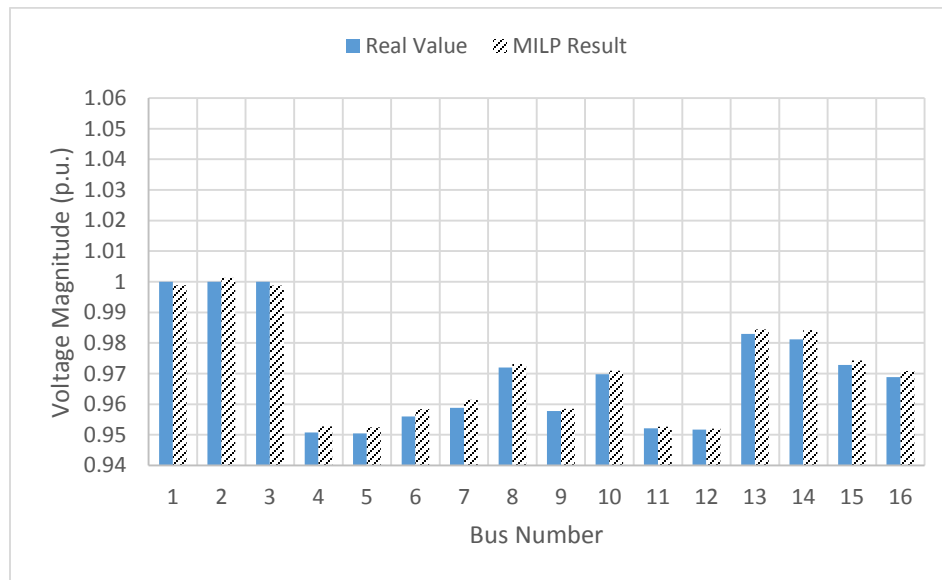


Figure 5.26 Voltage magnitudes - case 2 - fault A

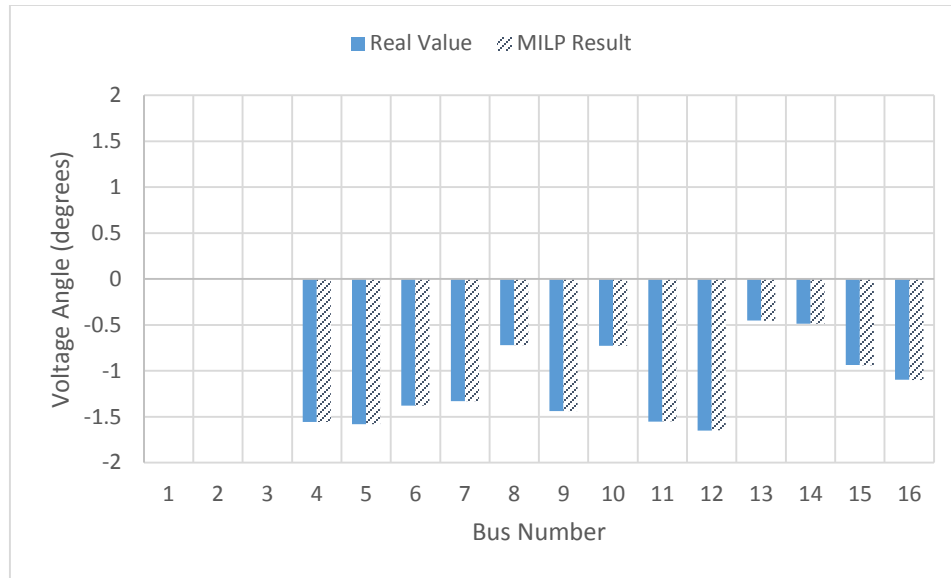


Figure 5.27 Voltage angles - case 2 - fault A

Fault B: Two feeders out of service

The configuration of the microgrid system after restoration from fault B is shown in Figure 5.28. Nodes with a line crossing them represent curtailed customers. In this case, load 9 was disconnected and both DGs were operating near their maximum power limits as can be seen from Table 5.26. Moreover, residential loads participating in curtailment programs were all curtailed up to the maximum limit as shown in Table 5.27.

Table 5.28 shows detailed reliability results including the ENS, SAIDI, SAIFI, and total cost of interruption of the fault, as well as the optimization computational time. The total operational cost is also indicated in Table 5.28 which is the combination of DGs output and the load curtailment cost. Note that there is a difference between the interruption cost and the load curtailment cost. The former is considered much greater, and it depends on the duration of the interruption. This basically represents the loss of economic activities or loss

of comfort caused from the interruption. However, the latter cost represents the compensation provided from the utility to the curtailed customers and it depends on the energy not served. The results of voltage magnitudes and angles after restoration are shown in Figures 5.29 and 5.30. All bus voltages were within the specified permissible limits after the process of restoration.

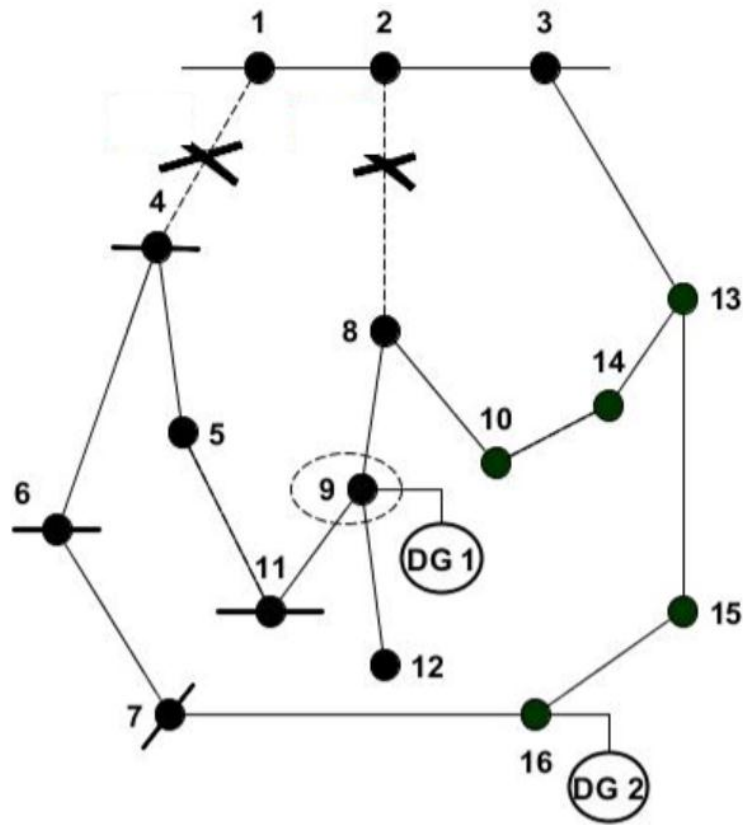


Figure 5.28 Restoration configuration result - case 2 – fault B

Table 5.26 DG outputs – case 2 – fault B

	DG Active Power Output (MW)	DG Reactive Power Output (MVAR)	DG Apparent Power Output (MVA)	Total DGs Operational Cost across MTTR (\$)
DG 1	5.4	4.4	7	4,050
DG 2	2.9	4	4.9	1,450
Total	8.3	8.4	11.9	5,500

Table 5.27 Curtailment data – case 2 – fault B

	Curtailed Power (MW)	Curtailment % of Nominal Load	Total Curtailment Cost across MTTR (\$)
Load 4	0.5	25	500
Load 6	0.5	25	500
Load 7	0.37	24.7	370
Load 11	0.15	25	150
Total	0.55	-	1,520

Table 5.28 Interruption results - case 2 - fault B

Fault	Lost Load Points	ENS (MWh)	SAIDI (hrs)	SAIFI	Interruption Cost (\$)	Operational Cost (\$)	CPU time (sec)
B	9	27.75	0.0559	0.0112	37,500	7,020	4.78

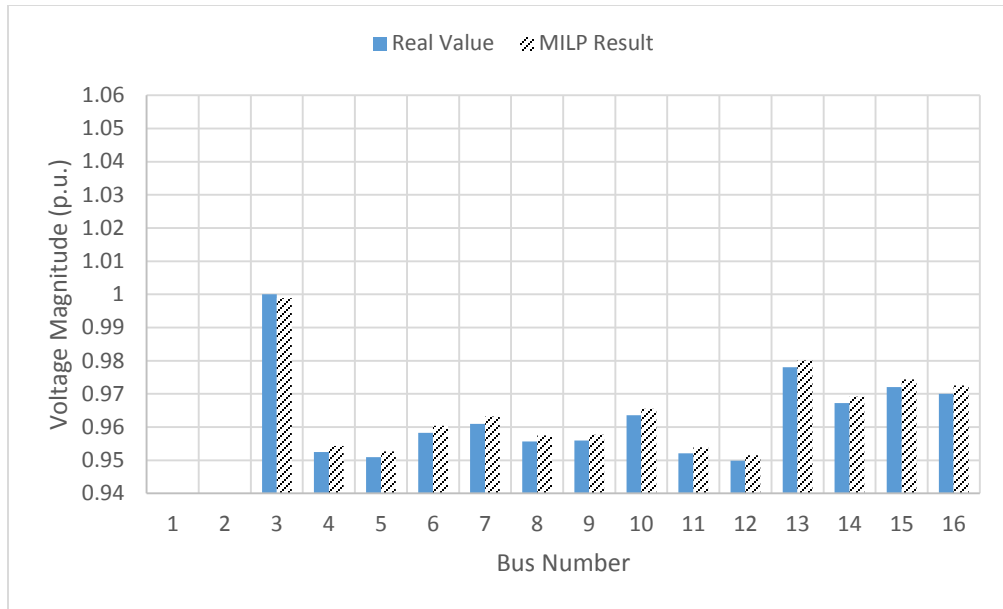


Figure 5.29 Voltage magnitudes - case 2 - fault B

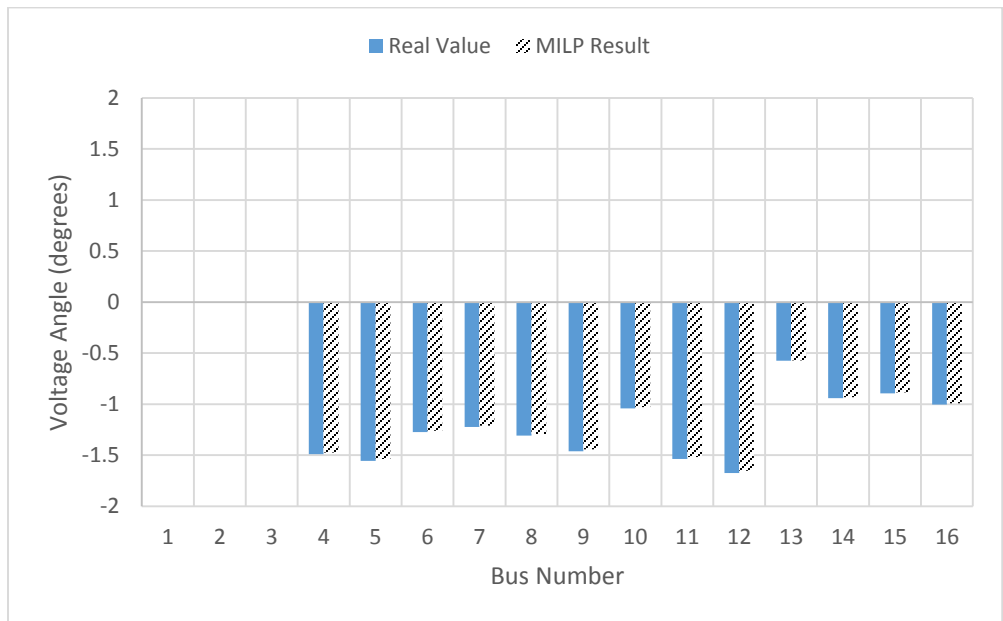


Figure 5.30 Voltage angles - case 2 - fault B

Fault C: Three feeders out of service

In this case, all feeders are out of service and the DGs are considered the only available source of energy. Be reminded that both DGs are assumed to be controllable in terms of active and reactive power, thereby, they are able to control their bus voltage as well. After the occurrence of fault on the three feeders, simultaneously, the system was isolated from the grid and operated in islanding mode as can be seen from configuration of the microgrid system after restoration in Figure 5.31. Due to the fact that this is a high emergency situation, both DGs were operating at their rated limits as seen in Table 5.29. Five loads were completely shed out summing to be 61% of total system load. Also, all residential loads faced an action of curtailment as illustrated in Table 5.30. It can be seen from Table 5.30 that some loads still have allowable range of curtailment since the maximum is set to 25% of nominal load. However, the total remaining allowed curtailment from all residential loads sums to be 0.13MW which cannot satisfy any disconnected load. Thereby, in order to minimize the operational cost, this remaining amount was not curtailed.

Table 5.31 shows detailed reliability results including the ENS, SAIDI, SAIFI, and total cost of interruption of the fault, as well as the optimization computational time. Also, the operational cost is indicated in the same table. The results of voltage magnitudes and angles after restoration are shown in Figures 5.32 and 5.33, respectively. It can be observed that the variation in voltage magnitude is less than the previous cases since only 34% of total loads are supplied. Another reason is that sources now are near load points which

minimizes the voltage drops. This simulates one of the important advantages of DGs in a microgrid system.

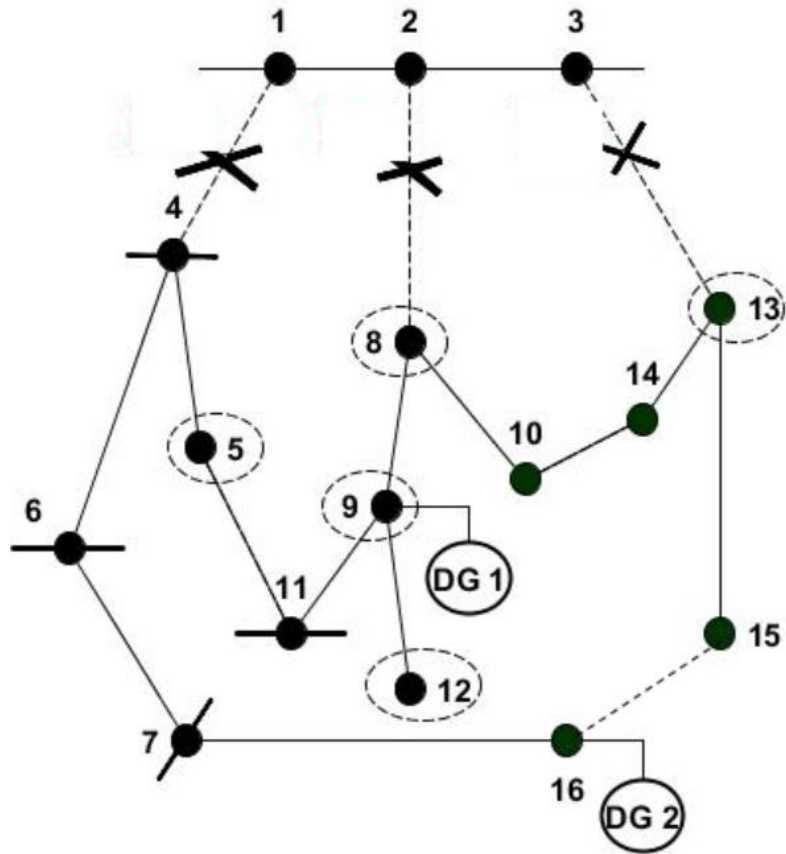


Figure 5.31 Restoration configuration result - case 2 – fault C

Table 5.29 DG Outputs – case 2 – fault C

	DG Active Power Output (MW)	DG Reactive Power Output (MVAR)	DG Apparent Power Output (MVA)	Total DGs Operational Cost across MTTR (\$)
DG 1	5.3	4.5	7	3,975
DG 2	4.6	1.9	5	2,250
Total	9.9	6.4	12	6,225

Table 5.30 Curtailment data – case 2 – fault C

	Curtailed Power (MW)	Curtailment % of Nominal Load	Total Curtailment Cost across MTTR (\$)
Load 4	0.5	25	500
Load 6	0.4	20	400
Load 7	0.37	24.7	370
Load 11	0.12	20	120
Total	1.39	-	1,390

Table 5.31 Interruption results - case 2 - fault C

Fault	Lost Load Points	ENS (MWh)	SAIDI (hrs)	SAIFI	Interruption Cost (\$)	Operational Cost (\$)	CPU time (sec)
C	5,8,9,12,13	94.45	0.2796	0.0559	187,500	7,615	4.73

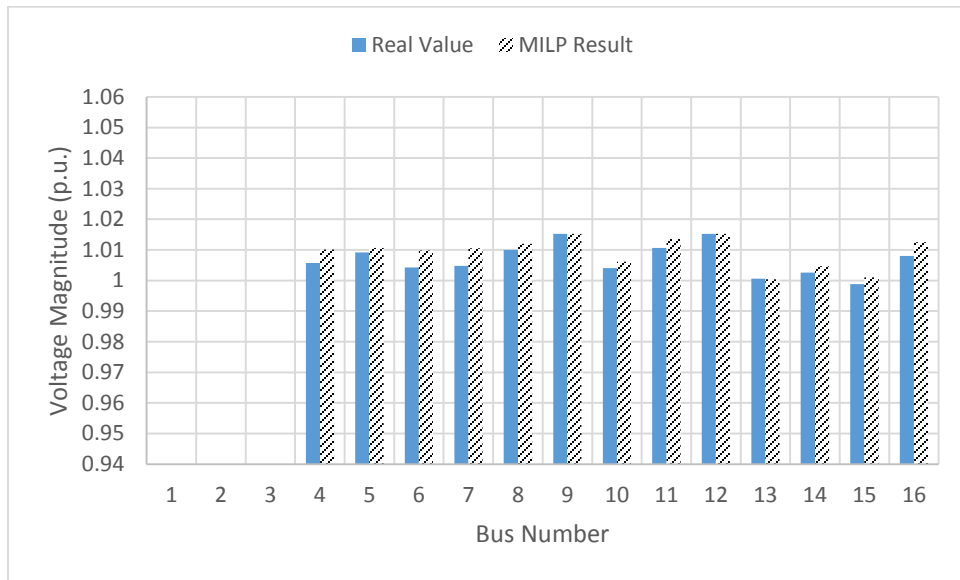


Figure 5.32 Voltage magnitudes - case 2 - fault C

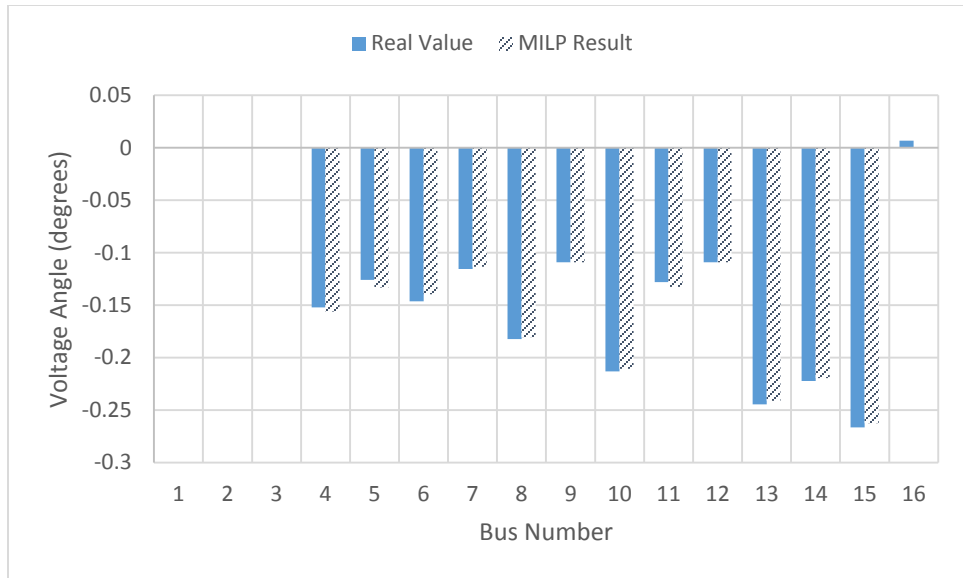


Figure 5.33 Voltage angles - case 2 - fault C

A comparison in terms of the total ENS, SAIDI, SAIFI, and associated cost between the conventional and microgrid cases is shown in Figures 5.34 – 5.37. The associated cost in the case of the microgrids includes both, the interruption cost and the operational cost together. In total, the microgrid case showed a remarkable reduction of 54.06%, 93.72%, 93.72%, and 70.05% in terms of ENS, SAIDI, SAIFI, and associated cost, respectively, as indicated in Table 5.32. For sure, these percentages can be further controlled and manipulated by utilizing the proposed prioritization method.

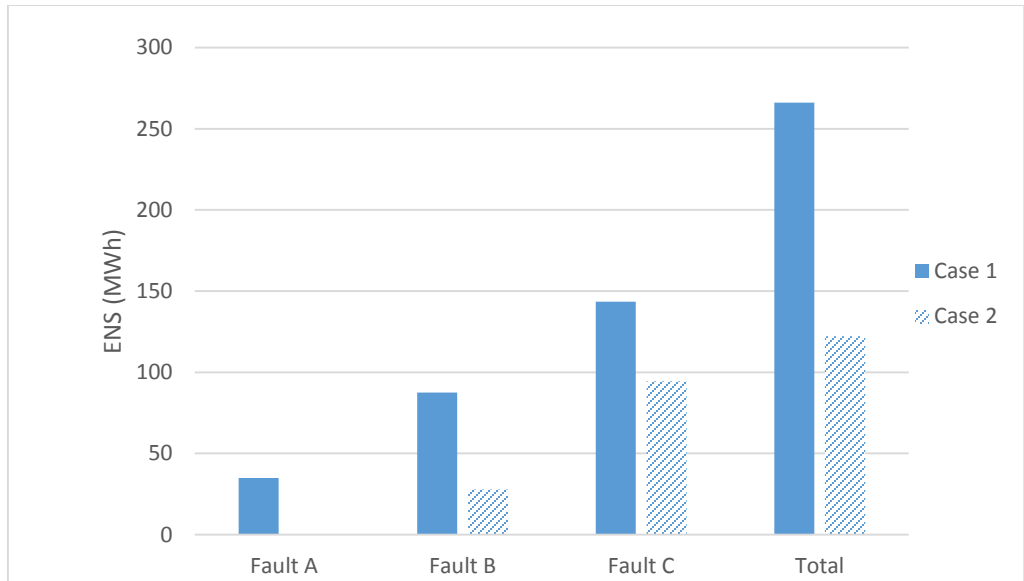


Figure 5.34 ENS comparison

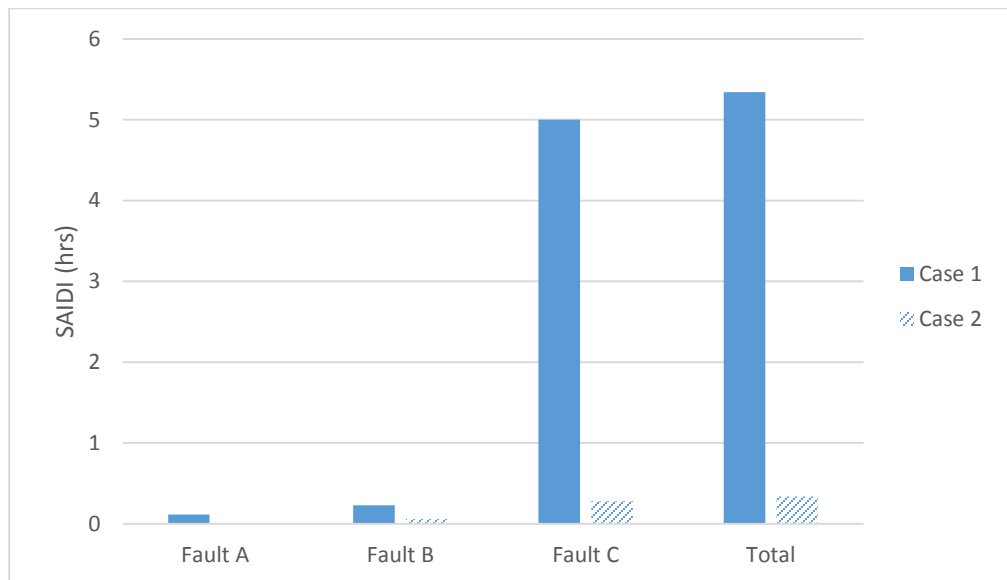


Figure 5.35 SAIDI comparison

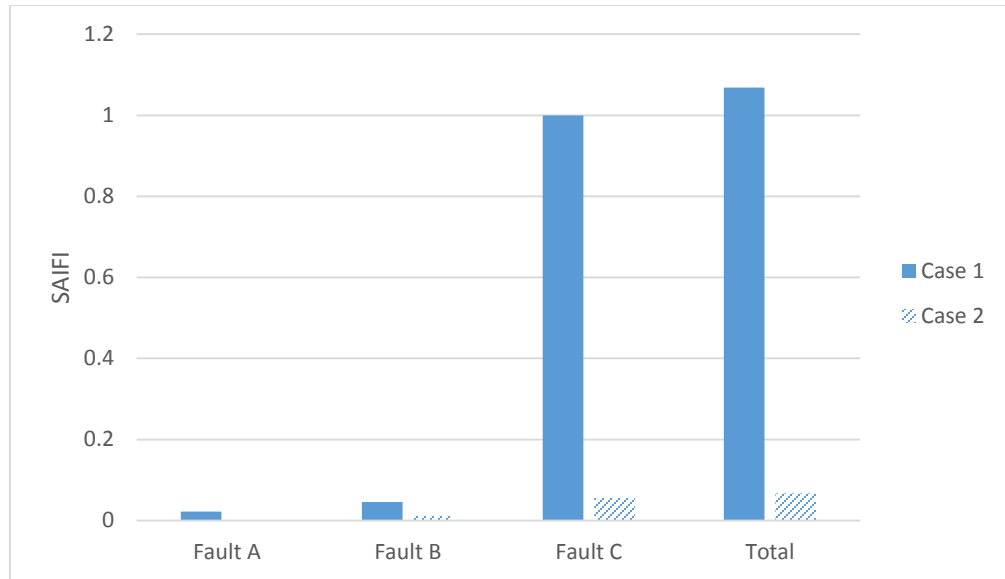


Figure 5.36 SAIIFI comparison

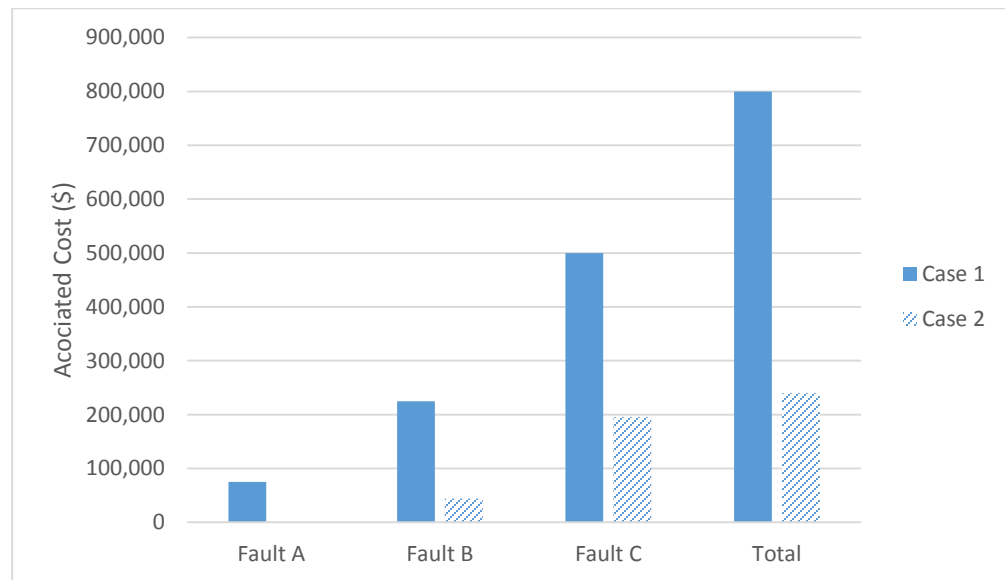


Figure 5.37 Associated cost comparison

Table 5.32 Coparison between case 1 and case 2

	ENS (MWh)	SAIDI (hrs)	SAIFI	Associated Cost (\$)
Case 1 : Conventional System	266	5.3412	1.06823	800,100
Case 2: Smart Microgrid	122.2	0.3355	0.0671	239,635
Total Reduction	54.06 %	93.72 %	93.72 %	70.05 %

It can be seen clearly from all previous cases that the restoration process was more successful in the microgrid system compared to the conventional distribution system. By including 2 DGs in the system, utilizing curtailment programs, and allowing meshed operation, the reliability of restoration was substantially improved. When one feeder was interrupted in fault A, two loads were lost in the conventional system case with ENS of 35MWh. In the other hand, the microgrid in fault A was able to supply all loads without any operational cost since the two DGs did not provide any active power and all curtailable loads were 100% served. This was achieved by allowing the meshed network operation and enhancing the voltage profile by injecting reactive power from the DGs. Note that the total DGs size was only 35.8% of total system load. If these sizes were to be increased, further improvement will surely be observed in the restoration process. Thereby, it can be confidently stated that considering the operation of a smart microgrid will defiantly increase the reliability and resilience of the system and may avoid several expected interruption.

5.5 Sensitivity Analysis

In this section, a single fault incident will be applied to the previously illustrated microgrid system. Then, the restoration optimization will be achieved several times considering different weights for the multi-objective function where the importance of restoring loads, DGs cost, and curtailment cost will be interchanged in each studied case. Note that similar DGs information and curtailable loads information shown in Tables 5.22 and 5.23, respectively, are utilized in this section. However, the maximum allowable curtailment percentage is increased to be 50%, instead of 25%, for all curtailable loads.

In all cases, the pre-fault configuration of the system is taken to be the optimal for loss reduction shown in Figure 5.4. The applied fault information are shown in Table 5.33. Also, the priority weights considered for each load point are similar to those shown in Table 5.17.

Table 5.33 Fault information

	Location	MTTR (hrs)
Fault	Feeders 1-4 & 3-13	5

The case studies considered in this section are illustrated in Table 5.34. Note that the objective of restoring loads was given a high weight in all cases. This is because low weight will yield not restoring loads since the optimization process will concentrate more on minimizing DGs and LC cost. Table 5.34 shows the restoration results for each case including switches to be open, lost load points, summation of priority weights for restored loads, total operational DGs cost and total load curtailment cost. Moreover, Tables 5.36

and 5.37 contain detailed information about the DGs output and load curtailed, respectively, for all cases.

Table 5.34 Cases of sensitivity study

Case No.	Weight of First Objective: Restoring Loads based on Priorities $\omega_{priority}^{Obj}$	Weight of Second Objective: DGs Operational Cost $\omega_{DG\ cost}^{Obj}$	Weight of Third Objective: Load Curtailment Cost $\omega_{LC\ cost}^{Obj}$
1	0.7	0.15	0.15
2	0.7	0.25	0.05
3	0.7	0.05	0.25

Table 5.35 Restoration results for sensitivity cases of study

Case No.	Switches to be open after Restoration	Lost Load Points	Total Priority Weights of Restored Loads	Total DGs Operational Cost across MTTR (\$)	Total Load Curtailment Cost across MTTR (\$)	CPU time
1	$S_{1,4}, S_{3,13}$	5, 12	4.558	2727.5	0	6.78
2	$S_{1,4}, S_{3,13}$	5, 9	4.533	1245	1750	7.38
3	$S_{1,4}, S_{3,13}$	9	4.8318	5820	0	5.25

Table 5.36 DGs operation information

Case No.	DG	Active Power Output (MW)	Reactive Power Output (MVAR)	Operational Cost across MTTR (\$)
1	DG1	0.59	5.08	442.5
	DG2	4.57	1.89	2285
2	DG1	0	1.17	0
	DG2	2.49	2.56	1245
3	DG1	5.02	4.81	3765
	DG2	4.11	2.75	2055

Table 5.37 Load curtailment information

Case No.	Load Point	Curtailed Power (MW)	Curtailment % of Nominal Load	Curtailment Cost across MTR (\$)
1	4	0	0	0
	6	0	0	0
	7	0	0	0
	11	0	0	0
2	4	0	0	0
	6	1	50	1000
	7	0.75	50	750
	11	0	0	0
3	4	0	0	0
	6	0	0	0
	7	0	0	0
	11	0	0	0

It can be observed from the results that when choosing equal weights for DGs and LC cost in case 1, no load curtailment occur. This was expected since the assumed cost for LC is higher than the cost of DGs. Thereby, operating DGs was preferable by the optimization process than curtailing loads. However, load curtailment was present at case 2 when the weight of DGs cost was higher than the weight of LC cost. Moreover, lower weight for DGs cost at case 3 increased the DGs power output compared to case 1 and 2 which resulted in restoring more load points.

CHAPTER 6

CONCLUSIONS AND REMARKS

6.1 Summary

In this study, a smart self-healing strategy for electrical microgrids was presented that was able to provide the optimal solution in terms of DGs output, amount of load curtailment, and system configuration. Also, a priority listing method was proposed that ranks loads depending on their cost of interruption, system reliability indices, and load management programs. The prioritization strategy was first implemented and studied on RBTS Bus 4 distribution system. Then, at later stage in section 5.3, it was integrated into the proposed MILP formulation and was examined on the IEEE 16 bus distribution system.

At the first stage of this thesis in chapter 2, system reliability and restoration was assist based on two main case studies. A local load study and a system study. In the local load study, the reliability of customers, including residential, commercial, and industrial sectors, was examined in four stages. The first stage consisted of the loads connected only to the utility. In the second stage, hybrid wind turbines and PV panels were integrated into the system. The third stage included the DSM and in the fourth stage DSM was included along with the hybrid renewable system. At each stage, the reliability was assessed in terms of unavailability in hours and ENS. In the second case of chapter 2, the impact of LM and the integration of renewable energy on the system restoration process was studied. Two faults on two different locations of the RBTS-BUS2 distribution system were simulated.

Several scenarios were analyzed by connecting different hybrid system sizes and by interchanging the LM factors. SAIFI, SAIDI and ENS indices of the system were obtained at each incident case. The voltage profiles were also examined in order to test system restoration capability.

The load prioritization method for MG systems was proposed in chapter 3. The method prioritizes all loads in the system by assigning calculated weights that depend on two levels. The first level classifies critical loads and the second level specifies four prioritization criteria. These criteria consist of the load effect on system ENS, the load effect on the SAIDI metric, the load effect on the SAIFI metric, and the cost of load interruption. The RBTS Bus 4 distribution system was used as an implementation model and was tested for two cases in which LPs were prioritized under different scenarios. The results demonstrate that the proposed load prioritization method is dynamic in time and takes into consideration the ENS, SAIDI, and SAIFI metrics and different load costs of interruption. Moreover, the methodology is capable of including customers participating in DSM programs as well as representing critical loads such as schools and hospitals

In chapter 4, system modeling and the mathematical formulation of the smart self-healing technique for electric microgrids was proposed. Three main control variables were considered which are, system configuration, DGs power output and amount of load curtailment. Several linearization techniques were utilized in order to model the non-linear behavior of the electric system as a MILP problem which then can be solved mathematically. The model takes into account controllable and non-controllable DGs, curtailable and non-curtailable loads, and switchable and non-switchable branches.

Although microgrids are expected to operate in a meshed manner, however, the radiality constraint was modeled to simulate the conventional distribution system which was then, compared with the microgrid system in terms of reliability of service restoration.

Chapter 5 was divided into four main case studies. Formulation verification, comparison based study, integrating and examining the proposed priority method, and finally, comparing the operation and restoration efficiency of a conventional distribution system and a smart microgrid.

6.2 Conclusions

From the results of the case studies presented in this thesis, the following can be concluded:

- With few modifications, the proposed MILP formulation was able to find the optimal configuration for loss minimization of the IEEE 16 bus system, as have been illustrated in section 5.1.
- Compared to formulation in [68], the proposed MILP formulation minimized the required integer constraints which expedited the optimization solution. In the comparison based study presented in section 5.2, it was shown that both formulation produced similar results. However, the proposed formulation reduced the computational time by 90.6% compared to formulation [68]. Moreover, the proposed formulation was able to find the optimum solution by exploring only 75 nodes compared to 9100 nodes when using the formulation in [68].
- By using the proposed load prioritizing method in load restoration, a reduction of 6.2%, 95.8%, 95.8%, and 37.3% in system ENS, SAIDI, SAIFI, and cost of

interruption, respectively, was achieved compared to the case when restoring the system without utilizing the proposed prioritizing method as was shown in section 5.3. Furthermore, the improvement of ENS, SAIDI, SAIFI, and minimizing interruption cost can be controlled by interchanging the presented importance weights.

- It was found from the three case studies presented in section 5.4 that the restoration process was more successful in the microgrid system compared to the conventional distribution system. By installing 2 DGs in the system with total size of 38.5% of system load, allowing meshed operation, and including curtailable customers, remarkable improvements in service restoration was recorded. Compared to the conventional system case, the microgrid reduced the resultant ENS, SAIDI, SAIFI, and interruption cost by 54.06%, 93.72%, 93.72%, and 70.05%, respectively.
- In the case of a one feeder outage, the conventional system lost 2 loads. However, the microgrid was able to restore all loads in the system by producing only reactive power from the connected DGs, and by that, improving the system voltage profile.
- In the case study with all feeders out of service, the conventional system faced a blackout losing all connected loads. However, the microgrid was able to operate in an islanded mode operating the DGs to their full limit and restoring around 38% of system total load.

6.3 Contributions

The main contributions of this thesis are summarized as follows:

- Proposing a load priority model that:
 - Encounters several prioritizing factors.
 - Flexible and can be controlled to satisfy the user requirements.
 - Improves system reliability and restoration efficiency.
- Proposing a MILP restoration model for microgrids that:
 - Models DGs active and reactive power outputs.
 - Models loads participating in LM programs.
 - Minimizes the branch and bound process in finding the optimal solution by decreasing integer variables.
 - Minimizes the computational time.
 - Controls the objective of the restoration to meet utilities requirements.

6.4 Future Work

As the path of research never ends, the following are topics suggested for future work:

- Optimizing the importance weights that were introduced in chapter 3 regarding the priority list method in order to provide the user or the utility with a general platform that can assure the best results relating to service restoration.
- Building several other self-healing strategies based on other optimization methods such as artificial intelligence and heuristic algorithms and to report a general comparison between these methods and the proposed mathematical programming method in terms of optimality simplicity, and computational time.

APPENDICES

A.1 Chronological Load Modeling Data

Table A.1 Weekly load peak fractions [21]

Week	Weekly Percentage	Week	Weekly Percentage
1	0.922	27	0.815
2	0.96	28	0.876
3	0.938	29	0.861
4	0.894	30	0.94
5	0.94	31	0.782
6	0.901	32	0.836
7	0.892	33	0.86
8	0.866	34	0.789
9	0.8	35	0.786
10	0.797	36	0.765
11	0.775	37	0.84
12	0.787	38	0.755
13	0.764	39	0.784
14	0.81	40	0.784
15	0.781	41	0.803
16	0.86	42	0.804
17	0.814	43	0.86
18	0.897	44	0.941
19	0.93	45	0.945
20	0.94	46	0.969
21	0.916	47	1
22	0.871	48	0.95
23	0.96	49	0.975
24	0.947	50	0.97
25	0.956	51	0.98
26	0.921	52	0.99

Table A.2 Daily fraction of the residential, commercial, and industrial peak load [21]

Day	Residential	Commercial	Industrial
Monday	0.96	1	1
Tuesday	1	1	1
Wednesday	0.98	1	1
Thursday	0.96	1	1
Friday	0.97	1	1
Saturday	0.83	1	1
Sunday	0.81	1	1

Table A.3 Hourly fraction of the residential, commercial, and industrial peak load [21]

Hour	Average Residential Day	Average Commercial Day	Industrial
1	0.55	0.01	0.337
2	0.5	0.01	0.337
3	0.43	0.01	0.337
4	0.37	0.01	0.337
5	0.36	0.01	0.337
6	0.38	0.03	0.337
7	0.385	0.04	1
8	0.425	0.25	1
9	0.45	0.85	1
10	0.55	0.9	1
11	0.6	0.91	1
12	0.7	0.92	1
13	0.7	0.985	1
14	0.75	0.975	1
15	0.75	0.88	1
16	0.75	0.865	1
17	0.8	0.89	1
18	0.85	0.9	1
19	0.85	0.9	1
20	0.86	0.64	1
21	0.86	0.6	1
22	0.8	0.42	1
23	0.75	0.4	1
24	0.65	0.025	1

A.2 Linearization Methods

The general formulation of any Mixed Integer Linear Programming (MILP) problem with number of control variables equal to N_{var} is as follows:

$$\min_x f^T x \quad (\text{A.1})$$

s. t

$$A_{in}x \leq B_{in}$$

$$A_{eq}x = B_{eq}$$

$$x^i \text{ are integers } \forall i \in \Gamma_{integers}$$

where

f : is a row vector of length N_{var} representing the objective function.

x : is a row vector of length N_{var} containing the control variables of the problem.

A_{in} : is an $N_{in} \times N_{var}$ matrix.

B_{in} : is a row vector of length N_{in} .

N_{in} : is the number of inequality constraints in the problem.

A_{eq} : is an $N_{eq} \times N_{var}$ matrix.

B_{eq} : is a row vector of length N_{eq} .

N_{eq} : is the number of equality constraints in the problem.

$\Gamma_{integers}$: is the set of variables that must take an integer value.

It is obvious from the previous formulation (A.1) that in an MILP problem, the objective function and all constraints must be linear. Thereby, in order to model the microgrid restoration optimization and the system behavior, which is non-linear in nature, as an MILP problem, different reformulation and linearization methods must be applied.

There exists several reformulation and approximation methods that model and linearize non-linear relations and equations. The accuracy of such approximation can be controlled by parameters that are introduced in the reformulation techniques. In this section, four well known methods are illustrated. These methods will be later utilized in modeling the electric system behavior and microgrid restoration optimization as an MILP problem. The explanation of those methods in this section will be general for any optimization problem and they are related to the thesis purpose in the mathematical formulation of the proposed self-healing technique in section 4.3.

A.2.1 Disjunctive or Decision Constraints

Several optimization problems include types of constraints that may or may not be considered depending on an auxiliary binary control variable. For instance, suppose that the constraint $\sum_i a_i \cdot x_i \leq b$ is only considered when the binary control variable c is equal to 1. Otherwise, when $c = 0$, the constraint is relaxed. The modeling of such constraint can be achieved by including the constant M in the constraint as follows [70]:

$$\sum_i a_i \cdot x_i - b \leq M(1 - c) \quad (\text{A.2})$$

If the numerical value of M is ensured to be always greater than $\sum_i a_i \cdot x_i - b$, the preceding constraint is then controlled by the binary variable c .

A.2.2 Polygonal Inner-Approximation

Suppose that it is required to include the following constraint in an MILP problem:

$$x_1^2 + x_2^2 \leq r^2 \quad (\text{A.3})$$

Where x_1 and x_2 are control variables and r is a constant. It is obvious that this constraint is non-linear and must be re-formulated to be incorporated in the MILP problem.

A technique which was used in [71] is to approximate the circle of $x_1^2 + x_2^2 = r^2$ as a regular polygon. Assuming that $r = 1$, the polygonal approximation of the circle of $x_1^2 + x_2^2 = 1$ with different number of edges is shown in Figure A.1.

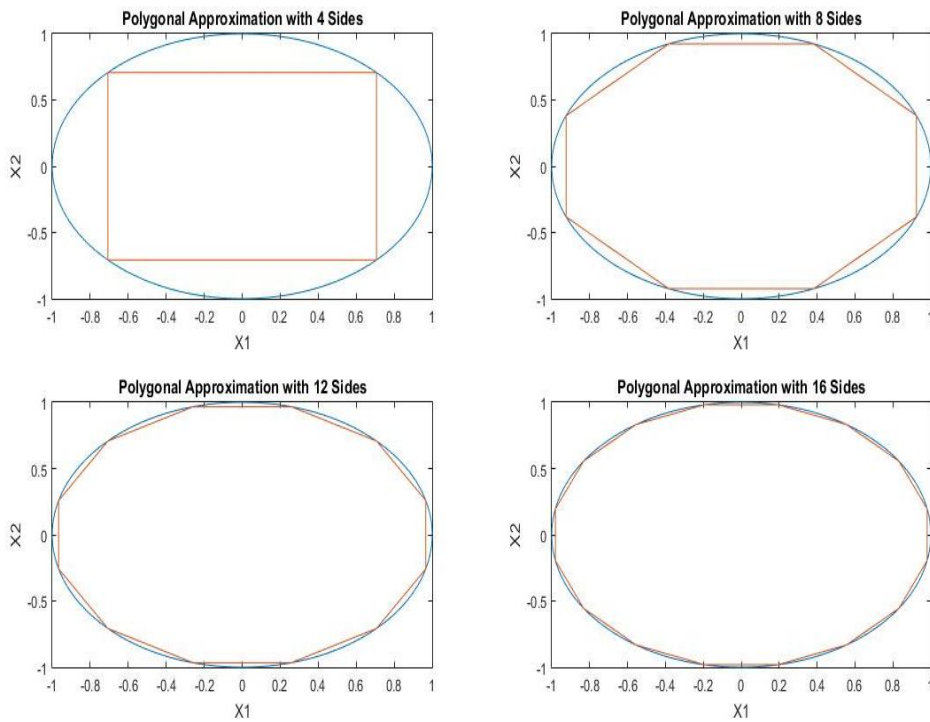


Figure A.1 Polygonal inner approximation for a circle with radius=1 considering different number of edges

It can be seen from Figure A.1 that the approximation becomes more accurate as the number of polygonal edges increase. Note that any polygonal can be represented by a

finite number of lines which can be then represented as linear equations. Hence, the constraint in (A.3) can be linearly re-formulated considering a polygonal with E edges as follows:

$$\bar{x}_1^p \cdot x_1 + \bar{x}_2^p \cdot x_2 \leq r^2 \quad \forall p \in \{1, 2, \dots, E\} \quad (\text{A. 4})$$

Where the coefficients \bar{x}_1^p and \bar{x}_2^p can be found as:

$$\bar{x}_1^p = r \cdot \cos \left[(p - 0.5) \cdot \frac{2\pi}{E} \right] \quad (\text{A. 5})$$

$$\bar{x}_2^p = r \cdot \sin \left[(p - 0.5) \cdot \frac{2\pi}{E} \right] \quad (\text{A. 6})$$

It is worth mentioning that there is a trade off between the accuracy and the computational performance whereas E increase, the approximation becomes more accurate but the number of constraint is also increased. Polygonal approximation with E edges require E constraints.

The probability of an error in this approximation can be calculated as the difference in percentage between the area of the circle A_c and the area of the polygonal A_p as follows:

$$\text{error probability} = \frac{A_c - A_p}{A_c} \times 100\% \quad (\text{A. 7})$$

Where

$$A_c = \pi r^2 \quad (\text{A. 8})$$

$$A_p = \frac{Er^2}{2} \sin \left(\frac{2\pi}{E} \right) \quad (\text{A. 9})$$

Figure A.2 plots the error probability versus the number of considered edges. Note that this plot is fixed regardless of the circle radius to be approximated since the ratio in (A.7) will cancel the term r^2 .

It can be seen from Figure A.2 that the probability of an error decreases exponentially as we increase the number of edges where an acceptable approximation would be in range of $E > 35$. The exact value of E will depend on the desired accuracy of approximation.

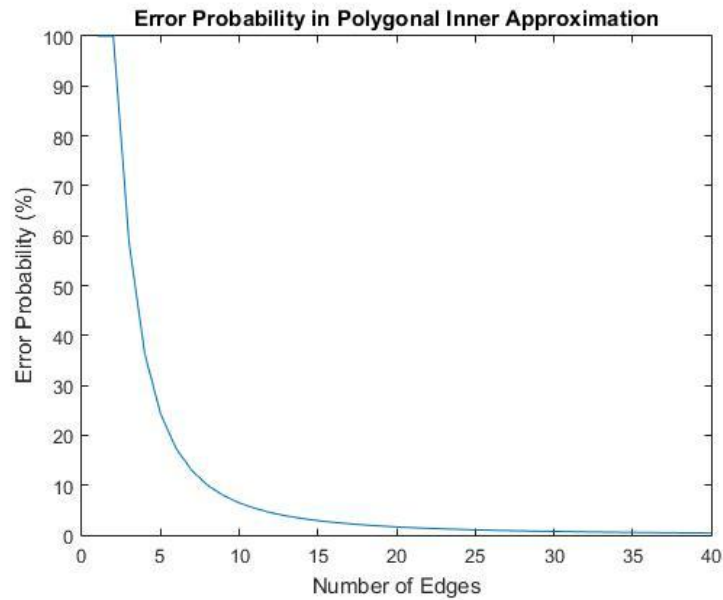


Figure A.2 Error probability in polygonal inner approximation

A.2.3 Linear Envelopes for Bilinear Products

A bilinear product is defined as the product of two continuous control variables such as $x_1 \cdot x_2$. This product is for sure non-linear and must be re-formulated in a linear fashion to be included in the MILP problem. A possible method is to replace the product by an auxiliary variable, say u , and then limit the value of u by linear constraints that

represent an envelope and are functions of x_1 and x_2 . Certainly, as the envelope becomes tighter, the approximation error is reduced.

In this thesis, McCormick's envelope [72] is considered which is known to be the tightest possible envelope representing a bilinear product. Assuming that x_1 is bounded in the interval $x_1^{min} \leq x_1 \leq x_1^{max}$ and $x_2^{min} \leq x_2 \leq x_2^{max}$, then McCormick's envelope can be linearly defined as follows:

$$x_1^{min} \cdot x_2 + x_2^{min} \cdot x_1 - x_1^{min} \cdot x_2^{min} \leq u \quad (\text{A.10})$$

$$x_1^{max} \cdot x_2 + x_2^{max} \cdot x_1 - x_1^{max} \cdot x_2^{max} \leq u \quad (\text{A.11})$$

$$x_1^{min} \cdot x_2 + x_2^{max} \cdot x_1 - x_1^{min} \cdot x_2^{max} \geq u \quad (\text{A.12})$$

$$x_1^{max} \cdot x_2 + x_2^{min} \cdot x_1 - x_1^{max} \cdot x_2^{min} \geq u \quad (\text{A.13})$$

Equations A.10 and A.11 define lower-bound envelopes for the bilinear product and equations A.12 and A.13 define upper-bound envelopes. In order to visualize the McCormick's envelopes procedure, an example is illustrated graphically. Suppose it is required to approximate the multiplication of $x_1 \cdot x_2$ where the ranges of these variables are $1 \leq x_1 \leq 2$ and $3 \leq x_2 \leq 4$. Figure A.3 shows the actual function of the bilinear product $x_1 \cdot x_2$. Figures A.4 and A.5 display the lower and upper bounds, respectively.

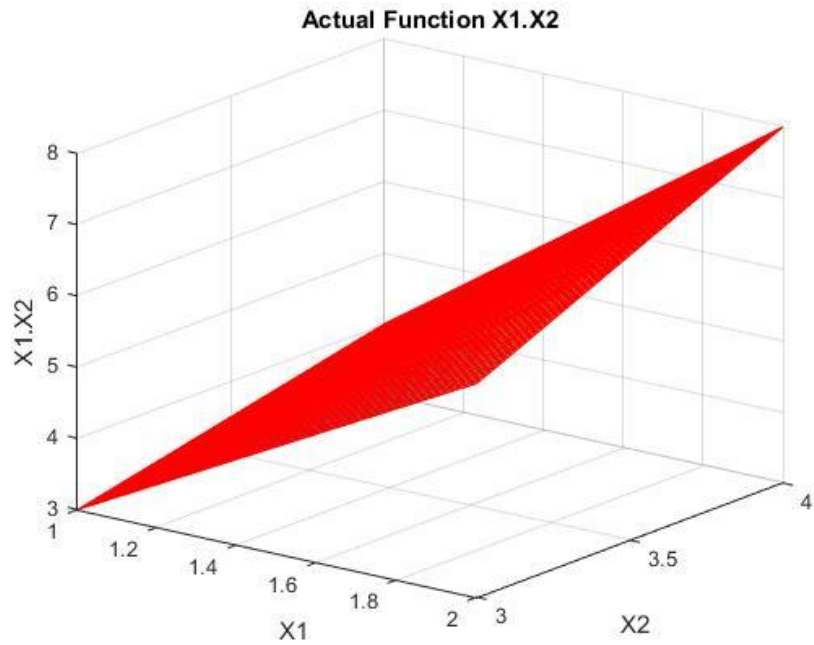


Figure A.3 Actual function of bilinear product

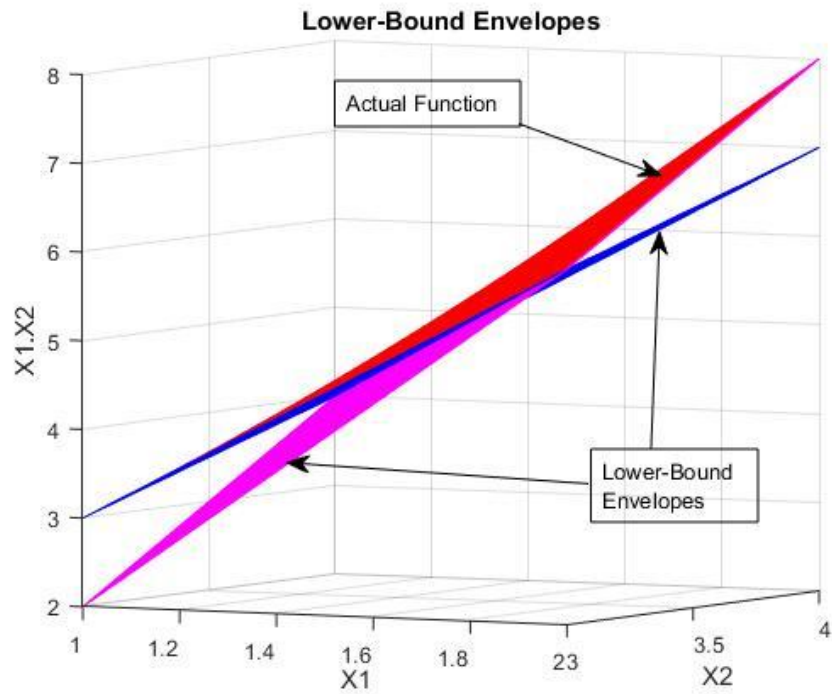


Figure A.4 Lower bound McCormick's envelopes

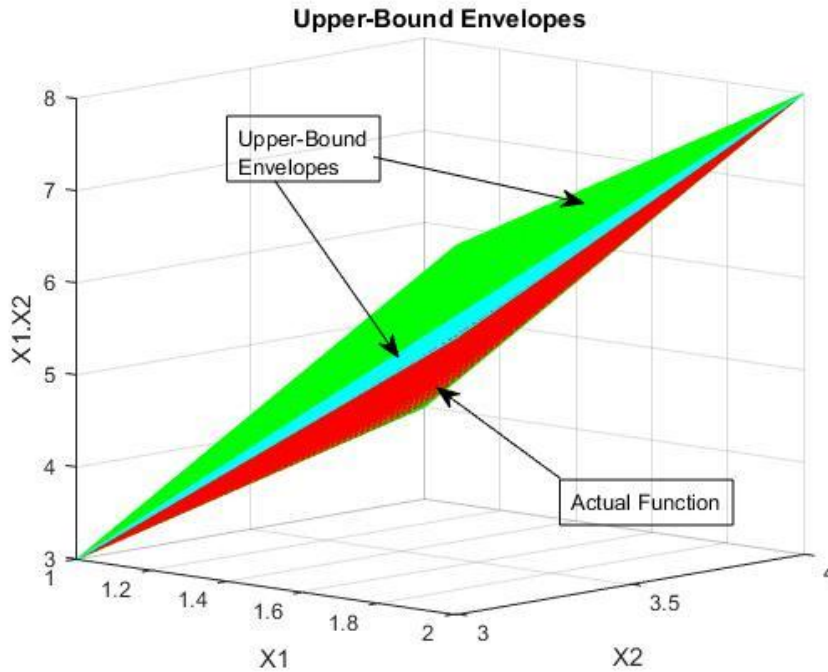


Figure A.5 Upper bound McCormick's envelopes

Each envelope in Figures A.4 and A.5 represents a plane that is described by equations (A.10-A.13). These planes are set as linear constraints in the MILP formulation, where the result value of the bilinear product is set to be within these specifies planes.

A.2.4 Piecewise Linearization and Special Order Sets of Type 2 (SOS2)

In the previous part, an equation that is characterized as a bilinear product was linearly approximated to be included in an MILP problem. In many optimization cases, equations to be approximated are not necessarily bilinear product. Hence, other reformulation techniques are needed. One of the basic most famous linearization techniques for non-linear functions is the use of piecewise-linearization segments. Consider the example in Figure A.3 where the function $f(x)$ (represented by the dashed blue line) is approximated to be the piecewise linear function $f_{pw}(x)$ (represented by the

continuous red line). The approximation was achieved using six evaluated points \tilde{f}_i at each \tilde{x}_i evaluation point resulting five line segments. These evaluation points are used to approximate the value of $f(x)$ at any x point. To generalize the idea, assume that n evaluation points are used, then the approximation of $f(x)$ to $f_{pw}(x)$ at point x is found using the following linear equations [73, 74]:

$$\sum_{i=1}^n \alpha_i \tilde{x}_i = x \quad (\text{A.14})$$

$$\sum_{i=1}^n \alpha_i \tilde{f}_i = f_{pw}(x) \quad (\text{A.15})$$

$$\sum_{i=1}^n \alpha_i = 1 \quad (\text{A.16})$$

Where each α_i , $i \in \{1, 2, \dots, n\}$, is the weight associated with each evaluation point \tilde{x}_i in (A.14) to result the value of x and all α_i must be positive. The same weights are then used in equation (A.15) to get the final approximated value of $f(x)$. It is worth mentioning that equations (A.14), (A.15), and (A.16) are usually referred to as the reference row, the function row, and the convexity row, respectively.

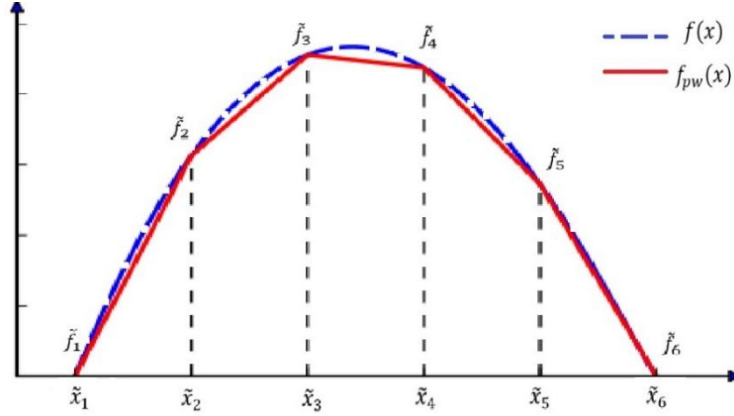


Figure A.6 Piecewise linearization

It must be noted that in order to accurately approximate a value of $f(x)$, only two consecutive evaluated points $\tilde{f}_{i-1}, \tilde{f}_i$ or $\tilde{f}_i, \tilde{f}_{i+1}$ must be used in equation (A.15). In contrast, if, for example, \tilde{f}_2 and \tilde{f}_5 in Figure A.6 are used to approximate $f(x)$, this will result in a line segment that clearly do not resemble the original function. Thereby, only two weights α can be allowed to be non-zeros and they should also be consecutive forming what is usually referred to as a special order set of type 2 (SOS2). This constraint can be added to the MILP problem as illustrated in [75] by introducing n binary variables, one for each weight α_i , as follows:

$$\alpha_1 \leq \delta_1 \quad (\text{A.17})$$

$$\alpha_i \leq \delta_i + \delta_{i-1} \quad \forall i \in \{2, \dots, n\} \quad (\text{A.18})$$

$$\sum_{i=1}^n \delta_i = 1 \quad (\text{A.19})$$

Suppose now that the non-linear function to be piecewise approximated depends on two variables $f(x, y)$. The mathematical formulation of this case can be achieved by

using a rectangular grid of evaluation points $(\tilde{x}_i, \tilde{y}_j)$ where $i \in \{1, \dots, n_x\}$ and $j \in \{1, \dots, n_y\}$ [2] resulting $n_x \times n_y$ evaluated $\tilde{f}_{i,j}$ points. To approximate the value of $f(x, y)$ to $f_{pw}(x, y)$, the following set of linear equations are used:

$$\sum_{i=1}^{n_x} \alpha_i^x \tilde{x}_i = x \quad (\text{A.20})$$

$$\sum_{j=1}^{n_y} \alpha_j^y \tilde{y}_j = y \quad (\text{A.21})$$

$$\sum_{i=1}^{n_x} \sum_{j=1}^{n_y} \alpha_{i,j}^f \tilde{f}_{i,j} = f_{pw}(x, y) \quad (\text{A.22})$$

$$\sum_{i=1}^{n_x} \alpha_i^x = 1 \quad (\text{A.23})$$

$$\sum_{j=1}^{n_y} \alpha_j^y = 1 \quad (\text{A.24})$$

$$\sum_{j=1}^{n_y} \alpha_{i,j}^f = \alpha_i^x \quad (\text{A.25})$$

$$\sum_{i=1}^{n_x} \alpha_{i,j}^f = \alpha_j^y \quad (\text{A.26})$$

Similarly, in order to force the evaluation points to be adjacent, the following constraints are used by introducing the binary variables δ_i^x with $i \in \{2, \dots, n_x\}$ and δ_j^y with $j \in \{2, \dots, n_y\}$ as follows:

$$\alpha_1^x \leq \delta_1^x \quad (\text{A.27})$$

$$\alpha_i^x \leq \delta_i^x + \delta_{i-1}^x \quad \forall i \in \{2, \dots, n_x\} \quad (\text{A. 28})$$

$$\sum_{i=1}^{n_x} \delta_i^x = 1 \quad (\text{A. 29})$$

$$\alpha_1^y \leq \delta_1^y \quad (\text{A. 30})$$

$$\alpha_j^y \leq \delta_j^y + \delta_{j-1}^y \quad \forall j \in \{2, \dots, n_y\} \quad (\text{A. 31})$$

$$\sum_{j=1}^{n_y} \delta_j^y = 1 \quad (\text{A. 32})$$

Observe that all equations previously listed are linear and can be directly integrated in the MILP formulation. Also, it must be noted that the accuracy of the piecewise linear approximation highly depends on the number of evaluation points \tilde{x}_i and \tilde{y}_j to be considered where larger number of evaluation points will results in a better accuracy. In the other hand, the computational performance will obviously be negatively effected due to the increased number of variables $\alpha_i^x, \alpha_j^y, \alpha_{i,j}^f, \delta_i^x$ and δ_i^y and the increased number of constraints to be added especially those that force δ_i^x and δ_i^y to be integers.

These four mentioned methods are utilized to model the electric system behavior and the microgrid restoration optimization as an MILP problem. They are referred to as reformulation methods 1 to 4 in the formulation section 4.3 of this thesis.

NOMENCLATURE

The following symbols are used in chapter 4.

Sets

Symbol	Set Definition
Γ_N	Nodes in the system
Γ_B	Branches in the system
Γ_{sw}	Switchable branches
Γ_{DG}	DGs in the system
Γ_{CDG}	Controllable DGs
Γ_L	Loads in the system
Γ_{CL}	Curtable loads
Γ_{loop}	Loops in the system
Γ_{sub}	Substations connected to the system
$\Gamma_{DG,absorb Q}$	DGs absorbing reactive power
$\Gamma_{DG,supply Q}$	DGs supplying reactive power

Input Parameters

Symbol	Parameter Definition
R_{km}	Resistance of branch km
X_{km}	Reactance of branch km
$\overline{I}_{km}^p, \overline{I}_{km}^p$	Parameters used to model branch km current limit

$\overline{DG_k^P}, \overline{DG_k^Q}$	Parameters used to model rated power constraint of DG k
L_k^P	Active power demand of load k – considered a parameter for non-curtailable loads
L_k^Q	Reactive power demand of load k – considered a parameter for non-curtailable loads
L_k^S	Apparent power demand of load k – considered a parameter for non-curtailable loads

Continuous Decision Variables

Symbol	Variable Definition
V_k^{re}, V_k^{im}	Respectively, real and imaginary voltages of node k
I_{km}^{re}, I_{km}^{im}	Respectively, real and imaginary currents flowing from node k to node m .
$I_{d,k}^{re}, I_{d,k}^{im}$	Respectively, real and imaginary demand currents of load k
$I_{DG,k}^{re}, I_{DG,k}^{im}$	Respectively, real and imaginary generated currents from DG k or substation k in the system
L_k^P	Active power demand of load
L_k^Q	Reactive power demand of load
L_k^S	Apparent power demand of load k
DG_k^P	Active power output from DG k or substation k in the system
DG_k^Q	Reactive power output from DG k or substation k in the system
DG_k^S	Apparent power output of DG k or substation k in the system

LC_k	Amount of demand curtailed from load k
θ_k	Voltage phase angle of node k
ϕ_k^{DG}	Power angle of DG k
ϕ_k^L	Power angle of load k
ζ_k	Variable approximating the square of real voltage of node k
η_k	Variable approximating the square of imaginary voltage of node k
$g_k^{P,Vre}$	Variable approximating the bilinear product $I_{DG,k}^{re} \cdot \zeta_k$
$g_k^{P,Vim}$	Variable approximating the bilinear product $I_{DG,k}^{re} \cdot \eta_k$
$g_k^{Q,Vre}$	Variable approximating the bilinear product $I_{DG,k}^{im} \cdot \zeta_k$
$g_k^{Q,Vim}$	Variable approximating the bilinear product $I_{DG,k}^{im} \cdot \eta_k$
$h_k^{P,Vre}$	Variable approximating the bilinear product $V_k^{re} \cdot DG_k^P$
$h_k^{P,Vim}$	Variable approximating the bilinear product $V_k^{im} \cdot DG_k^P$
$h_k^{Q,Vre}$	Variable approximating the bilinear product $V_k^{re} \cdot DG_k^Q$
$h_k^{Q,Vim}$	Variable approximating the bilinear product $V_k^{im} \cdot DG_k^Q$
$l_k^{P,Vre}$	Variable approximating the bilinear product $I_{L,k}^{re} \cdot \zeta_k$
$l_k^{P,Vim}$	Variable approximating the bilinear product $I_{L,k}^{re} \cdot \eta_k$
$l_k^{Q,Vre}$	Variable approximating the bilinear product $I_{L,k}^{im} \cdot \zeta_k$
$l_k^{Q,Vim}$	Variable approximating the bilinear product $I_{L,k}^{im} \cdot \eta_k$
$m_k^{P,Vre}$	Variable approximating the bilinear product $V_k^{re} \cdot L_k^P$
$m_k^{P,Vim}$	Variable approximating the bilinear product $V_k^{im} \cdot L_k^P$

$m_k^{Q,Vre}$	Variable approximating the bilinear product $V_k^{re} \cdot L_k^Q$
$m_k^{Q,Vim}$	Variable approximating the bilinear product $V_k^{im} \cdot L_k^Q$
μ_k	Binary decision variable representing load k status (shed=0, not shed=1)
y_{km}	Binary decision variable representing switch km status (opened=0, closed=1)

REFERENCES

- [1] Mohamed E. El-Hawary, “The Smart Grid—State-of-the-art and Future Trends”, Department of Electrical and Computer Engineering, Dalhousie University, Halifax, Nova Scotia, Canada.
- [2] “Cost of Power Interruptions to Electricity Consumers in the United States (U.S.)”, LBNL-58164, by Kristina Hamachi LaCommare, and Joseph H. Eto, February, 2006.
- [3] U.S Energy Information Administration – EIA – Independent Statistics and Analysis <http://www.eia.doe.gov/cneaf/electricity/>
- [4] “Waiting for the sunrise (solar energy forecast) (Science and Technology)”, The Economist (US), May 19, 1990.
- [5] Solar Energy Industry Forecast: Perspectives on U.S. Solar Market Trajectory, U.S. DOE Solar Energy Technologies Program May 30, 2008.
- [6] “20% wind Energy by 2030”, May 2008, published by Energy Efficiency and Renewable Energy, Department of Energy, USA.
- [7] Ignacio Marti, “Evaluation of Advanced Wind Power Forecasting Models”, Presented at European Wind Energy Conference, Athens, Feb 27- Mar 2, 2006.
- [8] Leonardo Energy. Electrical load management in industry. Paris, France: IE Working Group;1996.
- [9] Federal Energy Regulatory Commission, "Assessment of Demand Response and Advanced Metering", Staff Report Docket Number: AD-06-2-000, August 2006.
- [10] U.S. Department of Energy, "Grid Energy Storage", December 2013.
- [11] Dange Huang and Roy Billinton, "Impacts of Demand Side Management on Bulk System Reliability Evaluation Considering Load Forecast Uncertainty", 2011 IEEE Electrical Power and Energy Conference.
- [12] Chenye Wu, Hamed Mohsenian-Rad, Jianwei Huang, and Yuexuan Wang, " Demand Side Management for Wind Power Integration in Microgrid Using Dynamic Potential Game Theory" IEEE International Workshop on Smart Grid Communications and Networks 2011.
- [13] A. Mehrtash, P. Wang and L. Goel, " Reliability Evaluation of Generation System Incorporating Renewable Generators in a Spot Power Market", 2011 IEEE.
- [14] K. Matsumoto, T. Sakaguchi, R. Kafka, and M. M. Adibi, “Knowledge- based systems as operational aids in power system restoration,” Proc. IEEE, vol. 80, no. 5, pp. 689–697, May 1992.

- [15] Cuong P. Nguyen, and Alexander J. Flueck, "Agent Based Restoration with Distributed Energy Storage Support in Smart Grids", IEEE Transactions On Smartgrid, Vol.3, No.2, June 2012.
- [16] Lasseter, Robert H. "Microgrids." Power Engineering Society Winter Meeting, 2002. IEEE. Vol. 1. IEEE, 2002.
- [17] Microgrid at Illinois Institute of Technology <http://www.iitmicogrid.net/microgrid>
- [18] Huang, Dange, Roy Billinton, and Wijarn Wangdee. "Effects of demand side management on bulk system adequacy evaluation." Probabilistic Methods Applied to Power Systems (PMAPS), 2010 IEEE 11th International Conference on. IEEE, 2010.
- [19] Celli, G., Ghiani, E., Mocci, S., Pilo, F., & Pazzola, E. (2005, June). Demand Side Management as a support to distributed generation in active networks. In Electricity Distribution, 2005. CIRED 2005. 18th International Conference and Exhibition on (pp. 1-4). IET.
- [20] Prema, V., K. Uma Rao, and Amit S. Closepet. "A novel predictive DSM strategy to match power outage pattern for optimal cost with solar and diesel power." Innovative Smart Grid Technologies-Asia (ISGT Asia), 2014 IEEE. IEEE, 2014.
- [21] A. Sankarakrishnan, R. Billinton, "Sequential Monte Carlo simulation for composite power system reliability analysis with time varying loads," IEEE Transactions on Power Systems, v. 10, no. 3, August 1995, pp. 1540-1545.
- [22] Y. Aslan, S. Yavasca and C. Yasar, "Long Term Electric Peak Load Forecasting of Kutahya using Different Approaches," International Journal on Technical and Physical Problems of Engineering, June 2011.
- [23] Hao Jing, Liu Dawei, Li Zhenxin, Chen Zilai and Kong Lingguo, "Power System Load Forecasting Based on Fuzzy Clustering and Gray Target Theory," International Conference on Future Energy, Environment, and Materials 2012.
- [24] Otávio A.S. Carpinteiro, Rafael C. Leme, Antonio C. Zambroni de Souza, Carlos A.M. Pinheiro and Edmilson M. Moreira, "Long-term load forecasting via a hierarchical neural model with time integrators," Electric Power Systems Research 77 (2007) 371–378, 2006.
- [25] Huang Wei, He Zijun and Fengli, "Reliability Evaluation of Microgrid with PV-WG Hybrid System," Henan electric power company, Henan, China 2011.
- [26] Boshell, F., and O. P. Veloza. "Review of developed demand side management programs including different concepts and their results." Transmission and Distribution Conference and Exposition: Latin America, 2008 IEEE/PES. IEEE, 2008

- [27] R.N.Allan, R.Billinton, I.Sjarief, L.Goel, and K.S.So, "A reliability test system for educational purposes basic distribution system data and results", IEE Transactions on Power Systems, Vo1.6, No. 2, May 1991.
- [28] Mirzaei, M., Ab Kadir, M. Z. A., Moazami, E., & Hizam, H. (2009). Review of fault location methods for distribution power system. *Australian Journal of Basic and Applied Sciences*, 3(3), 2670-2676.
- [29] Sanches, D. S., Lima, T. W., Santos, A. C., Delbem, A. C. B., & London, J. B. A. (2012, July). Node-depth encoding with recombination for multi-objective evolutionary algorithm to solve loss reduction problem in large-scale distribution systems. In *Power and Energy Society General Meeting, 2012 IEEE* (pp. 1-8). IEEE.
- [30] Santos, A. C., Delbem, A. C., London, J. B. A., & Bretas, N. G. (2010). Node-depth encoding and multiobjective evolutionary algorithm applied to large-scale distribution system reconfiguration. *Power Systems, IEEE Transactions on*,25(3), 1254-1265.
- [31] Mansour, M. R., Santos, A. C., London, J. B., Delbem, A. C. B., & Bretas, N. G. (2010, July). Node-depth encoding and evolutionary algorithms applied to service restoration in distribution systems. In *Power and Energy Society General Meeting, 2010 IEEE* (pp. 1-8). IEEE.
- [32] Kumar, Yogendra, Biswarup Das, and Jaydev Sharma. "Multiobjective, multiconstraint service restoration of electric power distribution system with priority customers." *Power Delivery, IEEE Transactions on* 23.1 (2008): 261-270.
- [33] Miu, Karen Nan, Hsiao-Dong Chiang, and Russell J. McNulty. "Multi-tier service restoration through network reconfiguration and capacitor control for large-scale radial distribution networks." *Power Systems, IEEE Transactions on* 15.3 (2000): 1001-1007.
- [34] Wei, W., Sun, M., Ren, R., & Wang, Y. (2012, May). Service restoration of distribution system with priority customers and distributed generation. In *Innovative Smart Grid Technologies-Asia (ISGT Asia), 2012 IEEE* (pp. 1-6). IEEE.
- [35] Hou, J., Xu, Z., Dong, Z. Y., & Wong, K. P. (2014). Permutation-based power system restoration in smart grid considering load prioritization. *Electric Power Components and Systems*, 42(3-4), 361-371.
- [36] Larry Kaufmann. "Services Quality Regulation for Detroit Edison: A Critical Assessment." Pacific Economics Group, March 2007.
- [37] LaCommare, Kristina H. "Tracking the reliability of the US electric power system: an assessment of publicly available information reported to state public utility commissions." Lawrence Berkeley National Laboratory (2008).

- [38] M. J. Sullivan, and D. M. Keane. "Outage Cost Estimation Guidebook," EPRI Research Project 2878-04 Final Report, December 1995.
- [39] Sullivan, M. J., Mercurio, M. G., Schellenberg, J. A., & Eto, J. H. (2010, July). How to estimate the value of service reliability improvements. In Power and Energy Society General Meeting, 2010 IEEE (pp. 1-5). IEEE.
- [40] Sullivan, Michael J. "Estimated value of service reliability for electric utility customers in the United States." Lawrence Berkeley National Laboratory(2009).
- [41] DcDermott, T. E., Drezga, I., & Broadwater, R. P. (1999). A heuristic nonlinear constructive method for distribution system reconfiguration. *Power Systems, IEEE Transactions on*, 14(2), 478-483.
- [42] Kafka, R. J., Penders, D. R., Bouchey, S. H., & Adibi, M. M. (1981). System restoration plan development for a metropolitan electric system. *Power Apparatus and Systems, IEEE Transactions on*, (8), 3703-3713.
- [43] Yuan-Yjh fiu, H.M. H~ang, H.C. KUO, S. K. Peng, C. W. Chang, K. J. Chang, H.S.Yu, C.E.Chow, R.T.Kuo, "Distribution System Service Restoratjon Using A Heuristic Search Approach", *IEEE Transactions on Power Delivery*, Vol. 7, NO. 2, April 1992
- [44] K. Hotta, et al., "Implementation of a real time expert system for a restoration guide in a dispatch center", *IEEE Trans. on Power Systems*, Vol. PWR SJ, pp. 1032-1038, 1990.
- [45] Y. Oualmakran, J. Meléndez, S.Herraiz, Mercedes López-Perea and Eloy González, "Survey on knowledge based methods to assist fault restoration in power distribution networks", *International Conference on Renewable Energies and Power Quality (ICREPQ'11) Las Palmas de Gran Canaria (Spain)*, 13th to 15th April, 2011.
- [46] Arturo S. Bretas, and Arun G. Phadke, "Artificial Neural Networks in Power System Restoration", *IEEE Transactions On Power Delivery*, Vol. 18, No. 4, October 2003
- [47] YogendraKumar, Biswarup Das, and Jaydev Sharma, "Genetic algorithm for supply restoration in distribution system with priority customers", *9th International Conference on Probabilistic Methods Applied to Power Systems KTH, Stockholm, Sweden-June 11-15, 2006-05-20*
- [48] T. Nagata, S. Hatakeyama, M. Yasouka, and H. Sasaki, "An efficient method for power distribution system restoration based on mathematical programming and operation strategy," in *Proc. Int. Conf. Power Syst. Technol.*, 2000.
- [49] J.A Huang, F.D. Galiana, and G.T. Vuong, "Power System Restoration Incorporating Interactive Graphics and Optimization", CH2948-8/91/0000-0216\$1.0001991 IEEE

- [50] T. Nagata, H. Sasaki, and R. Yokoyama, "Power System Restoration by Joint Usage of Expert System and Mathematical Programming Approach", IEEE Transactions on Power Systems, Vol. 10, No. 3, August 1995.
- [51] Hartmut Stadtler, "Linear and Mixed Integer Programming", University of Hamburg, Institute for Logistics and Transport, Von-Melle-Park 5,20146 Hamburg, Germany
- [52] Xiang Li, Tiejian Li, Jiahua Wei, Guangqian Wang, and William W.-G. Yeh, "Hydro Unit Commitment via Mixed Integer Linear Programming: A Case Study of the Three Gorges Project, China", IEEE Transactions on Power Systems, Vol. 29, No. 3, May 2014.
- [53] Mostafa Esmaeeli Sh., and A. Kazemi, "Stochastic Unit Commitment of Wind Farms Based on Mixed-Integer Linear Formulation", Innovative Smart Grid Technologies (ISGT), 2012 IEEE PES
- [54] Shahab Dehghan, IEEE, Nima Amjady, and Ahad Kazemi, "Two-Stage Robust Generation Expansion Planning: A Mixed Integer Linear Programming Model", IEEE Transactions On Power Systems, Vol. 29, No. 2, March 2014.
- [55] Hui Zhang, Vijay Vittal, Gerald Thomas Heydt, and Jaime Quintero, "A Mixed-Integer Linear Programming Approach for Multi-Stage Security-Constrained Transmission Expansion Planning ", IEEE Transactions On Power Systems, Vol. 27, No. 2, May 2012.
- [56] Rafael S. Ferreira, Carmen L. T. Borges, and Mario V. F. Pereira, "A Flexible Mixed-Integer Linear Programming Approach to the AC Optimal Power Flow in Distribution Systems", IEEE Transactions On Power Systems, Vol. 29, No. 5, September 2014.
- [57] B. Moradzadeh, K. Tomsovic, "Mixed Integer Programming-Based Reconfiguration of A Distribution System with Battery Storage", North American Power Symposium (NAPS), 2012
- [58] Wei Sun and Chen-Ching Liu, "Optimal Transmission Path Search in Power System Restoration", Bulk Power System Dynamics and Control - IX Optimization, Security and Control of the Emerging Power Grid (IREP), 2013 IREP Symposium.
- [59] V. Krishna., V.C.Ramesh, and N.Ong, "Optimisation approach to power restoration in steel mills", Electric Power Applications, IEE Proceedings Nov 1998.
- [60] M. Shahrin A. H., K. Nosu, H. Aoki, " Integrating Distributed Generator for Restoration Optimization", IEEE International Conference on Power and Energy (PECon), 2-5 December 2012, Kota Kinabalu Sabah, Malaysia.
- [61] Lei, Shaolan, et al. "Distribution service restoration using chaotic optimization and immune algorithm." Information Science and Technology (ICIST), 2011 International Conference on. IEEE, 2011.

- [62] De Sá Ferreira, Rafael. A Mixed-Integer Linear Programming Approach To The Ac Optimal Power Flow In Distribution Systems. Diss. Universidade Federal do Rio de Janeiro, 2013.
- [63] Jabr, Rabih A., Ravindra Singh, and Bikash C. Pal. "Minimum loss network reconfiguration using mixed-integer convex programming." *Power Systems, IEEE Transactions on* 27.2 (2012): 1106-1115.
- [64] Civanlar, Seyhan, et al. "Distribution feeder reconfiguration for loss reduction." *IEEE Trans. Power Del.* 3.3 (1988).
- [65] Hong, Ying-Yi, and Saw-Yu Ho. "Determination of network configuration considering multiobjective in distribution systems using genetic algorithms." *Power Systems, IEEE Transactions on* 20.2 (2005): 1062-1069.
- [66] Lin, Whei-Min, and Hong-Chan Chin. "A new approach for distribution feeder reconfiguration for loss reduction and service restoration." *Power Delivery, IEEE Transactions on* 13.3 (1998): 870-875.
- [67] Kim, Hoyong, Yunseok Ko, and Kyung-Hee Jung. "Artificial neural-network based feeder reconfiguration for loss reduction in distribution systems." *Power Delivery, IEEE Transactions on* 8.3 (1993): 1356-1366.
- [68] Chang, Hong-Chan, and Cheng-Chien Kuo. "Network reconfiguration in distribution systems using simulated annealing." *Electric Power Systems Research* 29.3 (1994): 227-238.
- [69] Su, Ching-Tzong, and Chu-Sheng Lee. "Network reconfiguration of distribution systems using improved mixed-integer hybrid differential evolution." *Power Delivery, IEEE Transactions on* 18.3 (2003): 1022-1027
- [70] L. A. Wolsey, *Integer programming*. John Wiley and Sons, New Jersey, 1998.
- [71] A. Borghetti, "Using mixed integer programming for the volt/var optimization in distribution feeders," *Elect. Power Syst. Res.*, vol. 98, pp. 39–50, May 2013.
- [72] G. McCormick, —Computability of global solutions to factorable nonconvex programs: Part I — Convex underestimating problems. *Mathematical Programming*. 10 (1976) 146–175.
- [73] M. S. Bazaraa, H. D. Sherali, and C. M. Shetty, *Nonlinear Programming—Theory and Algorithms*, JohnWiley&Sons,New York, NY, USA, 2nd edition, 1993.

- [74] F. S. Hillier and G. J. Lieberman, Introduction to Operations Research, McGraw-Hill, New York, NY, USA, 6th edition, 1995.
- [75] Ming-Hua Lin,¹ John Gunnar Carlsson,² Dongdong Ge,³ Jianming Shi,⁴ and Jung-Fa Tsai⁵, “A Review of Piecewise Linearization Methods”, Hindawi Publishing Corporation, Mathematical Problems in Engineering, Volume 2013, Article ID 101376.

VITAE

Personal Information

Name Maad Mohammed Abdullah Al-Owaifeer
Nationality Saudi
Date of Birth 19/11/1990
Email maad.alowaifeer@gmail.com
Address KFUPM, Dhahran, Saudi Arabia

Academic Background

- 2008-2013 “**King Fahd University of Petroleum and Minerals**”
Bachelor of Science degree in electrical engineering with honors recognition.
- 2013-2015 “**King Fahd University of Petroleum and Minerals**”
Master of Science Degree in power and energy engineering with honors recognition.

Experience

- Summer 2009 “**King Fahd University of Petroleum and Minerals**”
Working with King Abdul Aziz and His Companions Foundation for Giftedness and Creativity as an advisor.
- Jul – Dec 2012 “**General Electric Company**”
Abroad CO-OP training with Power Division, General Electric, NY
- Jan 2014 – current time “**King Fahd University of Petroleum and Minerals**”
Acting as a graduate assistant teaching power engineering undergraduate laboratory courses.
- Jan 2015 – current time “**Institute of Electrical and Electronic Engineers IEEE**”
Vice Chair of IEEE-KFUPM student branch.

Publications

- Maad AlOwaifeer, Mohammad AlMuhaini, and Abdulrahman AlSaggaf, “*The Impact of Load Management and Renewable DG on the Service Restoration of Future Power Distribution Systems*” IEEE 15th International Conference on Environment and Electrical Engineering, 2015.